Université du Québec
à Rimouski

ÉTUDE SUR L'OPTIMISATION DES PARAMÈTRES DU PROCÉDÉ DE TREMPE PAR INDUCTION EN UTILISANT UN CONCENTRATEUR DE FLUX

APPROCHE NUMÉRIQUE ET EXPÉRIMENTALE

Mémoire présenté

dans le cadre du programme de maîtrise en ingénierie

en vue de l'obtention du grade de maître ès sciences appliquées (M. Sc. A.)

PAR

© Mahyar Parvinzadeh

juillet 2022

Composition du jury :

Abderrazak El Ouafi, président du jury, Université du Québec à Rimouski

Noureddine Barka, directeur de recherche, Université du Québec à Rimouski

Maxime Berger, professeur, Université du Québec à Rimouski

Ilyes Maamri, examinateur externe, Tekna Plasma Systèmes

Dépôt initial le 22 Avril 2022 Dépôt final le 6 juillet 2022

[Taper ici la dédicace. Cette page est facultative; l'éliminer, de même que la page blanche suivante, s'il n'y a pas de dédicace.]

REMERCIEMENTS

Je tiens tout d'abord à remercier tout le personnel du département de mathématiques, d'informatique et de génie à l'Université du Québec à Rimouski qui m'ont guidé tout au long de mon projet de maîtrise et avec lesquelles j'ai développé des liens particuliers.

Je remercie également mon directeur de recherche, Monsieur Noureddine Barka, qui a fait partie des acteurs bienveillants de ma formation, et pour la confiance qu'il a eue à mon égard lorsqu'il m'a confié ce projet de recherche. Je ne saurais le remercier suffisamment pour ses précieux conseils et ses méthodes de travail qui m'aident quotidiennement.

Enfin, j'adresse mes remerciements à ma famille et tous mes amis qui ont été toujours présents à mes côtés, ainsi que pour leur soutien, leur patience et leurs encouragements tout le long de mon projet.

AVANT-PROPOS

[Cette page est facultative; l'éliminer, de même que la page blanche suivante, si elle n'est pas utilisée. L'avant-propos ne doit pas être confondu avec l'introduction. Il n'est pas d'ordre scientifique alors que l'introduction l'est. Il s'agit d'un discours préliminaire qui permet notamment à l'auteur d'exposer les raisons qui l'ont amené à étudier le sujet choisi, le but qu'il veut atteindre, ainsi que les possibilités et les limites de son travail. On peut inclure les remerciements à la fin de ce texte au lieu de les présenter sur une page distincte.]

RÉSUMÉ

La trempe par induction est un traitement thermique bien connu pour le durcissement superficiel du métal. La rentabilité, la constance de la qualité du résultat dans la production de masse, le gain de temps et le respect de l'environnement sont quelques-uns des avantages de cette méthode qui en font un bon choix pour la trempe superficielle des pièces complexes et sphériques comme les engrenages. La nécessité de durcir la surface extérieure des engrenages (tête et racine de la denture) plutôt que cœur fait de ces pièces une cible idéale pour le chauffage par induction à des fins industrielles. Des recherches appropriées sur cette méthode sont nécessaires pour comprendre plusieurs règles physiques et la métallurgique des matériaux concernés, ce qui rend cette méthode compliquée à étudier. Dans ce processus, de nombreux paramètres doivent être contrôlés en fonction du couplage physique complexe des phénomènes électromagnétiques et de transfert de chaleur. Ces paramètres affectent directement les caractéristiques mécaniques du résultat final qui peuvent être évaluées par la forme et la profondeur du profilé trempé. En outre, en fonction de la spécification du matériau traité et des propriétés telles que la résistance, la ductilité, la dureté, la fragilité, la ténacité, la rigidité, etc. que nous voulons atteindre à la fin du traitement thermique, il est nécessaire de connaître la métallurgie du matériau. Ainsi, pour obtenir le meilleur profil de dureté possible, il faut optimiser les paramètres de contrôle et trouver leur combinaison unique pour cette géométrie et ce matériau spécifique. La pièce étudiée dans ce projet est l'engrenage droit en acier 4340. Cet acier est un acier au carbone moyen à haute résistance qui réagit favorablement au traitement thermique. Il présente une bonne combinaison de ductilité et de résistance qui le rend fiable pour des applications telles que l'aérospatiale, l'armée, les systèmes automobiles et d'autres applications de machines-outils. En ce qui concerne les spécifications de l'engrenage droit et de l'alliage d'acier 4340, l'étape suivante consiste à étudier les effets des paramètres électromagnétiques, mécaniques et géométriques sur les effets de bord dans les géométries axisymétriques tridimensionnelles. La présente étude est réalisée en établissant un lien entre la simulation, le plan d'expériences, l'analyse statistique, les réseaux neuronaux, l'expérimentation et l'optimisation, afin de trouver un modèle prédictif du profil trempé. Simultanément, la minimisation de l'effet de bord en ajustant les paramètres de contrôle par l'application d'un concentrateur de flux est un autre objectif de ce projet. Les équations de Maxwell et de transfert de chaleur ont permis de simplifier la complication des lois de comportement du matériau en les remplaçant par les équations de densité de courant externe. La méthode des éléments finis du logiciel COMSOL 3D est appliquée pour faciliter l'amélioration du profil de dureté. Valider le modèle numérique créé, une combinaison de simulation, de tests expérimentaux et de mesures des profils de dureté sont effectuée à chaque étape du projet, ce qui a permis d'obtenir d'excellents résultats grâce à la simulation. Il en résulte des paramètres de processus d'induction améliorés qui aident les industries à produire des composants mécaniques d'une qualité et d'une performance plus souhaitables.

Mots clés : traitement thermique par induction, acier 4340, profil de dureté, effet de bord, concentrateurs de flux, engrenages, ANOVA.

ABSTRACT

Induction hardening is a well-known heat treatment for the surface hardening of metal. Cost-effectiveness, consistency in quality of the output in mass-production, time-efficient, and environment friendly are some of the advantages of this method that make it a good choice to surface hardening of the complex and spherical parts like gears. The necessity of hardening the outer surface of the gears (tip and root of the tooth) rather than the interior makes these parts a right target of induction heating for industrial purposes. Proper investigation on this method is needed to understand several physical rules and metallurgy of the involved materials which make this method complicate to study. In this process, many parameters are to be controlled based on the complex physical coupling of electromagnetic and heat transfer phenomena. These parameters directly affect the mechanical characteristics of the result that can be evaluated by the shape and depth of the hardened profile. Furthermore, according to the specification of the treated material and the properties such as strength, ductility, hardness, brittleness, toughness, stiffness etc., that we aim to reach at the end of the heat treating, knowing the metallurgy of the material is necessary to understand. Thus, having the best possible hardness profile needs to optimize control parameters and find their unique combination for that specific geometry and material. The studied part in this project is the 4340 steel spur gear. AISI 4340 is high-strength medium carbon steel with a favorable response to heat treatment and shows a good combination of ductility and strength that make it reliable for applications such as aerospace, military, automotive systems, and other machine tool applications. Regarding the specifications of the spur gear and 4340 steel alloy, the next step is to investigate the effects of the electromagnetic, mechanical, and geometrical parameters over edge effects in the three-dimensional axisymmetric geometries. The present study is carried out by linking among simulation, design of experiments, statistical analysis, neural networks, experimentation, and optimization, to find a predictive model of the hardened profile. Simultaneously, minimizing the edge effect by adjusting the control parameters by application of flux concentrator is another objective of this project. Maxwell's and heat transfer equations helped to simplify the complication of the material behavior laws by replacing them with the external current density equations. The finite element method of COMSOL 3D software is applied to ease the complication of enhancing the hardness profile. To validate the created model, a combination of simulation, experimental tests, and hardened profile measurements are conducted at each step of the project leading to the excellent results provided by the simulation. The result provides enhanced induction process parameters that help industries produce mechanical components with more desirable quality and performance.

Keywords: Induction heat treatment, 4340 steel, Hardness profile, Edge effect, Flux concentrators, Gears, ANOVA.

TABLE DES MATIÈRES

LISTE DES TABLEAUX

LISTE DES FIGURES

INTRODUCTION GÉNÉRALE

0.1 Contexte

De manière générale, la trempe superficielle de l'acier est classée en deux groupes: les traitements dans lesquels la microstructure subit des transformations microstructurales et thermochimiques. Dans la première méthode, la profondeur de cémentation est faible par rapport à la taille de la pièce (environ 0,8 à 3,5 mm) [1], par exemple, la trempe au laser [2-4], la trempe à la flamme [5, 6], la trempe par induction [7-10], la trempe au chalumeau à plasma et la trempe par faisceau d'électrons [11, 12]. La deuxième méthode implique des traitements thermochimiques tels que la cémentation, la nitruration et la carbonitruration. Dans ce cas, la diffusion d'éléments non métalliques à la surface de la pièce qui se produit entraîne une réduction de la dureté. On utilise des fours avec des combustibles tels que le propane (gaz naturel) ou l'ammoniac qui possèdent une forte concentration d'hydrocarbures ou d'azote gazeux.

Le procédé de trempe superficielle le plus performant parmi les autres procédés est le chauffage par induction qui a fait ses preuves dans les industries métallurgiques en raison de sa productivité exceptionnelle, de son efficacité énergétique et de sa capacité à faciliter le traitement de pièces métalliques aux formes géométriques complexes telles que les engrenages [10]. Cette méthode est très demandée dans de nombreuses industries pour des processus tels que le brasage [14, 15], le moulage [16, 17], ainsi que pour le durcissement des pièces qui est appliqué dans l'automobile et l'aérospatiale [18-20]. La spécificité la plus notable de la méthode de chauffage par induction est de chauffer la pièce sans aucun contact physique et direct entre la source d'énergie et la pièce fabriquée avec un matériau à perméabilité magnétique relativement élevée par l'intermédiaire d'un inducteur. Comme le montre la Figure 1, la génération de la chaleur est le résultat de la circulation en circuit fermé

de courants électriques sur la surface de la pièce. Ces courants sont connus sous le nom de courants induits ou courants de Foucault. Un courant alternatif externe circulant dans une bobine de cuivre produit un champ électromagnétique qui frappe la pièce et en y créant un courant électrique. La résistance électrique à l'intérieur de la pièce provoque la génération de chaleur [21, 22]. Le courant produit dans l'inducteur est caractérisé par sa fréquence (f) et la densité du courant induit (J_0). Durant le processus de chauffage, l'effet de peau distribue le courant de la surface et le distribue la chaleur sur la surface ou dans la peau de la pièce.

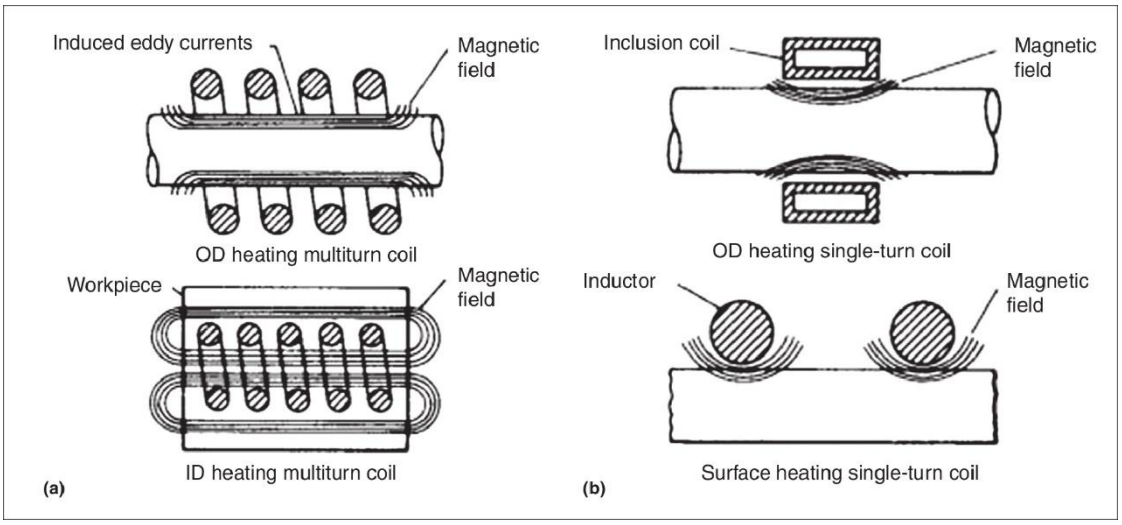

Figure 1. Disposition commune de l'inducteur et de la pièce traiter par le chauffage par induction (a) du diamètre extérieur et intérieur avec des bobines multi-spires et (b) du diamètre extérieur et de la surface avec des bobines à une spire [21]

Pour augmenter la dureté de la pièce, le chauffage doit être effectué au-dessus de la température minimale d'austénitisation et en dessous du point de fusion de cet acier spécifique. Un chauffage vite ou rapide doit être suivi d'une trempe rapide pour assurer une transformation de l'austénite en martensite. La structure martensitique de l'acier est connue pour être la structure la plus dure de ce type d'acier, ce qui le rend approprié pour les applications qui nécessitent une dureté pour de meilleures performances mécaniques. Pour produire de l'austénite à la surface de la pièce, la profondeur de la zone chauffée peut être ajustée en modifiant la fréquence, le courant et le temps de chauffage. Le réglage d'un niveau

de fréquence plus élevé conduit à faire circuler le courant davantage vers la surface que vers le cœur de la pièce.

0.2 PROBLÈMATIQUE

Le chauffage par induction est une combinaison de plusieurs phénomènes physiques tels que l'électromagnétisme, le transfert de chaleur et la métallurgie. En fonction de l'application du matériau souhaité, certains paramètres du procédé de chauffage par induction doivent être ajustés. La caractéristique de chauffage sans contact entre l'inducteur et la pièce de l'induction offre l'avantage d'appliquer une large gamme de pièces aux géométries simples ou complexes. Cependant, la combinaison des deux principaux phénomènes physiques entraîne une difficulté de réglage des paramètres. Ces deux phénomènes sont l'électromagnétisme et le transfert de la chaleur produite à l'intérieur de la pièce. Ces aspects ajoutent de la complexité à la simulation et à l'expérimentation. De plus, les données sur les propriétés des matériaux appliqués ne sont pas toujours précises et la réponse à la température peut varier par rapport aux attentes, ce qui est difficile à gérer.

En outre, le réglage du paramètre de chauffage du courant de la machine pendant le processus de chauffage est une tâche expérimentale qui est toujours difficile à maitriser ou contrôler avec précision en raison de la vitesse de chauffage très rapide. La prédiction des résultats du processus d'induction dépend de la connaissance du schéma de diffusion de la température à l'intérieur de la pièce tout au long du processus qui est lié à la fonction des champs électromagnétiques à l'intérieur de celle-ci. La principale cause de la chaleur produite à l'intérieur de la pièce est l'effet Joule qui, lui-même, est provoqué par la circulation de courants induits. La fréquence de ces courants est la même que la fréquence du courant alternatif externe circulant dans l'inducteur. Ces courants circulent principalement près de la surface (effet de peau) et des bords de la pièce, ce qui signifie que même dans les endroits très isolés, il y a une distribution non uniforme du courant. Ce phénomène ne se produit que lorsque le courant est alternatif et est connu sous le nom « d'effet de bord ». La conséquence de ce phénomène est illustrée à la Figure 2.

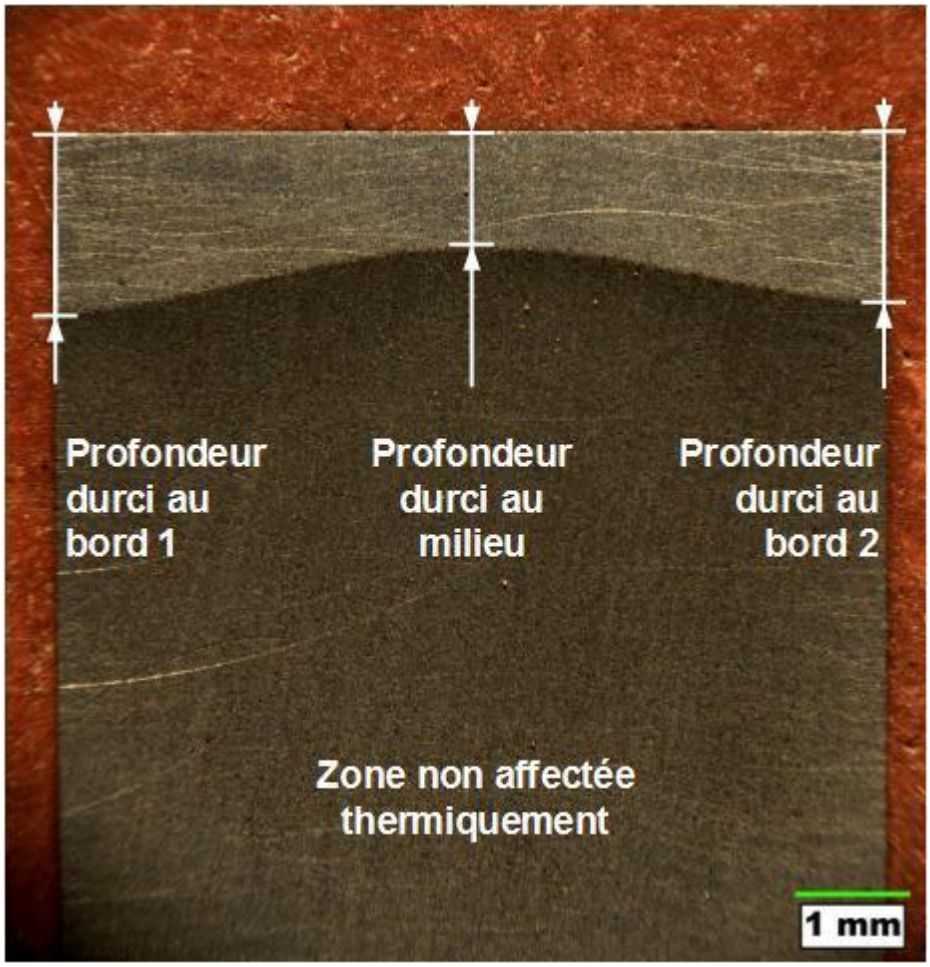

Figure 2. Démonstration de l'effet de bord en créant une profondeur durcie différente dans le plan moyen [24]

La densité des courants induits et de l'énergie par effet Joule a plus de profondeur sur les bords de la pièce et elle diminue au milieu. La profondeur maximale depuis la surface de la pièce est caractérisée par l'épaisseur δ. En règle générale, l'épaisseur est définie approximativement à 86% des courants induits [25]. Les valeurs de la profondeur dépendent de plusieurs paramètres tels que la fréquence, la géométrie de l'inducteur et du concentrateur de flux, la position relative de la pièce par rapport à la bobine et aux concentrateurs de flux, les propriétés magnétiques de la pièce, la méthode de trempe, etc. [26]. Cependant, la méthode d'induction est un processus industriel bien établi par rapport aux autres méthodes, mais comme il a été décrit, il y a quelques problèmes à améliorer tels que. Pour obtenir un

profil de dureté uniforme à la fin du processus de chauffage, il est nécessaire de prévoir la distribution des champs électromagnétiques créés par l'inducteur dans diverses situations. La raison est la distorsion du champ électromagnétique à certains endroits de la pièce, comme les coins, principalement dans les pièces cylindriques telles que les disques et les engrenages. Cette distorsion entraîne un profil de dureté non uniforme indésirable à la fin du traitement. Depuis les années 1970, plusieurs recherches ont été menées pour améliorer certains flux de la trempe par induction [26, 27]. Ces études ont été réalisées à l'aide de différentes procédures numériques et expérimentales afin de couvrir et d'améliorer tous les problèmes pratiques que les pièces subissent au cours des applications industrielles telles que le soudage, le moulage, la trempe par induction des matériaux métalliques eux-mêmes, etc., la modélisation du traitement thermique par induction [28-31], et des processus de cémentation [32, 33]. Les études mentionnées ont tenté de couvrir les difficultés de la combinaison du transfert de chaleur avec le champ électromagnétique. Dans la modélisation du procédé de la trempe par induction, la contribution des deux domaines mentionnés ainsi que les différentes réactions pratiques du matériau à partir de leur fiche technique constituent une autre difficulté de l'étude. Un autre facteur essentiel à connaître pendant l'étude est la mesure de la température de surface de la pièce à chaque étape de l'expérimentation, alors que la durée du processus est extrêmement courte, ce qui rend les études encore plus complexes. Pour éliminer ces problèmes, les chercheurs ont fusionné l'expérimentation avec des méthodes statistiques qui permettent de simplifier le processus. Les éléments constitutifs d'une étude statistique appropriée sont le choix des paramètres les plus efficaces, l'exécution des tests expérimentaux appropriés et, enfin, l'analyse des résultats en utilisant une méthode robuste et efficace. À cette fin, la simulation est l'approche la plus efficace, utilisée par les scientifiques [34-36], la simulation accompagnée de la validation des données [37, 38], des tests expérimentaux bien organisés [39-42]. Hömberg et al [43] ont utilisé la simulation pour étudier les transitions de phase et le changement des propriétés mécaniques pendant la trempe par induction multifréquence. Urquizo et al [44] ont étudié les effets mécaniques de la trempe dans le chauffage par induction de l'acier 42CrMo4. Jakubovičová et al [45] ont essayé d'améliorer la profondeur durcie non uniforme de la surface de la pièce. Barglik et al [46],

Cajner et al [47], and Sadeghipour et al [48] ont essayé d'utiliser la simulation et d'atteindre un modèle pour différentes pièces avec différentes géométries et matériaux. Kristoffersen et al [41] ont discuté la distribution des contraintes résiduelles et de ses effets sur le résultat final de la trempe par induction. Barka et al. [35] ont utilisé COMSOL pour la modélisation axisymétrique afin d'étudier l'effet des paramètres de la machine sur le profil de dureté de la trempe par induction d'échantillons en acier 4340. Les résultats des études mentionnées ont permis de mieux connaître les phénomènes électromagnétiques et le processus de trempe par induction, les effets des différentes méthodes de trempe, la contrainte résiduelle, la distribution de la température et leurs effets sur le profil de dureté. Dans le cas des engrenages, l'expérimentation pratique pouvait se faire en ajustant les paramètres et/ou la conception de la machine et en changeant la géométrie de la bobine, ce qui, dans les deux cas, prendrait beaucoup de temps et d'énergie, sans compter que la conception d'un nouvel inducteur à chaque étape rend l'expérimentation trop coûteuse. Comme l'indiquent les revues de littérature, pour résoudre ces problèmes, des modèles de simulation peuvent être appliqués pour analyser le profil de dureté des différents matériaux avec une variété de géométries en fonction des paramètres de la machine [21, 22] . Plusieurs études ont conclu que pour réduire l'effet de bord, une meilleure méthode et plus efficace devrait être utilisée pour avoir un meilleur contrôle sur la distribution de la chaleur sur la surface de la pièce [49-51]. En effet, pour atteindre cet objectif, dans la dernière étude, le chercheur a examiné l'utilisation de concentrateurs de flux dans la modélisation axisymétrique pour les pièces en forme de disque comme les engrenages [49] . Pour poursuivre et optimiser l'étude mentionnée, d'autres études avec la modélisation numérique axisymétrique 3D ont été réalisées [52] . Le flux magnétique non focalisé sur une section souhaitée de la pièce est l'un des problèmes courants du chauffage par induction qui provient de la nature dispersive du champ électromagnétique. Une étude menée par Barka et al [53] a démontré l'effet significatif de l'utilisation de concentrateurs ayant la même géométrie que l'engrenage droit lorsque la pièce principale est placée symétriquement entre les deux concentrateurs, comme le montre la Figure 3.

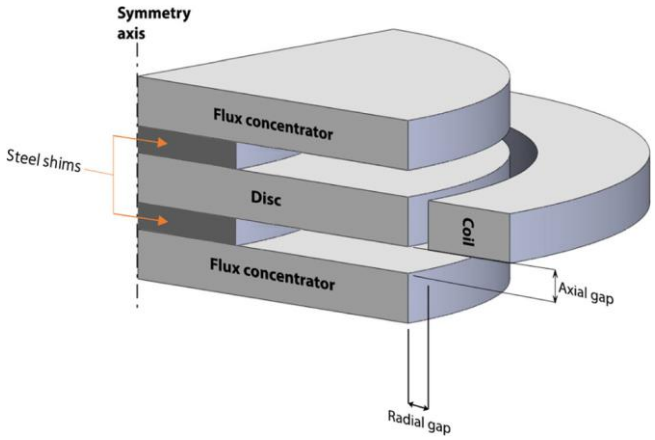

Figure 3. Présentation schématique du chauffage par induction avec deux concentrateurs de flux magnétique [54]

Les résultats ont confirmé que l'application d'un ensemble de concentrateurs de flux élimine la diffusion du flux magnétique sur les zones non souhaitées et les concentrer dans la zone la plus appropriée à chauffer. De plus, cela augmente l'uniformité de la profondeur du boîtier dans les zones prévues, comme le montre la Figure 4. Le choix de la forme et du matériau de construction du concentrateur de flux appliqué dépend de plusieurs paramètres tels que la forme et la géométrie de la pièce principale, la puissance et la gamme des fréquences utilisées. Les laminations découpées dans des alliages magnétiques à grains orientés sont le matériau habituellement utilisé pour construire les concentrateurs de flux [55].

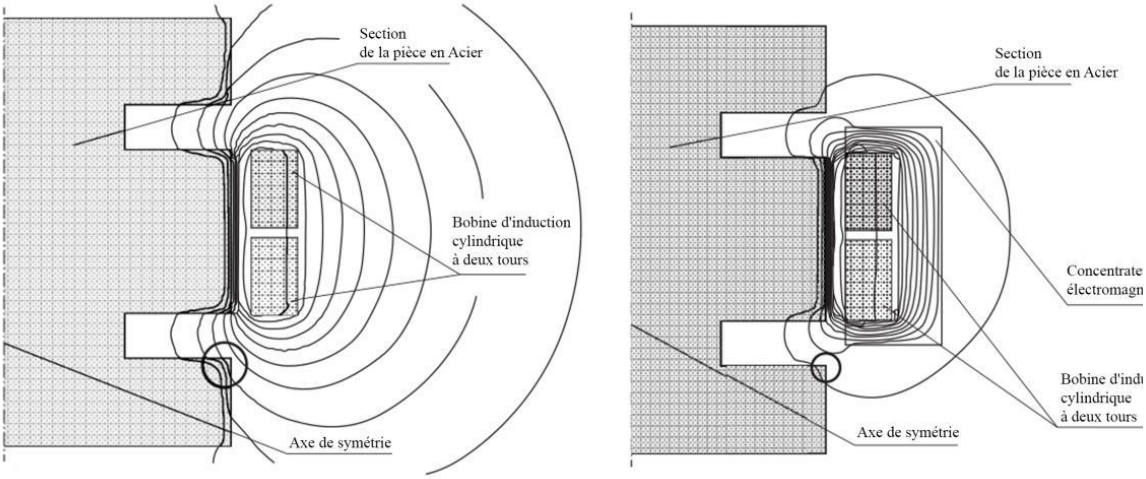

(a) (b)

Figure 4. Flux magnétique en concentration dans une bobine à deux spires (a) sans concentrateurs de flux (b) avec concentrateurs de flux.

Plusieurs recherches ont tenté de trouver d'autres paramètres actuels pour contrôler le modèle de la profondeur durcie sur la surface de la pièce afin d'obtenir une profondeur de cémentation plus uniforme [52, 56]. Deux concentrateurs concentrent et linéarisent le champ électromagnétique sur la surface de la pièce, ce qui réduit l'effet de bord et rend le processus plus coûteux et plus efficace.

0.3 OBJECTIFS

De nombreux types de recherche ont été menés dans le domaine de la trempe par induction et chacun d'entre eux a tenté d'apporter une amélioration à cette méthode, qu'il s'agisse de faciliter la manipulation et l'installation de la machine à induction et de la rendre plus conviviale, ou de la moderniser en la rendant plus puissante et plus efficace grâce à des améliorations telles qu'un générateur de puissance plus efficace et l'utilisation de concentrateurs de flux. Cependant, les autres études ont tenté d'améliorer les paramètres de la machine. Ceci peut être accompli en utilisant des expériences, des simulations ou une combinaison de ces deux méthodes.

Cette recherche vise à améliorer le profil de dureté final de pièces en acier 4340 traitées par induction, comme des disques et des engrenages droits, en appliquant un ensemble de concentrateurs de flux ayant la même géométrie que la pièce à traiter. L'étude utilise une série de paramètres basés sur des revues de la littérature et des recherches antérieures. Pour justifier le domaine le plus efficace et éliminer les paramètres inadaptés, il est essentiel d'établir des analyses statistiques robustes de la variation de la température qui aboutissent à la création de modèles de prédiction fiables.

Le premier objectif est d'améliorer la profondeur durcie de l'engrenage droit en acier 4340 en minimisant les phénomènes indésirables d'effet de bord tout en utilisant un ensemble de concentrateurs de flux ayant la même géométrie que l'engrenage principal. Le second objectif est d'étudier l'impact de l'effet de bord sur les disques simples. Dans ce cas, la géométrie simple du disque permet d'améliorer la profondeur durcie sur le bord dans un disque. Le troisième objectif est de maximiser la profondeur durcie et de minimiser l'effet de bord sur l'engrenage droit dans le cas d'un chauffage à double fréquence séquentielle (moyenne et haute fréquences).

0.4 MÉTHODOLOGIE

Pour atteindre le premier objectif, les séquences de réalisation des expériences, de collecte des données, d'analyse des données et de création du modèle sont planifiées sur la base de revues de la littérature. Lors des expérimentations, les échantillons sont durcis par une machine à induction de l'École de Technologie Supérieure de Montréal. Cet appareil possède un générateur de radiofréquence à thyristor (200 kHz) qui lui permet de produire la puissance maximale de 450kW. L'inducteur dont elle est équipée cette machine est usiné en cuivre et il a une section utile de 7 x 7 mm. Pour collecter les données, les essais de microdureté sont effectués pour déterminer les profils de dureté. Pour l'engrenage droit, quatre profondeurs ont été mesurées à la tête et à la racine de la denture. Ensuite, les résultats seront analysés statistiquement en appliquant l'analyse de la variance (ANOVA) et la méthodologie de la surface de réponse (RSM).

Des modèles utiles sont créés pour donner exprimer le profil de dureté en fonction des paramètres du procédé. Il est important de mentionner que le matériau choisi pour les expériences et les simulations est de l'acier 4340, qui est un alliage nickel-chrome-molybdène connu pour sa trempabilité, sa ductilité, sa ténacité et sa résistance élevées, ainsi que pour sa résistance à la fatigue élevée à l'état traité thermiquement.

Pour répondre au deuxième objectif, une première phase consiste à la réalisation des expériences de durcissement par induction appliqués sur des disques en acier 4340, la collecte des données, l'analyse des données et la création du modèle de prédiction. Dans ce cas-ci, une paire de concentrateurs de flux en même que le disque principal est utilisée. Comme pour les engrenages, les expériences sont réalisées avec la même machine à induction de l'École de Technologie Supérieure de Montréal. La collecte de données comprend les tests de microdureté. La même méthodologie sera suivie pour cette étude en ce qui concerne l'analyse statistique. Cependant, dans le cas des disques, seulement deux profondeurs seront mesurées au lieu de quatre dans le cas des engrenages. L'analyse statistique des données (ANOVA) et la méthodologie de la surface de réponse (RSM) vont permettre de déterminer les effets et les contributions des paramètres du procédé. Finalement, un modèle de prédiction sera développé pour exprimer le profil de dureté en fonction de paramètres du procédé.

La méthode pour atteindre le troisième objectif consiste à utiliser la méthode d'analyse par éléments finis pour créer un modèle numérique. En effet, le logiciel de simulation COMSOL est utilisé pour créer un modèle utilisant les modes monofréquence et à double fréquence séquentielle pour modéliser le procédé de chauffage par induction de l'engrenage droit en acier 4340. Le modèle sera basé sur le couplage des champés magnétiques et le transfert de chaleur pour déterminer les températures à la tête et à la racine d'une roue dentée. Pour le cas de l'étude, deux formulations des équations de Maxwell pour l'électromagnétisme et des équations de transfert de chaleur caractérisent mathématiquement la physique du chauffage par induction. La solution de ces équations sera démontrée par un modèle 3D. Pour

s'assurer que les résultats de la simulation ne sont pas affectés par le changement de la taille du maillage, toutes les simulations seront réalisées après avoir effectué une étude de convergence. Ensuite, les profondeurs durcies et les effets de bord pour chaque fréquence sont contrôlés. La dernière étape est de trouver la meilleure combinaison de la densité de courant J_0, du temps de chauffage t_c, de l'écart entre chaque concentrateur et la pièce) et l'écart entre la bobine et la pièce pour atteindre un profil de dureté en contour.

0.5 ORGANISATION DU MÉMOIRE

Comme indiqué, l'introduction générale a apporté une description des phénomènes de chauffage par induction, des paramètres, de ses préoccupations communes, des objectifs et de la méthodologie de l'étude présentée. Dans le premier chapitre, les effets des paramètres du processus de chauffage par induction et leurs interactions sur l'effet de bord dans la trempe de l'engrenage droit sont discutés. Le deuxième chapitre traite des effets de l'application de concentrateurs de flux avec la même géométrie que la pièce principale, qui est un disque, tout en cherchant la meilleure combinaison des paramètres du processus de chauffage par induction. Le troisième chapitre présente la simulation par éléments finis du procédé de chauffage par induction appliqué à un engrenage droit en utilisant le chauffage à double fréquence séquentielle. Enfin, le mémoire est complété par une conclusion générale permettant d’exposer les résultats des trois chapitres mentionnés pour ouvrir la voie à de nouvelles recherches dans ce domaine.

CHAPITRE 1
UNE NOUVELLE ÉTUDE SUR LA RÉDUCTION DE L'EFFET DE BORD D'UN ENGRENAGE DROIT EN ACIER 4340 PENDANT LE PROCESSUS DE TREMPE PAR INDUCTION

1.1 RESUME EN FRANÇAIS

La trempe par induction, une approche prometteuse pour la trempe sélective de pièces métalliques, est largement utilisée pour la trempe superficielle lorsqu'une surface dure est requise à côté d'un noyau résistant. En ce qui concerne la complexité de ce processus, la géométrie des pièces affecte profondément la distribution de la température et le profil de dureté en conséquence. Durant cette étude, deux concentrateurs de flux magnétique sont introduits dans notre ensemble de machines à induction afin de contrôler le flux magnétique et, par conséquent, le profil de dureté (profondeur durcie) des engrenages droits. La performance des concentrateurs de flux magnétique est examinée par l'effet des paramètres de la machine sur la profondeur durcie et l'effet de bord de l'engrenage droit en acier AISI 4340. Un plan d'expériences basé sur la méthode Taguchi est principalement utilisé pour optimiser le nombre d'essais expérimentaux. Ensuite, les profils de dureté des engrenages traités thermiquement à la tête et à la racine des engrenages sont mesurés par des essais de dureté par micro-indentation. Les résultats sont analysés à l'aide de l'analyse de la variance (ANOVA) et de la méthode de la surface de réponse (RSM) pour déterminer l'effet principal des paramètres du processus, ainsi que la meilleure combinaison de paramètres du processus qui maximise la profondeur durcie et minimise la caractéristique indésirable de l'effet de bord. Enfin, les modèles de prédiction de la profondeur durcie en fonction des paramètres du processus sont développés sur la base de la méthode de régression linéaire. À cette fin, quatre modèles prédictifs de la profondeur durcie à la tête et à la racine dans le plan du bord et le plan médian des engrenages droits sont générés. Les résultats indiquent que la profondeur

durcie maximale avec un effet de bord minimal à la racine et à la tête est obtenue en réglant la puissance maximale de la machine, le temps de chauffage le plus long et l'écart axial minimal entre les concentrateurs et l'engrenage droit. Cette étude fournit une bonne exploration de la profondeur durcie en présence de concentrateurs de flux magnétique sous différents paramètres de processus et donne une ligne directrice fiable concernant l'effet de bord pendant le processus de trempe par induction.

Mots clés **– Trempe par induction, engrenage droit, acier AISI 4340, ANOVA, RSM, profondeur durcie.**

Ce premier article, intitulé "A novel investigation into edge effect reduction of 4340 steel spur gear during induction hardening process", fut co-rédigé par moi-même ainsi que par le professeur Noureddine Barka, le professeur adjoint Sasan Sattarpanah Karganroudi, Mohamed Khalifa et Narges Omidi. Il a été accepté pour publication dans sa version finale en 26 janvier 2021 par les éditeurs de la revue "The International Journal of Advanced Manufacturing Technology". En tant que premier auteur, ma contribution à ce travail a été la recherche de l'état de l'art, le développement de la méthode, la gestion des données et des résultats, et la rédaction de l'article. Le professeur Noureddine Barka a fourni l'idée originale. Mohamed Khalifa a contribué à l'exécution des tests expérimentaux. Le professeur adjoint Sasan Sattarpanah Karganroudi et le professeur Noureddine Barka ont participé à la recherche de l'état de l'art, le développement de la méthode et la révision de l'article. Narges Omidi a également participé à la révision de l'article. Une version électronique de cet article a été présentée avec l’identifiant numérique suivant :

https://link.springer.com/article/10.1007/s00170-021-06639-w

1.2 A NOVEL INVESTIGATION INTO EDGE EFFECT REDUCTION OF 4340 STEEL SPUR GEAR DURING INDUCTION HARDENING PROCESS

1.2.1 ABSTRACT

Induction hardening, a promising approach for selective hardening of metal parts, is widely used for surface hardening, where a hard surface is required alongside a tough core. Regarding the complexity of this process, parts' geometry deeply affects the temperature distribution and hardness profile accordingly. In this study, two magnetic flux concentrators are introduced to our induction machine set in order to control the magnetic flux and consequently hardness profile (case depth) of spur gears. The performance of magnetic flux concentrators is examined by the effect of machine parameters on the case depth and the edge effect of AISI 4340 steel-made spur gear. Design of experiments based on Taguchi method is primarily used to optimize the number of experimental trials. Then, the hardness profiles of heat-treated gears at the tip and root of gears are measured by micro-indentation hardness tests. The results are analyzed using Analysis of Variance (ANOVA) and Response Surface Methodology (RSM) to determine the main effect of process parameters, also the best combination of process parameters that maximizes the case depth and minimizes the undesirable feature of edge effect. Finally, the predicted case depth models versus process parameters are developed based on linear regression method. To this end, four predictive models of case depth at tip and root in the edge plane and middle plane of spur gears are generated. Results imply that maximum case depth with minimum edge effect at root and tip is achieved by setting up the highest machine power, longest heating time, and minimum axial gap between concentrators and the spur gear. This study provides a good exploration of case depth in presence of magnetic flux concentrators under various process parameters and gives a reliable guideline towards edge effect during induction hardening process.

Keywords: **Induction hardening, Spur gear, AISI 4340 steel, ANOVA, RSM, Case hardening**

1.2.2 INTRODUCTION

Induction heating is a complex process that consists of several physical phenomena including thermal, electrical, and magnetic fields. In this process, the heat is generated on the surface of a magnetic object when it is exposed to an altering magnetic field. In fact, eddy currents derived from altering magnetic fields, flow over the object, and inherent electrical resistant of the material leads to heat generation in the object [57]. This method has proven its reliability for being used in mass productions. Induction heating for industrial purposes offers a fast generating of high-intensity heat at a well-defined location in parts with repeatable quality, low labor cost for operating induction machine, being energy-efficient and eco-friendly. Furthermore, it makes industries capable to treat metallic parts with complex-geometric shapes such as gears and splines. All these advantages lead to delivering fast products with desirable and constant quality and lower cost. Induction heating can be applied to annealing, bonding, brazing, carbide tapping, casting, curing and coating, forging, melting, plastic reflow, heat staking preheat and post-heat, shrink fitting, and soldering [26]. Besides, this method is widely used for case hardening, which is also known as surface hardening. The case hardening of a spur gear using the induction case hardening process is illustrated in Figure 5 wherein the yellow surface is induction-heated. The machine is equipped with a cooling system, that cools the gear rapidly after heating. This fast cooling increases the generation of martensite phase, in the heated area resulting in a more hardened gear surface compare to the gear core.

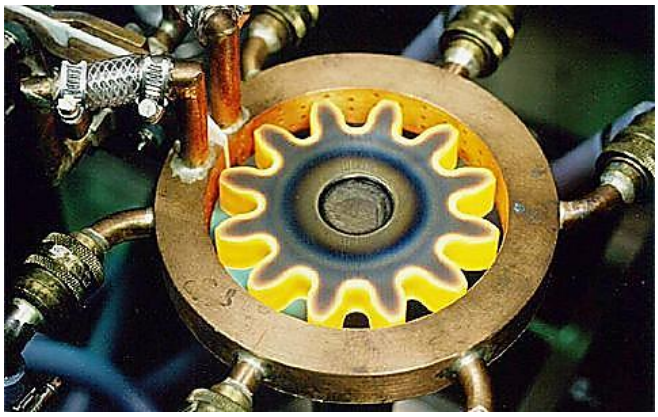

Figure 5. Induction hardening of a spur gear [58].

Generally, spur gears are subjected to altering forces that are the reason for gears' fatigue failure. Increasing wear-resistant in contact areas resulting in higher contact fatigue strength. One simple solution to this issue is quenching heat treatment, in which the whole part is undergone hardening heat treatment. This increases the martensite phase uniformly in a part, both on the surface and in the core, resulting in a brittle gear, which is not a desirable mechanical property for gears. In this regard, case hardening heat treatment would be a credible choice by providing a fine martensite phase only at the surface layers of the gear. Applying case hardening results in a hard gear surface without changing the hardness and metallurgical microstructure of the gear's core [26, 59]. In General, the result of case hardening highly depends on the components of steel alloys. Overall, steel alloys are categorized by the percentage of constituent alloys into low, medium, and high-alloy steels [35]. In this study, AISI 4340 steel is used, which is low alloy steel presenting the utmost possible toughness and strength in a heat-treated condition, as well as good fatigue resistance. In this study, the purpose of case hardening of AISI 4340 steel gear is to change, to the greatest degree, the perlite and bainite phase to martensite to enhance the surface hardness of gears and to provide fine martensite microstructure. To prevent producing any pearlite or bainite phases during cooling process, the austenite layer should be crystallized uniformly, during heating process [60]. A desirable austenite layer formation could be fulfilled by choosing proper process parameters in induction hardening in which the remaining martensite layer is guaranteed by using a suitable quenching method such as a water shower.

Conventional heat treatment procedures for AISI 4340 alloy steel parts is performed by heating the part within a range of 790 °C to 915 °C (850 °C in our study) to achieve a uniform austenite structure in its surface layer, then a rapid quenching to create maximum possible martensite layer [61-64].

Induction hardening of gears engages with several challenges. The major challenge is in induction heating wherein the edge effect is brought about due to the variable density of magnetic flux at different areas of a part [26, 65]. This variation in flux density causes diverse temperature map through the heated area. Generally, the hardness profile obtaining from hardening methods are not uniform. A typical quenching heat treatment creates a non-uniform martensite layer on the gear surface resulting from a non-uniform metallographic structure through the thickness of the part. In the case of induction hardening of external spur gears with the single-shot method and high-frequency current, the non-uniformity in temperature could be seen in two directions: radial and axial direction. The non-uniformity in axial direction causes a difference of temperature between the root and tip of the gear tooth that is due to the proximity of tooth tips to the induction coil compared to tooth roots. In axial direction, the issue referees to the fact that the generated heat between the middle plane and edge plane of a gear tooth, as shown in Figure 6.a, is not uniform. This is termed “edge effect”, which happens when the current is induced in thin bodies like slabs, stripes, foils, and thin gears in which the thickness of a part is considerably less than its width and length. When eddy currents bend to reverse direction in corners of close areas like gear edges near the end of corners, distortion of current takes place since current tends to break the corners. Overheating or underheating of these specific areas can create an uneven heat profile resulting in a non-uniform martensite layer on the gear [35, 66, 67]. The edge effect of a heat-treated gear using induction heating method is illustrated in Figure 6.b and 2.c wherein a different hardness profile between the edge plane of gear tooth (Figure 6.b) and the middle plane of gear tooth (Figure 6.c) can be observed. It is worth mentioning that the most case depth difference between two planes (middle and edge plane) happens at the teeth root of gears.

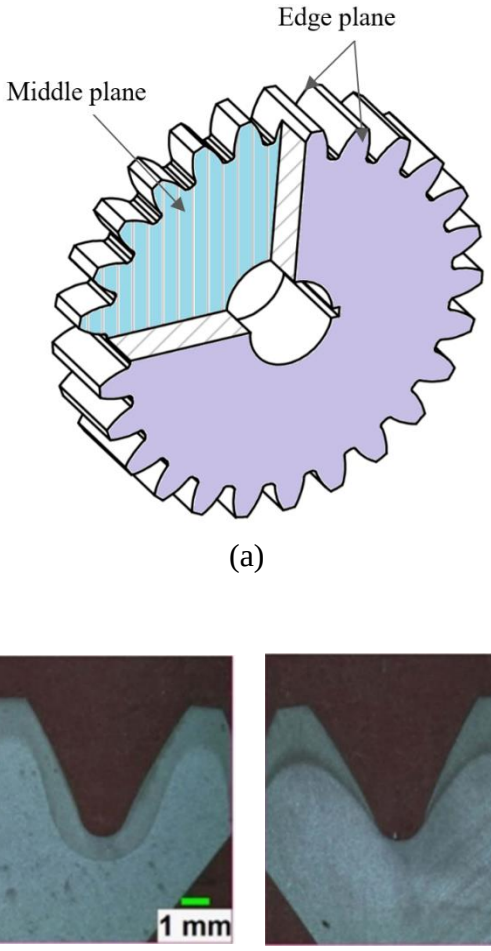

(a)

(b) (c)

Figure 6. (a)schematic representation of the edge plane and middle plane, and the case depths in (b) edge plane [53] and (c) middle plane [53] of a gear.

To the best of the authors' knowledge, there is no technology to eliminate this undesirable effect. However, efforts are done on hindering it as much as possible by utilizing flux concentrators. Process arrangements such as axial and radial gaps (Figure 8) are of importance in minimizing the edge effect. Therefore, minimizing the edge effect demands optimizing the induction heating machine parameters including machine power, frequency, heating time, and the axial and radial gaps. Over the last few decades researchers attempt to optimize induction heating process parameters with methods such as designing different-shaped coils, using variable power supplies, quenching systems for various part geometries

to achieve desirable hardened layer microstructure and case depth. Since the early years of thriving industrial experiences up to now, induction heating technology has seen many improvements such as creating solid-state power supplies instead of motor-generator and development of high current, which in their turn have caused more efficient processes with lower costs [26]. Studies are also carried out on the other objectives in the induction hardening field such as finding a relationship between fatigue tooth breakage start point and machine parameter, and case depth using power circulating gear testing machine for steel spur gear [68]. Zhichao et al. [69] investigate the effect of preheating of parts on the residual stress and cracking during quenching of large parts of 4340 steel. Barglik [70] presented the spatial temperature distribution through a dual-frequency induction heated gear and validate the model by experimental studies. Kristoffersen et al. [41] presented research that studies the relationship between residual stress and hardening depth for two microstructures of cylindrical parts by using an X-ray diffraction method. Cajner et al. [47] studied the effects of induction hardening machine parameters on cylindrical workpieces using computer simulation for an electromagnetic process, thermodynamic, microstructural transformations, and hardness distribution in a part. Residual stresses of surface hardened steel parts using induction heating method are also investigated both experimentally, using X-ray diffraction technique, and numerically, using multiphysics finite element modeling [7]. Candeo et al. [28] conducted computer simulations with electromagnetic, thermal, and metallurgical finite element analyses for induction hardening of spur gears. Munikamal et al. [10] exploited ABAQUS^{TM} simulation software to determine the case depth and hardness in surface hardening of automotive steel components such as crankshaft and spur gears. Montalvo et al. [44] used computer simulation to demonstrate the effect of quenching rate on Transformation-Induced-Plasticity (TRIP) effect in a high-frequency induction heating process wherein results showed that the effect is not negligible. Barglik et al. [46] established temperature profiles and the final hardness of a gear wheel using 3D numerical analysis with temperature-dependent parameters of the hardening process. Other research works have also been carried out using 3D simulation to analyze and predict AISI 1045 steel behavior during spot induction hardening (SIH) [71], and to estimate residual stresses in small spur gears

hardened by induction heating [72]. Moreover, 3D simulations of multi-frequency induction hardening were accomplished for a mathematical model including Maxwell's equations and nonlinear heating equation to eventually link thermal and electromagnetic equations [73]. Computer simulations are also used to determine temperature distribution in a workpiece in multi-frequency-induction-hardening with a single coil for parts with complex geometries [43], and to predict material properties for spot continual induction hardening [30]. Recent researches [74-76] are fulfilled to develop numerical studies on dual-frequency hardening process of AISI 300M gear. They introduce a mathematical model of the process with the help of Time-Temperature- Austenitization (TTA) and Continuous-Cooling-Temperature (CCT) diagrams [77]. Marco Baldan et al, investigated the induction heating process from another point of view, wherein multi-fidelity optimization approach is implemented to reduce process time [78]. Li et al. also tried to optimize the induction heating temperature of 55CrMo Steel ball screws in which they used the martensite fraction value as main criterion of their study. The outcome of the study shows that the more temperature, the more hardness and the more martensite volume fraction generation [79].

To investigate the effects of heat treatment process parameters on pipes residual stress in medium-frequency induction, 3D analysis of medium-frequency induction heating of steel pipes are conducted [8]. More recently, Xiaobin et al. [29] carried out numerical and experimental studies on local induction heating of large-diameter gear rolling. It is worth noting that Tong et al. [80] applied a couple of simulations and numerical models together to investigate residual stress distributions of gear tooth in an asynchronous dual-frequency (ADF) induction hardening process for spur gears. Our research group implemented new techniques to accomplish enhancement in the surface hardening of gears. We used a 3D model simulation of spur gears to the determinate extensive effect of machine parameters and coil geometry on the final temperature distribution on specimens [81]. The most effective machine parameters on the case depth of spur gears [34] and the effects of machine parameters on the case depth of flat cylinders by using computational simulation [35] were studied. More recently, we studied the effect of flux concentrators on the case depth of gears using experiments, analytics, and simulation software to achieve a more efficient method. In

this regard, we investigated using COMSOL^{TM} simulation for a 3D finite element model on spur gears [35]. We further evaluated the effects of flux concentrators on the edge effect of gear tooth [53]. Researches studying the effect of flux concentrators on the final temperature distribution and case depth in the induction heating of spur gears using finite element analysis, Analysis of Variance (ANOVA), and artificial neural network methods are also conducted to predict models leading to the edge effect reduction [82, 83].

Although preceding researches have investigated the case depth of simple and symmetrical shapes, edge effect control in complex shapes such as gears is still a challenge. To the best of the author's knowledge, no study analyzes and prioritizes the influence of induction machine parameters on the case depth of spur gears in both experimental approach and statistical analyses. In this research, an experimental method is adopted, and results are explored using ANOVA to analyze the effect of induction surface heating parameters on the case depth. This statistic approach is planned, to perform most precisely yet with the optimum number of tests. This proposed statistical approach is developed in progressive steps. The first step is to prepare an experimental plan according to Taguchi planning method [84]. The second step is involved in defining the induction hardening ranges for spur gears. The third step is consisted of acquiring the experimental results and analyzing the data using ANOVA [85]. Based on ANOVA analyses and linear regressions, predictive models are developed to assess the case depth in the tip and root of gear teeth. This model is executed to achieve an optimized condition in the induction heating process for the case depth of spur gears. The effect of flux concentrators on edge effect and the consequences of using them in induction heating of thin spur gears are also investigated in this study. The feasibility and effectiveness of the proposed approach led to an accurate and reliable statistical model for predicting the case depth of spur gears. This article is formed as follows: Section 2 presents the methodology of our experimental tests based on induction surface heating and its related parameters. Results of experimentation, statistical and sensitivity analyses, and edge effect discussions are then reported in section 3. In the end, section 4 presents conclusions and ideas for future works in this field.

1.2.3 EXPERIMENT PROCEDURE

1.2.3.1 Materials and induction heating process

The induction heating experiments in this study have been performed on spur gears made of AISI 4340 steel, that are used widely in power transmission gears due to high strength in heat-treated condition and excellent fatigue strength. The chemical composition of AISI 4340 steel and its mechanical characteristics are presented in Table 1 and 2 respectively.

Table 1. AISI 4340 steel chemical composition in wt % [86].

Element	***Ni***	***Cr***	***Mn***	***C***	***Mo***	***Si***	***S***	***P***
Content (%)	1.65-2.00	0.70-0.90	0.60-0.80	0.38-0.43	0.20-0.30	0.15-0.30	0.04	0.035

Table 2. Mechanical properties of AISI 4340 steel Q and T [87].

Yield strength [MPa]	**Ultimate tensile strength [MPa]**	**Elongation at break [%]**	**Hardness Rockwell C [HRC]**
847	1020	20.6	34

Induction hardening tests were carried out by the induction machine illustrated in Figure 7. The machine exploits two generators to produce a varying range of frequencies from medium to high frequency. The frequency rate is controlled by generator power in a way that the maximum frequency will be achieved by the machine's maximum power, which in its turn is obtained by combining the maximum power of two generators. In order to reach the maximum frequency, first, the audio-frequency of 10 kHz is obtained at the maximum generator power of 550 KW using solid-state converters. Then, 200 kHz frequency is generated by a radiofrequency (RF) transistor generator at the maximum power of the second generator in 450 kW. In this study, the radiofrequency (RF) transistor generator operates at 200 kHz. The real-time monitoring (RTM) module is also applied to ensure the quality of the

process in a way that the parameters are checked whether the actual parameters are the same as the operator's intended parameters.

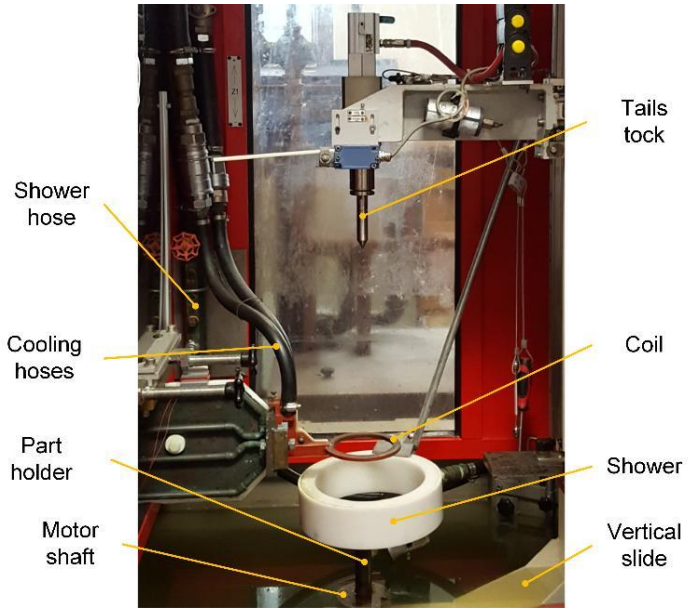

Figure 7. Induction machine and operation system [24].

The schematic of a spur gear and flux concentrators is illustrated in Figure 8. Two flux concentrators are gears exactly similar to the master spur gear. They have positioned above and under the spur gear employing an available stand kit and using AISI 1010 steel shims to ensure axial gaps. The thickness and the outer diameter of these shims are 0.2 ±0.05 mm and 31.75 mm respectively. The master spur gear is surrounded by a coil with 140 mm of outer diameter, 110 mm of inner diameter, a useful section of 7 × 7 mm, and 2 mm thickness. Finally, the machine is equipped with a cooling system comprising a jet of coolant solution containing 92% water and 8% polymers. The quenching heat treatment is performed by a cooling system which is situated under the gears as shown in Figure 7.

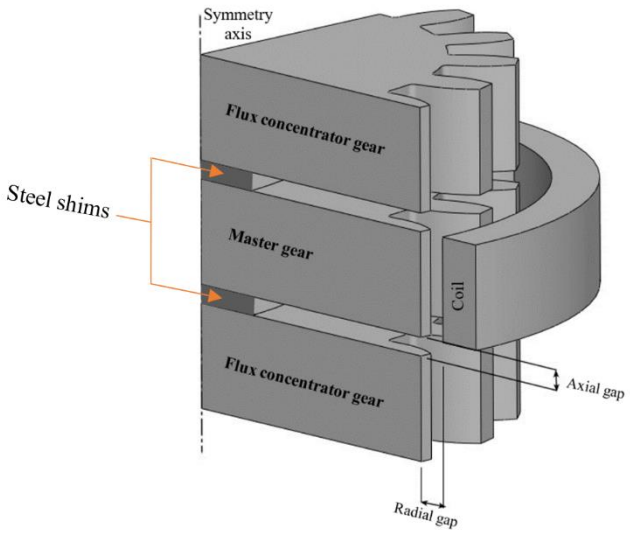

Figure 8. Schematic presentation of the model's geometry

All used gears in this research are made of AISI 4340 steel with identical shape and geometry with an outer diameter of 104.3 mm, and a thickness of 6.5 mm. To make sure that gears are containing homogenous mechanical and microstructural properties, the gears were undergone quenching and tempering heat treatments. Using microhardness tests the uniform hardness of gears reaches approximately 40 HRC in this step. It should be noted that due to the geometrical complexity of gears, the roots and tips of gear teeth are exposed to different magnetic flux densities. To prevent overheating, the temperature should not exceed the austenite transformation temperature. As already mentioned, induction heating of gears is a function of the process parameters. To avoid redundancy and to find an optimum number of parameter variations for experimental tests, a design of experiment method is implemented. The efficiency and simplicity of factorial design and more specifically Taguchi planning method, make it the most commonly used method allowing choosing factor levels and simultaneous mode of factor variations, studying the effect of each factor on the process [84, 88]. To predict experimentally the case depth in tip and root of spur gears, Taguchi method is used to minimize the number of our tests while providing expressive results for statistic analyses.

1.2.3.2 Design of experiments based on Taguchi method

The generated heat is adjustable by machine input variables consisting of machine power, heating time, and frequency. However, modifying frequency in induction heating is not as straightforward as machine power and heating time. The concentrator gap also plays an important role in controlling the induction heating of gears. The axial and radial gaps, the most important geometrical factors of the process, are determined as a gap between the gear and coil as well as the gear and concentrator respectively (Figure 8). In this research, the axial gap is considered as a study-term while the radial gap is preserved as a constant at 2.3 mm. In this regard, researches on the variation of radial gap and its effect could be the subject of investigation in further studies. Regarding Taguchi method, three (3) levels for each parameter are considered to cover all practical parameter ranges including low, medium, and high levels which is presented in Table 3. The controlling parameters are power (P), heating time (T), and the gap between a concentrator and the master gear (G)

Table 3. Experimental factors and range of variables for each level applied to Taguchi method.

Parameter	**Unit**	**Abbreviation**	**Level 1**	**Level 2**	**Level 3**
Power	kW	P	143.0	156.5	170.0
Time	s	T	0.45	0.50	0.55
Gap	mm	G	0.20	0.60	1.00

As already mentioned, to develop a reliable analytical model through analysis of induction heat treatment experiments, it is essential to carry out a properly designed test plan to perform a minimum efficient number of experimentations using Taguchi experiment planning. The suitable range of factors along with the Taguchi experimental design makes the process more robust, efficient, and with a more consistent performance in a minimal number of trials [89, 90]. In the case of induction hardening processes, it is important to search for the variation of experimental parameters allowing minimal and maximal case depth transformation. To this end, the maximal and minimal parameter range tuning is necessary before establishing parameter levels. This is defined during our preliminary tests

as mentioned before in this section. Based on Taguchi planning method, the design of experiments that addresses this experiment is an L_9 orthogonal matrix corresponding to nine (9) tests. Consequently, each test consists of a unique combination of parameter levels which are shown in Table 4.

Table 4. Design of experiences, L_9 orthogonal matrix, and experimental results.

Tests No	P [kW]	T [s]	G [mm]
1	143.0	0.45	0.2
2	156.5	0.50	0.2
3	170.0	0.55	0.2
4	143.0	0.50	0.6
5	156.5	0.55	0.6
6	170.0	0.45	0.6
7	143.0	0.55	1.0
8	156.5	0.45	1.0
9	170.0	0.50	1.0

1.2.3.3 Case depth measurement

In order to measure the case depth of gear after the case hardening process, micro-indentation tests using Clemex microhardness [91] testing machine is performed on the edge and middle planes of gears (Figure 6.a). Micro-indentation tests are repeated on each of nine induction heated gear to evaluate the effect of process parameters on case hardening. These results are shown in Table 5 which presents the case depth measurement at gears tooth root in the middle plane (d_{RM}) and the edge plane (d_{RE}) as well as at gears tooth tip in the middle plane (d_{TM}) and the edge plane (d_{TE}).

Table 5. Microhardness test results of the tooth root (R) and tooth tip (T); hardness has been measured on the middle plane (M) and the edge plane (E).

Test no.	**Parameters**			**Root**		**Tip**	
	P [kW]	T [s]	G [mm]	d_{RM} [mm]	d_{RE} [mm]	d_{TM} [mm]	d_{TE} [mm]
1	143.0	0.45	0.2	0.35	0.10	2.45	2.20
2	156.5	0.50	0.2	0.50	0.40	3.35	2.90
3	170.0	0.55	0.2	0.60	0.65	3.95	3.70
4	143.0	0.50	0.6	0.45	0.20	2.90	2.30
5	156.5	0.55	0.6	0.55	0.50	3.60	3.10
6	170.0	0.45	0.6	0.50	0.45	3.50	2.65
7	143.0	0.55	1.0	0.55	0.50	3.60	2.80
8	156.5	0.45	1.0	0.55	0.40	3.20	2.20
9	170.0	0.50	1.0	0.60	0.60	3.90	3.25

It can be observed in Table 5 that increasing P and T may result in reducing d_R, however, no significant effect could be seen for d_T. These results imply that the maximum and minimum case depth occurs in tests 3 and 1 respectively. The hardness profile of the gear on tip and root area resulting from tests 1 and 3 are compared in Figure 9 and Figure 10. Three regions could be noticed in theses graphs: the first region presents a hardened surface layer due to martensitic microstructure formation, the second region displays a hardness drop to approximately the core material hardness, and the third region preserves the initial hardness of gear as it did not receive the thermal flow [92]. Figure 9.a demonstrates the maximum and minimum obtained case depth at middle-root (d_{RM}) resulted respectively from test 3 and test 1. Figure 9.b shows the maximum and minimum case depth at edge-root (d_{RE}). In Figure 10.a, the maximum and the minimum attained case depths at middle-tip (d_{TM}) of test 1 and test 3 are compared together. Moreover, the comparison between the maximum and minimum case depth at edge-tip (d_{TE}) is presented in Figure 10.b.

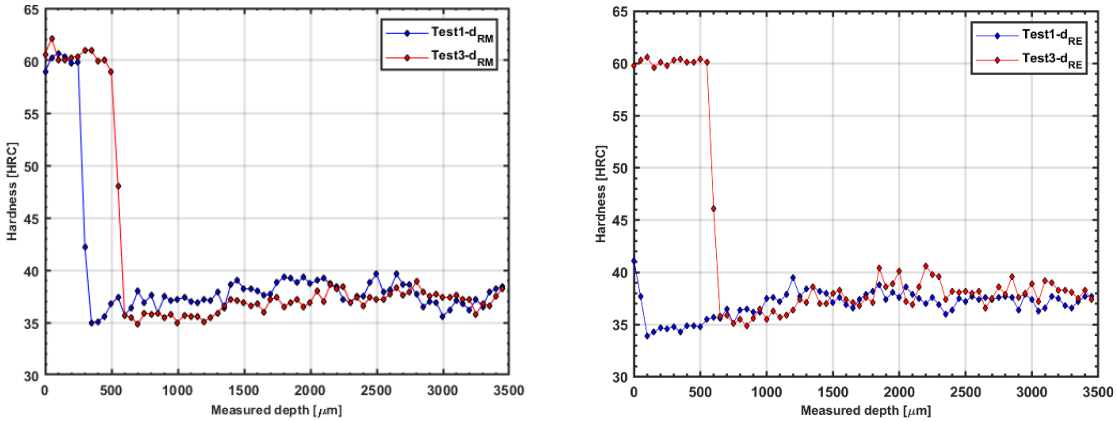

(a) (b)

Figure 9. Microhardness of teeth root for test 1 and test 3 (a) in middle plane d_{RM} (b) in edge plane d_{RE}.

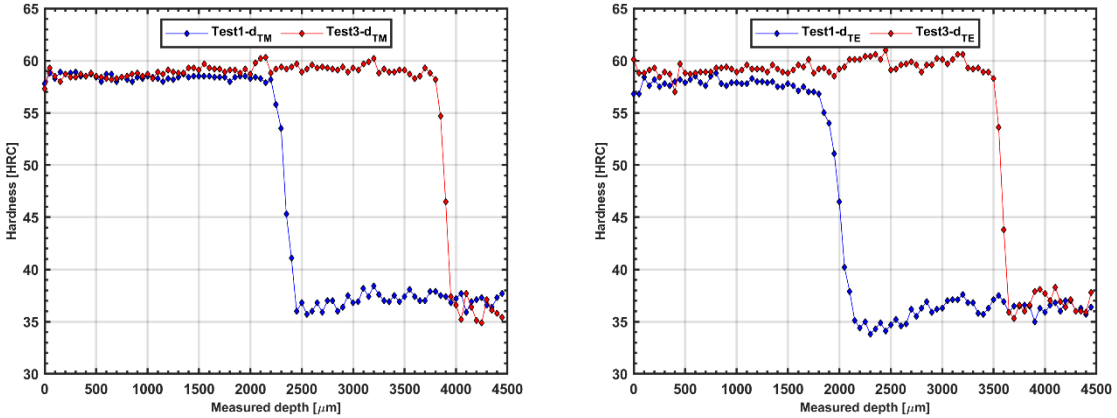

(a) (b)

Figure 10. Microhardness of teeth tip for test 1 and test 3 (a) in middle plane d_{TM} (b) in edge plane d_{TE}.

Three main conclusions can be drawn from Table 5. First, the maximum case depth for both root and tip can be achieved at the highest machine power and the longest heating time that are 170.0 kW and 0.55 s respectively. In contrast, the minimum case depth can be carried out at the lowest level of parameters (143.0 kW and 0.45 s). This is due to the fact that the more heating time, lets the heat to convey through more surface, resulting in a more heated area. Second, in each gear, generally, the case depths in the middle plane are deeper than the case depth in the edge plane. This is an affirmation of generating more current density at the

middle of teeth compared to the edges due to the induction edge effect. Third, a proper variation of collected case depths in terms of having fine coverage between the maximum and minimum depths in roots and tips, remarks on the credibility of well-designed tests with Taguchi method.

1.2.4 Effect of parameters on hardness profile

1.2.4.1 Statistical analysis and parameters contribution

To investigate the effect and influence of each parameter on the case depth of spur gears, analyses of variance (ANOVA) are applied [93, 94]. The exactitude of the regression model is evaluated by an F-test based on ANOVA. General systematic details are presented in Table 9-9. Terms that present the results of the analyses are Degrees of freedom (DoF), Sum of squares, Contribution percentage, F-Value, and P-Value [93, 95]. To determine whether the effect of process parameters on the case depth is statistically significant, ANOVA calculates p-value based on F-test. Comparing p-value with the designated significance level (α) determines whether the null hypothesis can be rejected or not. The null hypothesis, in this case, states that the effect of studied parameters is not significant on the case depth. We reject the null hypothesis when the calculated p-value is less than the designated significance level. In this study, we use a significance level (α) of 0.05 which indicates that there is a 5% risk of concluding that a parameter has a significant effect on the process when there is no actual effect.

In this study, linear regression is developed based on ANOVA results wherein the case depths are estimated as a dependent variable (d_{RE}, d_{RM}, d_{TE}, and d_{TM}), and power (P), heating time (T), and concentrator's gap (G) as independent variables. Preliminary effect analyses for each of the dependent variables (d_{RE}, d_{RM}, d_{TE}, d_{TM}), using interaction diagrams of factors in three levels, show that there are no significant interactions between independent variables. In this regard, adding factor interactions into ANOVA model can use the DoF up, and make the model complicated and incalculable [96]. During preliminary ANOVA analyses, first-

order interaction of factors (T×P, T×G, and P×G) are added to the ANOVA model along with the factors (P, T, and G) to determine the significance of their effect on d_{RM}, d_{RE}, d_{TE}, and d_{TM}. These results showed that the calculated p-value for interactions was much higher than the significance level (0.05), which infers that the interactions are not significant in these cases. These large p-values raise a red flag for an overfitted model which can consequently lead to erroneous predictive models [97]. For this reason and to provide a reliable goodness-of-fit regression model, ANOVA analyses for d_{RM}, d_{RE}, d_{TE}, d_{TM} are performed without the interaction of independent factors.

Table 6 shows ANOVA analyses for d_{RM} in which the p-value for P, G, and T are respectively 0.004, 0.008, and 0.017. These p-values are less than 0.05, hence, the null hypothesis of nonsignificant factors for these terms is rejected. It can be observed that machine power (P) is the most effective parameter, then heating time (T), and finally concentrator's gap (G) with respect to their incremental quantity of p-values. Thinking back to p-values for d_{RM} and considering the contribution percentage variables, it can be concluded that P is the most effective term in d_{RM}. In the same way, for d_{RE} in Table 7, P and T respectively are the most effective parameters. Considering contribution percentage of 53.88% and p-value of 0.001 for d_{RE}, declares that P is the most effective term in d_{RE}.

Table 6. Results of ANOVA for micro-hardness tests at root and on middle plane ($d_{RM.}$) of gear.

Factors	DoF	Sum of squares	Contribution	F-Value	P-Value
P	1	0.020417	40.83%	24.50	0.004
T	1	0.015000	30.00%	18.00	0.008
G	1	0.010417	20.83%	12.50	0.017
Error	5	0.004167	8.34%		
Total	8	0.050000	100.00%		

Table 7. Results of ANOVA for micro-hardness tests at root and on edge plane (d_{RE}) of gear.

Factors	DoF	Sum of squares	Contribution	F-Value	P-Value
P	1	0.13500	53.88%	50.10	0.001
T	1	0.08167	32.59%	30.31	0.003
G	1	0.02042	8.15%	7.58	0.040
Error	5	0.01347	5.38%		
Total	8	0.25056	100.00%		

Table 8 for d_{TM} remarks p-value of 0.000 for P and 0.001 for T. p-value of 0.000 for P implies that the null hypothesis is rejected with high confidence. Considering a contribution of 52.32%, the effect of P in d_{TM} is very significant. p-value of 0.001 and the contribution of 36.33% for T shows also the significant effect of this parameter. Results in Table 9 expresses that in d_{TE}, the p-value of T is 0.000, and of P is 0.001. This indicates that T is the primary effective parameter and P is the secondary effective term in d_{TE}. It should be noted that the effect of G was not significant enough to be considered as a contributing factor, and this factor is eliminated during iterations of ANOVA.

Table 8. Results of ANOVA for micro-hardness tests at tip and on middle plane (d_{TM}) of gear.

Factors	DoF	Sum of squares	Contribution	F-Value	P-Value
P	1	0.96000	52.32%	82.88	0.000
T	1	0.66667	36.33%	57.55	0.001
G	1	0.15042	8.20%	12.99	0.015
Error	5	0.05792	3.15%		
Total	8	1.83500	100.00%		

Table 9. Results of ANOVA for micro-hardness tests at tip and on edge plane (d_{TE}) of gear.

Factors	DoF	Sum of squares	Contribution	F-Value	P-Value
P	1	0.8817	41.91%	38.20	0.001
T	1	1.0837	51.51%	46.96	0.000
Error	6	0.1385	6.58%		
Total	8	2.1039	100.00%		

1.2.4.2 The main effect of process parameters

For easier correlation determination between dependent and independent variables, statistical methods are used to specify the effect trend of each parameter on the response. Using the sum of squares calculated for each parameter in ANOVA tables, the contribution of each factor in the total sum of squares indicates the effect of parameter values on the response variation. To this end, the results of ANOVA analysis are used to determine the contribution ratio of each parameter (P, T, and G) in the case depths for root (d_{RE}, and d_{RM}) and tip (d_{TE}, and d_{TM}) of the gear. As shown in Table 6-9, the contribution percentage of each process parameter (P, T, and G) confirms in most cases, that the highest contribution percentages belong to the parameters P and T, while G has a minimum influence on the case depth. The contribution percentages of P are 40.83%, 53.88%, 52.32%, 41.91%, and of T are 30.00%, 32.59%, 36.33%, and 51.51% for d_{RM}, d_{RE}, d_{TM}, and d_{TE} in turn. These contribution percentages concerning G are 20.83%, 8.15%, 8.20%, for d_{RM}, d_{RE}, and d_{TM} respectively.

In order to have a better visual perspective of the impact of each parameter on responses, the main effect plots are drawn in MATLAB^{TM}, in which the statistical mean value of responses in each level of parameters presents the trend of each parameter on the response. In this regard, the steeper is the plot, the more influencing is the studied parameter. The main plots present separately the effectiveness of each parameter at varying levels. Through these plots, each level of P, T, and G are linked to their response mean value at the parameter level. Hence, to examine differences between level means of independent variables (P, T, G) on each of four responses (d_{RE}, d_{RM}, d_{TE}, and d_{TM}), main effect plots are presented in Figure 11 a and b.

Figure 11.a is dedicated to show the case depths of tooth root where d_{RM} and d_{RE} are respectively distinct by red and blue lines. Generally, the steepness of lines from a level to the next level shows the effect of each parameter on the case depth response; the steeper the line, the more effective the parameter on case depths. It could be observed in Figure 11.a, for

d_{RM} with red lines, that P and T are the most effective parameters over the three levels due to the biggest range of the case depth from the first to the thirst level. From the first to the second level, P shows the largest effect, which is also the most significant effect. However, from the second level to the third, G shows more contribution. It means the considerable effect of G on the case depth happens at the higher values of G. Overall, regarding the case depth changes, P is the most effective parameter and the next important parameters are T and G with close effects on d_{RM}. Blue lines in Figure 11.a expose a dominant influence of P compare to T and G, because of a steeper line of P over the three levels. Case depth changes over the three levels are more vivid in the edge plane wherein P and T mainly affect the case depth, then G with a considerable difference. It worth mentioning that G plays the same role as in the middle plane; very low effect from the first to the second level (the representative line for this part is almost flat) and steeper from the second to the third level.

Steep red lines of d_{TM}, presented in Figure 11.b, emphasize the most influential rule of P and T on d_{TM}. Almost the same length and steep line and the same starting and finishing point of P and T in their levels approve this deduction. This is while the influence of G on d_{TM} is not comparable to P and T. Blue representative lines of d_{TE} show that the effect of T is the most in all three levels while P is also considered as having the main effect on the case depth. In contrast, G has a minor effect compared to P and T.

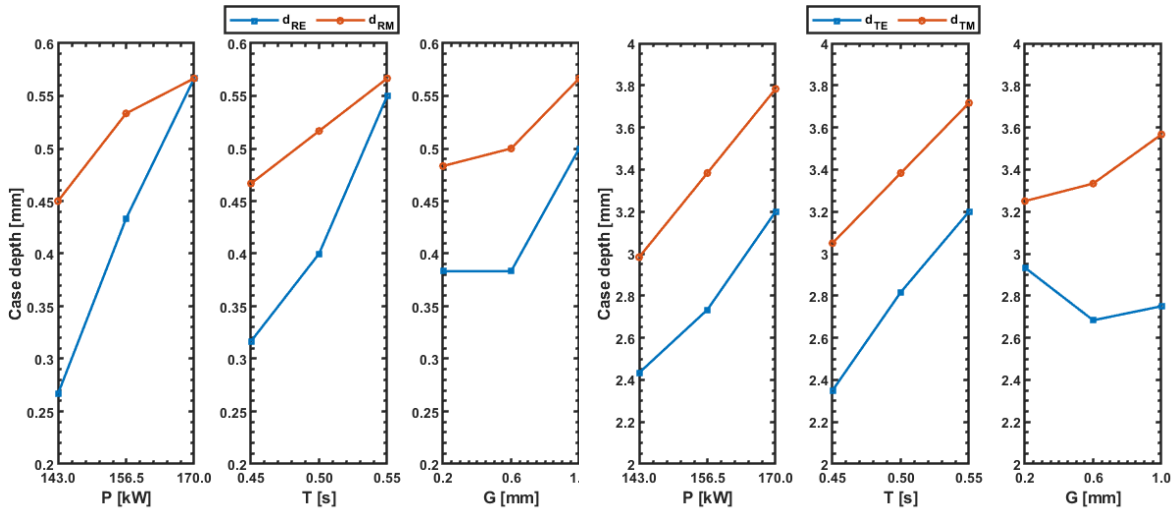

(a) (b)

Figure 11. Main effect plots of case depth on middle and edge planes at (a) root (b) tip.

1.2.4.3 PREDICTIVE MODELS BASED ON LINEAR REGRESSION

To explain a mathematical relationship between the dependent and independent variables in a predictive model, regression equations based on minimizing mean squared errors, are exerted. The regression equations estimate responses (d_{RM}, d_{RE}, d_{TM}, and d_{TE}) depending on the parameters of this study (P, T, and G). As presented in section 3.1, the highly effective parameters concerning each response are analyzed by ANOVA and presented in Table 6-9. The regression equations based on these analyzed parameters are presented for d_{RM}, d_{RE}, d_{TM}, and d_{TE} respectively in Equations 1 to 4.

$$d_{RM} = -0.722 + 0.1042 \times G + 0.004321 \times P + 1.000 \times T \quad (1)$$

$$d_{RE} = -2.572 + 0.1458 \times G + 0.01111 \times P + 2.333 \times T \quad (2)$$

$$d_{TM} = -4.825 + 0.396 \times G + 0.02963 \times P + 6.667 \times T \quad (3)$$

$$d_{TE} = -5.905 + 0.02840 \times P + 8.05 \times T \quad (4)$$

The coefficient (denoted by R^2 or R-squared) is an indicator to evaluate the precision of regression models. The R^2 assesses the reliability of regression equations in the range of test variation. The R^2 for Equation 1 is calculated 91.67%, which declares that the equation can predict 91.67% of the variation case depth in d_{RM}. The R^2 for predictive equations of d_{RE},

d_{TM}, and d_{TE} (Equation 2 to 3) are 94.62%, 96.84%, and 93.42% respectively. These R^2 values show that the regression equations are well fitted to experimental results. The graphical presentations of these predictive models (Predicted), experiment results (Measured), and the difference between (Residual) versus case depths (d_{RM}, d_{RE}, d_{TM}, and d_{TE}) are demonstrated in Figure 12 and Figure 13. These curves present a visual comparison between predictive model and experimentation results. To evaluate quantitatively the preciseness of predictive models, for each of the four responses (d_{RM}, d_{RE}, d_{TM}, and d_{TE}), obtained case depths of models are compared to their experimentation outcomes. To this end, Equation 5 is utilized to quantify statistically the error percentage of models.

$$Error\ (\%) = \frac{|\ Predicted - Measured\ |}{Measured} \times 100 \tag{5}$$

The average estimated errors for the response models (d_{RM}, d_{RE}, d_{TM}, and d_{TE}) are respectively 3.65%, 9.54%, 2.00%, and 8.03%. Results imply that case depths d_{RM}, d_{RE}, d_{TM}, and d_{TE} are computed with a good accuracy wherein the average estimation errors are less than 10%.

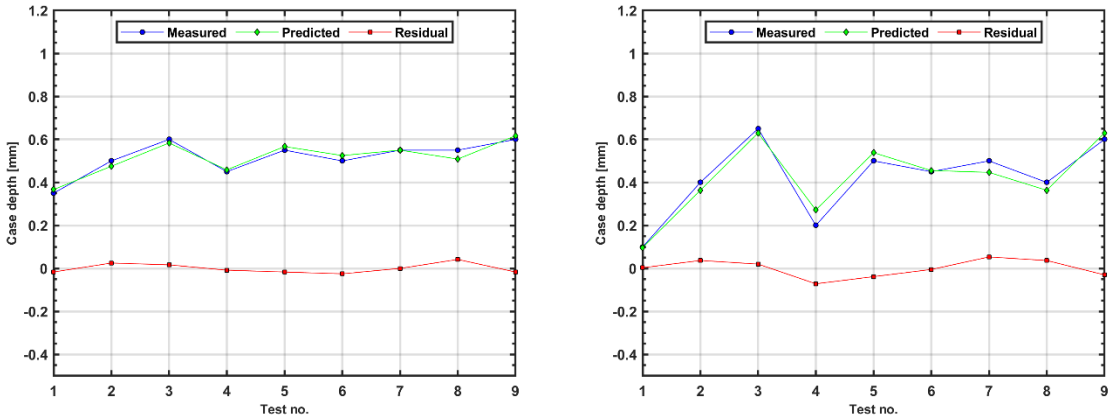

(a) (b)

Figure 12. Case depth measured by experiments, predicted by regression equations and their residuals in (a) d_{RM} b) d_{RE}.

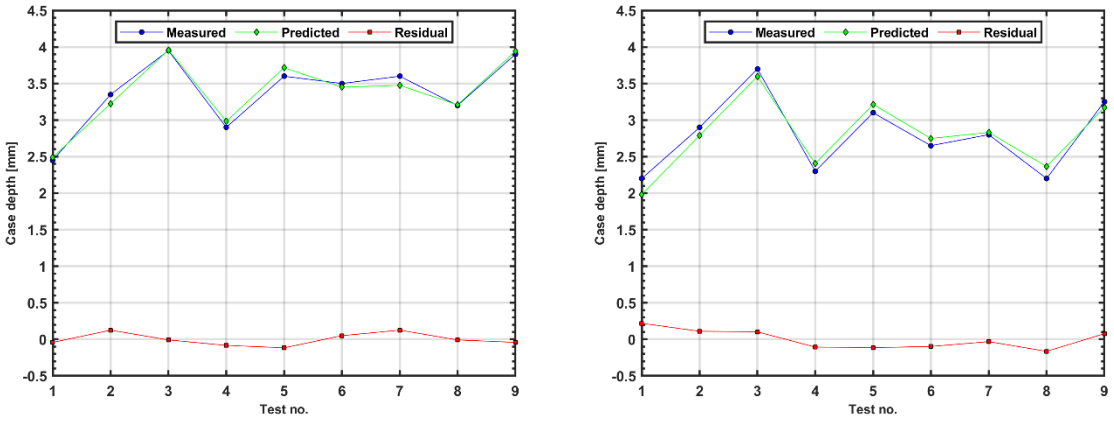

(a) (b)

Figure 13. Case depth measured by experiments, predicted by regression equations and their residuals in a) d_{TM} b) d_{TE}.

1.2.4.4 Response surfaces and sensitivity analysis

To investigate the trend of predictive response models (d_{RM}, d_{RE}, d_{TM}, and d_{TE}) with respect to their most effective terms, contour plots are drawn in Figure 14 and Figure 15 using MATLAB^{TM}. Contour plots are color-based maps drawn through two independent variables, presented on vertical and horizontal axes, displaying the variation a response by color gradient and isolines. These plots are useful when the objective is to specify which level combinations of parameters optimize the response. considering that the most important factors in our experimental responses are machine power (P) and heating time (T), the trend of case depth versus the variation of these parameters are presented in this study. The contour plot of d_{RM} is presented in Figure 14.a where a linear relationship between machine power and heating time versus case depth is illustrated, which represents graphically Equation 1 for d_{RM}. It can be inferred from this plot that increasing P and T results in a deeper case depth in middle plane at tooth root of gear. In this regard, the maximum case depth can be obtained at the highest level of P and T. In Figure 14.b, the linear relation between independent variables (P and T) and response (d_{RE}) is found similar to that of d_{RM}. Increasing P and T leads to increasing the case depth. Thus, the highest case depth in d_{RE} is also obtainable with the highest level of P and T.

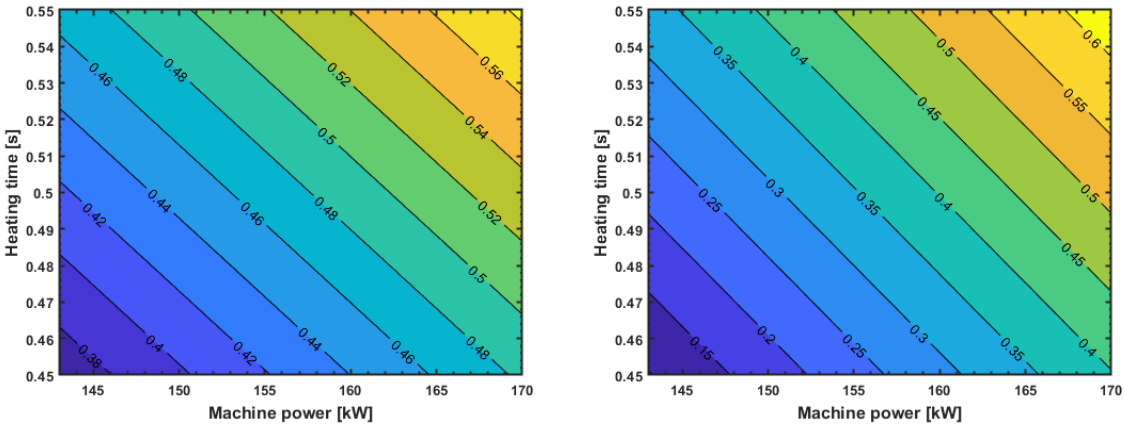

(a) (b)

Figure 14. Contour plots of P and T versus case depths at gear's root in (a) middle plane (d_{RM}) (b) edge plane (d_{RE}).

Figure 15.a presents the contour plot of P and T versus the case depth at gear's tooth in its middle plane. It demonstrates more intense effects of P and T on case depth compare to their effect at the gear's root, which is due to the proximity of tooth tip to the coil. This is concluded from a comparison of the highest d_{TM} (3.8) which is shown in yellow color in Figure 15.a. The effects of changing P and T on d_{TE} are displayed in Figure 15.b in which d_{TE} raises with increasing P and T. Highest d_{TE} could be achieved at the highest P and T. It is worth noting that the maximum case depth of d_{TE} is slightly less than d_{TM} in the range of our experimentations. The general conclusion in this section is that the case depth increases with the increase of P and T.

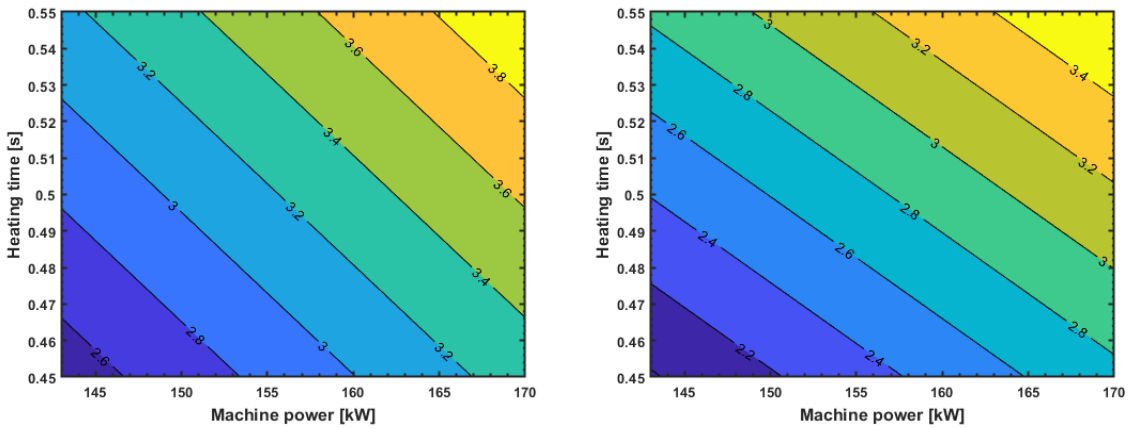

(a) (b)

Figure 15. Contour plots of P and T versus case depths at gear's tip in (a) middle plane (d_{TM},) (b) edge plane (d_{TE}).

1.2.4.5 Edge effect discussion

The more radial distance of the coil from tip of gear results in a nonuniform case depth (as previously shown in Figure 6.c), where the case depth on the tip is more pronounced compared with the root of gear teeth. Referring to previous studies, induced eddy currents affect the case depth profile causing overheating of some areas, depending on the geometry of part which is exposed to induction heating. This leads to a case depth profile in edge plane that is different from the one in middle plane. The main purpose of this study is to investigate, analytically and experimentally, the machine parameters in order to minimize the edge effect, case depth difference in edge plane (d_{RE} and d_{RM}) over middle plane (d_{TE} and d_{TM}), using flux concentrators. To this end, the less case depth differences between middle and edge planes consider as a more ideal case depth profile in spur gears. Studying the effect of machine parameters on the case depth profile, monitoring it separately in middle and edge planes, it is concluded that increasing P and T results in a deeper case depth. Although reaching deeper case depth fulfills our goal to reach maximum induction heating performance, an ideal case depth profile is the one with the least edge effect. To measure the edge effect quantitatively, we introduce edge effect indicators of gears tooth at root, the difference of case depths measured in middle plain and edge of tooth root (Δ_{dR}), and tip, the difference of case depths

measured in middle plain and edge of tooth tip (Δ_{dT}). The case depth difference between middle and edge planes at root and tip is shown in Figure 10.

The red line in Figure 10 represents edge effect at tip of gears tooth. It shows a general enhancement in edge effect at tooth tip with respect to tests from 1 to 9. However, the increasing trend is not uniform, and a considerable reduction in edge effect happens in tests 3, 5, 7, and 9. This is because of an increase of both T and P in these tests compared to the others with an exception for test number 7 that a significant enhancement in T (0.1 s) compensate for P reduction from 170 kW to 143 kW. The minimum edge effect, and consequently the best-case profiles at tip are achieved in tests number 1 and 3, where parameters P and T are at their minimum and maximum level respectively; 143 kW and 0.45 s for test number 1, and 170 kW and 0.55 s for test number 3. It should be mentioned that the effect of G is negligible compare to T and P due to their higher contribution percentage (Table 11 and 9).

The blue line in Figure 10 represents the edge effect at root of gear's tooth. It shows a different trend compared to the edge effect at tip. The edge effect is less pronounced in tooth root compare to the tip since the case depth is generally less than tip due to its proximity to the induction coil. In this regard, the effect of G is not negligible at root (the contribution effect of G is 20.83% in middle plane and 8.15% in edge plane). From tests 1 to 9, G increased from 0.2 mm to 1 mm which shows a general decreasing trend in edge effect. The minimum edge effects happen at test numbers 3, 5, 6, and 9. However, test number 3 is the one in which the edge effect is minimum for both tip and root and provides higher case depth. Therefore, we can conclude that the optimum case depth profile is obtainable in test 3 wherein P and T are at their maximum level, 170 kW, and 0.55 s respectively.

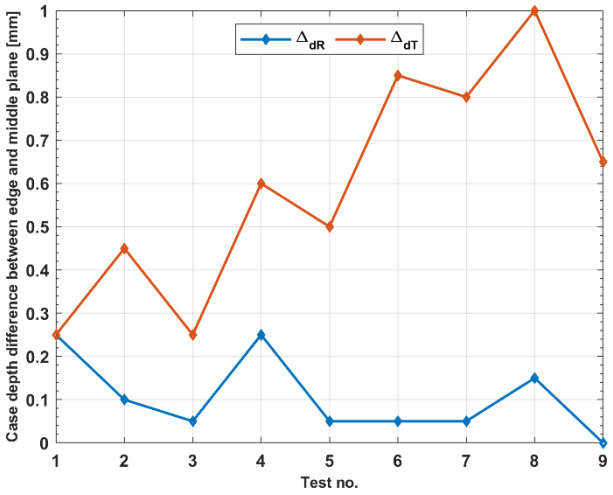

Figure 12: Edge effect comparison of experimental tests at root (ΔdR) and tip (ΔdT) of gear's tooth.

1.2.5 Conclusions

In this article, 4340 steel-made spur gears are used to investigate the effects of induction heating process parameters namely machine power, axial gap between flux concentrators and the master gear, and heating time as independent variables (inputs) on the edge effect. The case depth is measured in four different areas on each gear: at tip and root of gears in edge plane and middle plane. Using Taguchi method, nine experiments are designed to combine four mentioned process parameters in three levels each. Measuring the case depths, the results are statically studied by analyses of variance (ANOVA). The predicted regression model of case depth in four areas of gears, at gear tips (d_{TM} and d_{TE}) and roots (d_{RM}, d_{RE}) are developed. The main effect plots, regression equations, error residuals, and contour plots of each response are developed and analyzed in this study. The results indicate that the total accuracy of predictive models is fine since the average errors of models are in an acceptable range: 3.65%, 9.54%, 2.00%, and 8.03%. for d_{RM}, d_{RE}, d_{TM}, d_{TE} respectively. Results demonstrate that power and heating time are the dominant parameters in case depth. The contribution percentage of machine power are 40.83%, 53.88%, 52.32%, 41.91%, and of heating time are 30.00%, 32.59%, 36.33%, and 51.51% for d_{RM}, d_{RE}, d_{TM},

and d_{TE} in turn. Generally, the axial gap does not show a significant effect on the case depth. It does not affect the case depth in low levels, while it shows moderate effects in higher levels of the gap. The overall conclusion determines that case depth profile in middle plane is controllable via machine parameters, and the best-exploited range of parameters can maximize case depth while minimizing edge effect. The highest machine power and longest heating time in conjunction with the smallest axial gap contribute to an optimized case depth.

Although the results of this study are promising, some improvements and applications can be foreseen. As already mentions, this work can be improved by taking into consideration the effect of the radial gap of flux concentrators concerning the case depth of induction-heated gears. To optimize surface treatment of the other parts like discs, bevel gears, and helical gears which have different shapes than spur gears, experimental test benches as well as predictive models can be developed. In this regard, applying artificial intelligence to create and enhance the models on helical gear could be the next project to perform.

CHAPITRE 2
UNE NOUVELLE ÉTUDE SUR LA RÉDUCTION DE L'EFFET DE BORD D'UN DISQUE EN ACIER 4340 PAR UN PROCESSUS DE TREMPE PAR INDUCTION UTILISANT DES CONCENTRATEURS DE FLUX MAGNÉTIQUE

2.1 RESUME EN FRANÇAIS

La trempe par induction est l'un des meilleurs procédés de production de masse utilisés récemment en raison de sa capacité à générer rapidement une chaleur de haute intensité à un endroit bien défini de la pièce. Les nombreux avantages de cette méthode en font une technique fiable pour produire une fine couche de martensite sur la surface de la pièce qui présente des contraintes résiduelles de compression. À cet égard, l'étude présentée est consacrée à l'utilisation du chauffage par induction pour la trempe superficielle d'un disque en acier AISI 4340. L'objectif est d'évaluer les performances des concentrateurs de flux magnétique et les effets des paramètres du processus d'induction sur la profondeur durcie et l'effet de bord dans la trempe superficielle du disque. Une fois que la gamme appropriée de paramètres est définie, la planification de l'expérimentation Taguchi est utilisée pour encadrer une expérimentation complète avec le minimum d'essais possible. Ensuite, la profondeur durcie des disques est évaluée sur leurs sections transversales (plan du bord et plan médian) par la mesure du profil de dureté des échantillons à l'aide d'une machine de dureté par micro-indentation. Les résultats sont ensuite analysés statistiquement à l'aide de l'analyse de la variance (ANOVA) et de la méthode de la surface de réponse (RSM) afin de déterminer la meilleure combinaison de paramètres pour obtenir une profondeur durcie maximale tout en minimisant l'effet de bord. Les modèles de régression de la qualité de l'ajustement sont ensuite développés pour prédire le profil de la profondeur durcie en fonction des paramètres de la machine sur la base d'une régression linéaire utilisant les réponses de la profondeur

durcie dans le plan du bord et du milieu des disques. Les résultats indiquent que la profondeur durcie maximale avec un effet de bord minimal peut être obtenue en utilisant le temps de chauffage le plus élevé ainsi que l'amplitude moyenne de la puissance, de l'écart axial et de l'écart radial. Cette étude donne une bonne exploration des profondeurs durcies optimisées par la mise en place des paramètres du processus lorsque le concentrateur de flux magnétique est utilisé, ainsi, une ligne directrice pour réduire l'effet de bord des disques dans l'application de la trempe de surface par induction est donnée.

Mots clés **- Trempe par induction, concentrateur de flux magnétique, disque en acier AISI 4340, ANOVA, RSM, profondeur durcie**

Ce deuxième article, intitulé " A novel investigation into the edge effect reduction of 4340 steel disc through induction hardening process using magnetic flux concentrators", fut co-rédigé par moi-même ainsi que par le professeur Noureddine Barka, le professeur adjoint Sasan Sattarpanah Karganroudi, Mohamed Khalifa et Narges Omidi. Il a été accepté pour publication dans sa version finale en 31 mai 2021 par les éditeurs de la revue "The International Journal of Advanced Manufacturing Technology". En tant que premier auteur, ma contribution à ce travail a été la recherche de l'état de l'art, le développement de la méthode, la gestion des données et des résultats, et la rédaction de l'article. Le professeur Noureddine Barka a fourni l'idée originale. Mohamed Khalifa a contribué à l'exécution des tests expérimentaux. Le professeur adjoint Sasan Sattarpanah Karganroudi et le professeur Noureddine Barka ont participé à la recherche de l'état de l'art, le développement de la méthode, et la révision de l'article. Narges Omidi a également participé à la révision de l'article. Une version électronique de cet article a été présentée avec l’identifiant numérique suivant :

https://link.springer.com/article/10.1007/s00170-021-07351-5

2.2 A NOVEL INVESTIGATION INTO THE EDGE EFFECT REDUCTION OF 4340 STEEL DISC THROUGH INDUCTION HARDENING PROCESS USING MAGNETIC FLUX CONCENTRATORS

2.2.1 ABSTRACT

Induction hardening serves as one of the best mass production processes used recently due to its ability to quickly generating high-intensity heat in a well-defined location of the part. Numerous advantages of this method make it a reliable technique to produce a thin martensite layer on the part surface that has compressive residual stresses. In this regard, the presented study is devoted to investigating utilizing induction heating for surface hardening of AISI 4340 steel disc. The purpose is to evaluate the performance of magnetic flux concentrators and the effects of the induction process parameter on the case-depth and edge effect in the surface hardening of the disc. Once the proper range of parameters is defined, Taguchi experimentation planning is used to frame comprehensive experimentation with the minimum possible trial. Then, the case-depth of discs is evaluated on their cross-sections (edge and middle plane) through hardness profile measurement of samples using a micro-indentation hardness machine. The results are then statistically analyzed using Analysis of Variance (ANOVA) and Response Surface Methodology (RSM) to determine the best combination of parameters to achieve maximum case-depth yet minimum edge effect. The goodness-of-fit regression models are then developed to predict the case-depth profile as a function of machine parameters based on linear regression utilizing case-depth responses in the edge and middle plane of discs. Results imply that maximum case-depth with minimum edge effect can be produced by using the highest heating time along with the average amplitude of the power, axial gap, and radial gap. This study gives a good exploration of case-depths optimized by setting up process parameters when magnetic flux concentrator is utilized, thus, a guideline to reduce discs edge effect in induction surface hardening application is given.

Keywords: Induction hardening, Magnetic flux concentrator, AISI 4340 steel disc, ANOVA, RSM, Case hardening

2.2.2 Introduction

The importance of Induction heat treatment and its numerous applications have been increased over the last decades. One of the most sought-after usages of this phenomenon is the hardening of metals [71, 98]. Multiple advantages of induction heat treatment make it superior to traditional methods: capability to produce high power density in a shorter time that results in saving time, being high energy efficient, limiting the risks of distortion and deformation during conventional heat treatments [99]. It is a fast and clean-energy process and repeatable in terms of treating parts with the same quality. Also, the ability of fast heat generation in well-defined points of the specimen and eliminating other undesired-treated parts, being environmental-friendly along with other mentioned characteristics make this method well-received for mass production and industrial purposes [26]. The ability to generate localized heat during the heating process in hardening processes is one of the most important industrial applications of induction heating employing improving wear and fatigue resistance of the parts such as bearings, shafts, and disc-shaped parts like gears [80, 100].

Parts geometry, surface topology, chemical composition as well as induction heating processing parameters are crucial elements in induction surface hardening [101]. This study aims at investigating the effects of induction machine parameters on parts with plain geometry like a disc. While the result of this simplification can be generalized to gears [102], considering simpler geometries like disc rather than gear can eliminate some redundant parameters which are related to gear-shaped parts and geometrical complications (Figure 16).

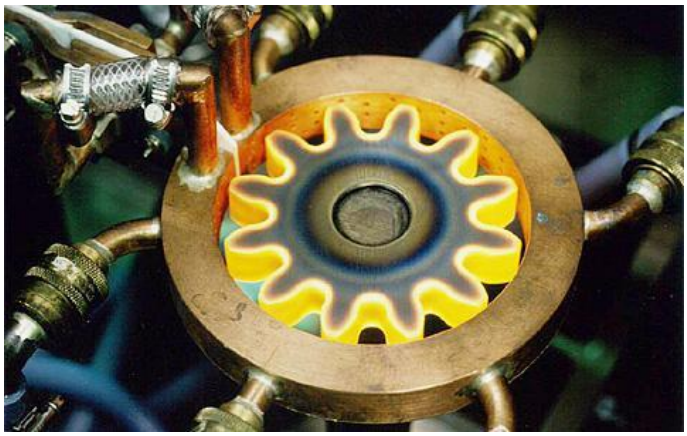

Figure 16. Induction hardening of the gear [102].

Similar to conventional hardening methods, the induction hardening process is based on increasing the temperature up to the austenitic area, then cooling the part rapidly. As a result, the martensite phase, a very hard steel structure, is formed. However, the hardenability of the metal alloy plays a key role in the final percentage of the martensite phase. In this study, AISI 4340 steel, which is known for its heat treatable properties, is used to achieve high strength, good fatigue resistance, and proper atmospheric corrosion resistance behaviors. Referring to the main goal of the study, obtaining a hard surface on 4340 steel discs, creating maximum martensite in surface layers is intended since the formation of any pearlite or bainite phase causes a drop in the hardness of the material. To eliminate producing pearlite or bainite formation, rapid quenching of a uniform austenite layer is essential [60]. A desirable form of austenite layer highly depends on induction process parameters that could maximize the austenite phase formation. The subsequent step of quenching is done by a water shower to create a uniform martensitic layer on the part's surface. According to these facts, a typical heat treatment temperature for AISI 4340 alloy steel parts is within a range of 790°C to 915°C (850 °C in our study) to create a uniform austenite layer, and a rapid quenching to produce the maximum possible percentage of martensite layer [61-64].

Despite the brilliant advantages of induction hardening, the process yet involves some challenges that lead to undesirable results. The major issue in induction heat treatment is the edge effect due to the disproportionate density of magnetic flux in different areas of a part

[26, 65]. This variation causes non-uniform generated temperatures over the surface of parts. Subsequently, an uneven formation of martensite phases will occur on the surface of the specimen following the quenching may lead to undesirable metallographic structure. These physical phenomena arising from magnetic flux characteristics coupled with coil geometry limitation provide a varying temperature distribution in radial and axial directions. In the case of high-frequency induction hardening of a small disc with a single-shot method, two facts could be concluded to justify the non-uniform temperature distribution. First, the temperature gradient in the radial direction due to the more proximity in the outer layer of the disc to the induction coil compared with the distant layer to the coil toward the center of the disc's geometry. The second reason for nonuniform temperature distribution comes from the distortion of magnetic field at coil and bending of the induced current in the edge regions of the workpiece; namely, the edge effect phenomenon. This results in a temperature gradient in the axial direction wherein the generated heat profile between the middle plate and side plates of a disc is not uniform as shown in Figure 17. Thermal gradient because of the edge effect is negligible for big parts, though this is not applicable for small parts. The smaller workpiece the more serious challenge in the quality of the final product [35, 66, 67]. Due to the complexity of this physical phenomenon, there is no definite solution to eliminate it, however, a great deal of researches has been dedicated to reducing its consequences as much as possible. One efficient solution is to utilize magnetic flux concentrators. Axial/radial gaps between magnetic flux concentrators and coil/disc are two effective parameters in the edge effect that are included in this study. This study investigates the effect of the concentrators position (radial and axial gap) as well as the induction heating process parameters including machine power, frequency, heating time on the edge effect aiming at tuning them to minimize the edge effect. Figure 18 demonstrates a schematic presentation of the position of the coil, concentrator, and workpiece.

Since the discovery of the induction phenomenon in 1831, plenty of efforts have been hailed on detecting all effective elements and improving the induction machine component to make this process more productive and user-friendly. In the last few decades, the development of computer technology has brought a great deal of facilitation in this field

alongside experimental investigation. Indeed, numerical computer simulation currently plays a fundamental role in the development of this complex and multi-physical process. Investigations on residual stress profiles produced by induction surface heating and quenching [103] and numerical simulation to find a relation between induction process parameters and phase transition in surface hardening [104] can be cited as examples.

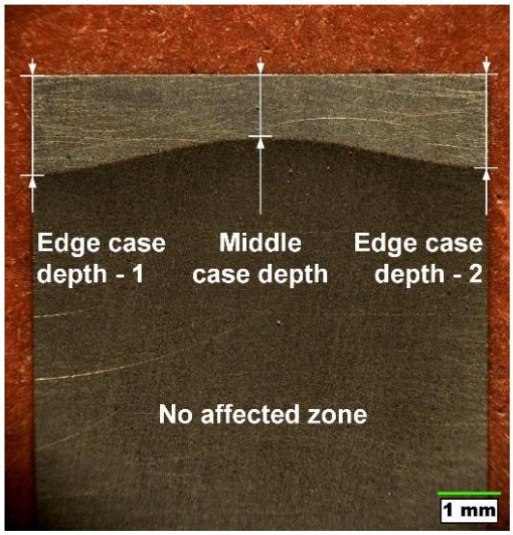

Figure 17. Axial cross-section of an induction hardened sample[58].

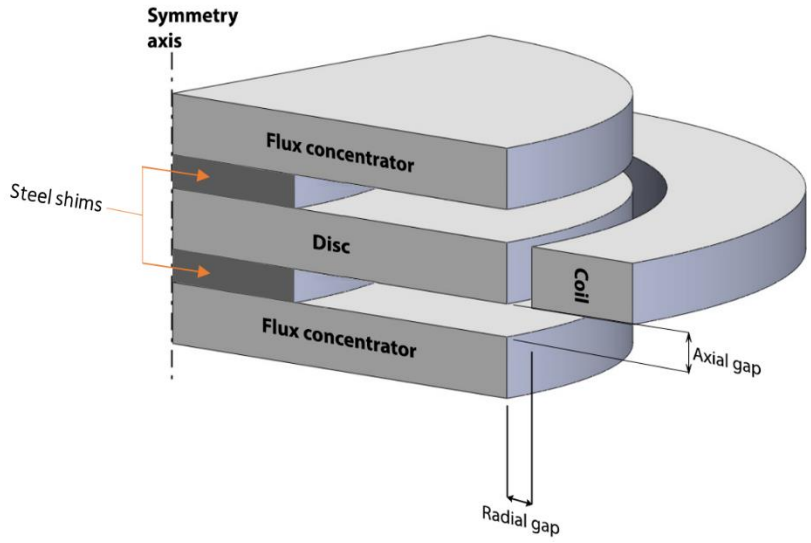

Figure 18. Schematic presentation of induction heating with magnetic flux concentrators.

Furthermore, looking at academic researchers on induction heating and heat-treating shows applying computer modeling along with experimental has replaced the word ‘‘usefulness’’ with the word ‘‘necessity’’. Studies such as the formation of surface stresses in forming rolls hardened by induction hardening are analyzed by FEM simulation [105]. In another research, case hardening of gray and ductile iron was studied by induction hardening [106]. In a practical approach, the kinetics of structural transformation of roll steels was examined [107]. Dutka et al. [108] utilized computers along with experiments to predict phase transformation during the induction process applied for cutting tools. Also, the functionality of spray cooling was tested for induction hardening of the gearwheels [109]. Multiphysics modeling was executed to make experimental faster and more accurate for induction hardening of the ring gear [28]. Furthermore, initial microstructure and heating rate were investigated for induction hardening of 5150 steel [110]. In more recent studies, induction heating was performed to enhance the fatigue strength of AISI E52100 bearing steel [111]. Experiment analyses are also applied to study distortion of cold-drawn and induction-hardened components [112]. Jeong et al. [113] tried to predict the deformation of curve shape steel plates in high-frequency induction heating. The eddy-current method is used to define the case-depth of cast iron hardened by induction [114]. Estimation of stress

and distortion during the induction case hardening tube was performed by Nemkov et al. [115], and another experimental approach has been done to investigate the numerical modeling of the induction process [116]. To improve fatigue strength and avoid cracks in stress and strain during induction hardening, numerical simulations were performed by Ivanov et al. [9]. The effects of initial microstructure of 4140 steel on the fatigue behavior after induction hardening was also explored [117], and multiple investigations applied finite element analysis (FEA) to determine effective process parameters and to find ways for microstructural enhancement of the final induction-hardened product [30, 43, 118]. Utilizing ELTA software induction heat treatment of steel is simulated [119] wherein a combination of numerical and experimental investigations is applied for local induction hardening of large-diameter gear rolling [29]. This research team has recently utilized both experimental and FEA simultaneously to enhance induction hardening process applied to gears. 2D simulation is used to observe the effect of changing in the geometry of the component on hardness profile [49] and 3D simulation is applied to improve the case-depth of induction-hardened helical gears [50]. In another research using 2D models, the effects of induction heating process parameters on hardness profiles of 4340 steel bearing shoulders were studied [120]. The effect of frequency on the hardness profile of spline shaft heat-treated by induction is also examined [100]. Another study was focused on the effects of induction machine parameters on the case-depths of 4340 spur gear with a 2D model [34], and explore how machine parameters and geometrical factors are effective on the hardness profile of 4340 steel disc hardened by induction hardening [24]. Furthermore, surface methodology and artificial neural network modeling were exploited to observe the effects of flux concentrators on changing of edge effect in spur gear treated by induction [82]. Barglik et al. [77], are recently performed a numerical study on dual frequency hardening process of a AISI 300M gear. They introduce a mathematical model of the process by the help of CCT and TTA diagrams**.** In 2019, Baldan et al. [78], investigated the induction heating process from another point of view; implementing multi-fidelity optimization approach to reduce process time. In early 2019, Li et al. [54] tried to optimize the induction heating temperature of 55CrMo steel ball screw specimen and used the martensite fraction value as a main criterion of their study.

The outcome of the study shows that the temperature increase is in favor of martensite formation and hardness gain.

This study aims at determining the most effective process parameter on edge effect in induction hardening of disk-shaped parts while flux concentrators are applied. As previously mentioned, employing disk-shaped parts in this study could helpfully eliminate some difficulties of using parts with complex geometry like gears while the result can be applied for both shapes. In this experimental effort, the ANOVA statistical method is used to model and analyze case-depth for different combinations of process parameters and location of concentrators. This method has proved its reliability in statistic approaches and shows the way to understanding the effect and measure of each multi-physical parameter and helps to reduce errors and wasting time on calculations. In this regard, the first step is to identify the most effective range of the process parameters by preliminary tests. The second step is to plan the most effective tests with the minimum number of trials employing Taguchi planning method. The last steps are respectively performing the planned tests, statistical analysis, and then discussing the results and finally, elaborating conclusion according to the evidence. These proceeds led to yield an effective, accurate, and robust statistical model that can be used to predict the case-depth of disk-shaped workpieces. This article is formed as follows: section 2 presents the methodology of our experimental tests based on induction surface heating and its related parameters, while results of experimentation, statistical, and sensitivity analyses are reported in section 3. In the end, section 4 presents conclusions and ideas for future works in this field.

2.2.3 Experimental procedure

2.2.3.1 Materials and method

Induction hardening is applied to 4340 steel discs aiming at fast surface heat treatment, which is low alloy steel known for its high toughness and strength in the heat-treated condition while preserving fatigue resistance. Mentioned characteristics make it a reliable

choice for making industrial disc shape parts. The chemical composition of AISI 4340 steel and its mechanical characteristics are noted in Table 9 and 10 respectively.

Table 9. AISI 4340 steel chemical composition in wt % [86].

Element	**Ni**	**Cr**	**Mn**	**C**	**Mo**	**Si**	**S**	**P**
Content (%)	1.65-2.00	0.70-0.90	0.60-0.80	0.38-0.43	0.20-0.30	0.15-0.30	0.04	0.035

Table 10. Mechanical properties of AISI 4340 steel [87].

Yield strength [MPa]	**Ultimate tensile strength [MPa]**	**Elongation at break [%]**	**Hardness Rockwell C [HRC]**
710	1110	13.2	35

The induction heating machine that is used for this study employs two generator sets of a medium and high frequency to produce a wide range of frequencies. The maximum range of frequency, approximately 1 MW, could achieve by a combination of the two generators. Here is the machine procedure to drive the maximum range of frequency: first is to create maximum power of 550 kW by using audio-frequency technology with solid-state converters that operate at 10 kHz, and the second is to deliver maximum power of 450 kW by running a transistor radiofrequency generator at 200 kHz. To achieve high frequency, a thyristor radiofrequency (RF) generator operates at 200 kHz. Process controlled utilizing real-time monitoring (RTM) module to ensure the state of machine parameters during the process validating whether the actual parameters are the same as the input parameters.

A disc is positioned on a ready-made stand kit between two magnetic flux concentrators. Discs and flux concentrators are in the same material, shape, and geometry; AISI 4340 steel with an outer diameter of 104.3 mm, and a thickness of 6.5 mm. AISI 1010 steel shims are inserted between disc and concentrators to ensure distance between them (axial gap). The thickness and the outer diameter of each shim are 0.2 ± 0.05 mm and 31.75

mm respectively. The geometrical specification of copper-made coil is 140 mm for outer diameter and 110 mm for inner diameter with a useful section of 7 mm × 7 mm and thickness of 2 mm. Figure 18 displays a schematic position of magnetic flux concentrators, master disc, and coil. Finally, a jet of a cooling solution containing 92% water and 8% of polymers is used as coolant fluid for quenching the disc after induction heating. It should be mentioned that all disc samples have undergone a uniform quenching and tempering treatment to have approximately a uniform hardening of 45 HRC through the discs. This is to prepare an equal initial condition for all samples before starting the induction heating process. As previously mentioned, because of the variety of flux densities in different areas of the disc, different amounts of heat will be generated through the disc and can be stocked in some areas. Therefore, the area that is exposed to the more magnetic flux is considered critical, that must be heated within the range of austenization (above Ac_3) to avoid overheating more or less than this specific temperature range. To serve this purpose, a typical guideline for the induction hardening of the AISA 4340 disc is followed.

To avoid useless trial and error tests, an optimized number of tests should be done, therefore a rigid method for designing the experiments is adopted to provide the maximum amount of information from the minimum number of experiments. In this study, Taguchi planning method is applied because of the capability of this method in executing efficient and simplified factorial results [84, 88]. To apply this optimized experimental planning method, a list of effective parameters required with a defined level of each. During the induction heating, machine power, heating time, and frequency are three input variables of the induction machine that control the generated heat and consequently the temperature amplitude on the part. It should be considered, in contrast to the power and heating time, frequency is not tunable. Other effective factors are the axial gap (the gap between each concentrator and master disc), and the radial gap (the gap between the coil and discs) as shown in Figure 18. Accordingly, the input parameters are power, time, axial and radial gap. The levels of input parameters and their ranges were defined by low, medium, and high levels as presented in Table 11. Regarding the abbreviation list in Table 11, in the following P, T, AG, RG are used instead of power, heating time, axial gap, and radial gap respectively.

Table 11. Experimental factors and range of values for each level.

Parameter	Unit	Abbreviation	Level 1	Level 2	Level 3
Power	kW	P	85.0	100.0	115.0
Time	s	T	0.40	0.50	0.60
Axial Gap	mm	AG	0.20	0.80	1.40
Radial Gap	mm	RG	2.60	2.80	3.10

Taguchi experiment planning is well-known as one of the most reliable and robust planning-designer to perform a minimum efficient number of experiments. A proper range of factors by preliminary tests along with using Taguchi experimental design makes the process more robust, efficient, and with a minimum number of trials [89, 90]. Indeed, performing an induction hardening within the maximum and minimum range of parameters is of critical importance to create maximal and minimal case-depth transformation. An L_9 orthogonal matrix corresponding to nine (9) experimental tests is addressed by Taguchi planning method; consequently, each test consisted of a unique combination of parameter levels as shown in Table 12.

Table 12. Design of experiences, L_9 orthogonal matrix.

Tests No	AG [mm]	P [kW]	T [s]	RG [mm]
1	0.2	85	0.4	2.6
2	0.2	100	0.5	2.8
3	0.2	115	0.6	3.1
4	0.8	85	0.5	3.1
5	0.8	100	0.6	2.6
6	0.8	115	0.4	2.8
7	1.4	85	0.6	2.8
8	1.4	100	0.4	3.1
9	1.4	115	0.5	2.6

2.2.3.2 Micro-indentation hardness tests

Micro-indentation tests using Clemex machine are performed to measure the hardness of specimens at their cross-section. After surface-hardening process by induction heating method, discs specimens are cut into two halves. In the following, the middle plane refers to the surface that cut the thickness of disc in two equal parts parallel to the edge plane. The edge plane, in its turn, refers to the outer surfaces of the disc as depicted in Figure 19. Micro-indentation tests are then performed in both edge and middle planes, and results are summarized in Table 13. These responses present the measured case-depths of discs at the edge and middle of discs respectively denoted as d_E, d_M. It worth mentioning that the defined case-depths on edge planes are calculated as the mean value of case-depths measured on the two exterior surfaces of the disc (edge planes). Doing so could avoid complications in analyses related to outliers.

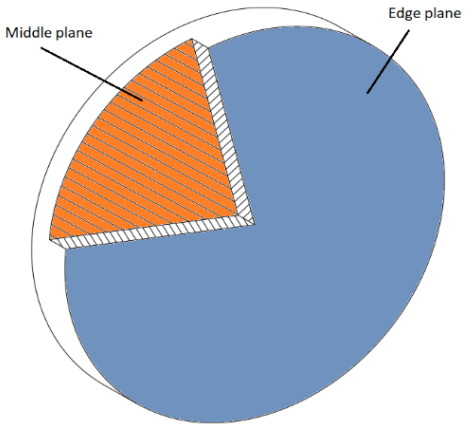

Figure 19. Schematic of the disc representative for middle and edge plane.

The results in Table 13 implies that the maximum case-depth in both middle and edge planes is occurred using test 9 parameters, while the minimum case-depth in middle and edge planes is observed in test 1. In detail results of tests 9 and 1 are presented in Figure 20.a and b, in which the hardness profile of induction heat-treated discs is evaluated. Three distinguished regions could be defined in these figures; the first region presents a hardened surface layer due to martensitic phase formation (the line approximately parallel horizontal

axis), the second region displays a hardness drop to approximately the core material hardness (the part with deep slope) and the third region in which discs tempered before the tests and preserve the initial core material hardness (approximately 45 HRC) [92]. Figure 20.a demonstrates the hardness profile and obtained case-depth at edge plane (d_E) resulted respectively from test 9 and test 1, while Figure 20.b shows the hardness profile and case-depth at the middle plane (d_M).

Table 13. Microhardness test results in middle plane (d_M) and edge plane (d_E).

Test No	**Parameters (variables)**				**Responses**	
	AG [mm]	T [s]	P [kW]	RG [mm]	d_E [mm]	d_M [mm]
1	0.2	0.4	85	2.6	0.525	0.90
2	0.2	0.5	100	2.8	1.225	1.30
3	0.2	0.6	115	3.1	1.475	1.550
4	0.8	0.5	85	3.1	0.80	1.050
5	0.8	0.6	100	2.6	1.575	1.550
6	0.8	0.4	115	2.8	1.125	1.250
7	1.4	0.6	85	2.8	1.30	1.30
8	1.4	0.4	100	3.1	0.930	1.10
9	1.4	0.5	115	2.6	1.725	1.550

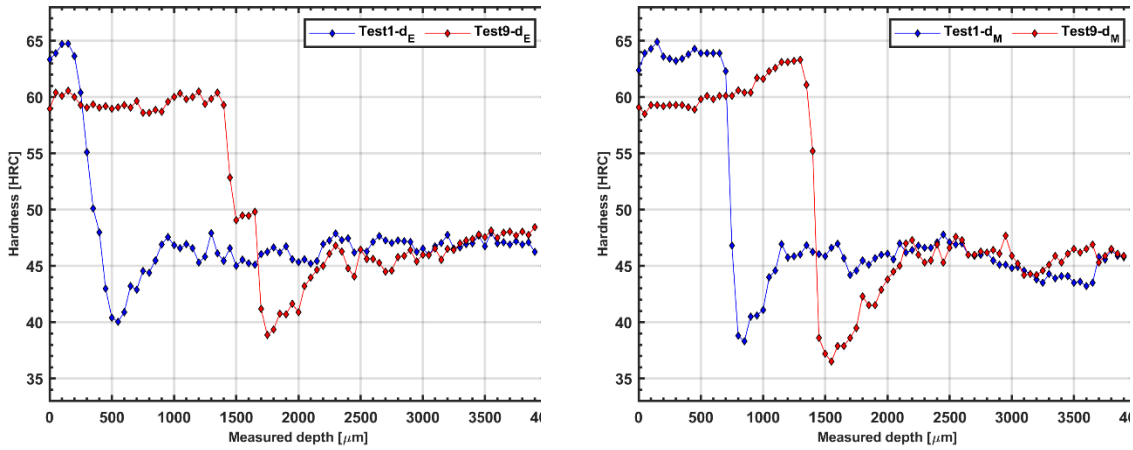

(a) (b)

Figure 20. Hardness profile of test 1 and test 9; (a) in middle plane d_E, (b) in edge plane d_M.

There are three main conclusions to be drawn from Table 13. First, the maximum case-depth at the edge plane happens in the maximum level of power and axial gap, and a minimum level of radial gap. Meanwhile, the minimum case-depth at edge plane occurs when P, T, AG, and RG are set at their minimum level. Second, the minimum amplitude of the case-depth difference between middle and edge plane (Δd), which is an indication of reaching a minimum edge effect, is reached when heating time is in its maximum level of variations. Third, a proper variation of process parameters in terms of covering the measured maximum and minimum case-depths confirms the credibility of designed tests based on Taguchi method.

2.2.4 Effects of parameters on hardness profile

2.2.4.1 Statistical analysis and parameters contribution

To estimate the effectiveness degree of each variable in the experimental, outputs are analyzed utilizing the statistical method of analysis of variance (ANOVA) [93, 94]. ANOVA uses F-test to appraise the regression model. To evaluate the degree of parameters' participation in responses (case-depth at middle and edge plane), the main effect diagram for each dependent variable (specific range combination of the parameters) is first plotted. The

results of ANOVA concerning the case-depth at edge and middle planes are shown in Table 14 and Table 15 respectively. In these tables, the degrees of freedom (DoF), sum of squares, contribution percentage, F-value, and p-value are the terms that declare the results of the analyses. Also, to estimate the precision of the regression model, the coefficient of determination (denoted by R^2 or R-squared) is calculated. The term p-value determines statistically whether the effect of process parameters on the case-depth is significant. In other words, ANOVA calculates the p-value and compares it with the significance level (α) to determine whether the null hypothesis is rejected. In fact, the null hypothesis states that the effect of studied parameters is insignificant. The null hypothesis can be rejected when the calculated p-value is lower than or equal to the designated significance level. The defined significance level (α) for this study is 95%, which means that there is a 5% risk of considering a specific parameter as having a noticeable effect on the process when there is no real effect.

Linear regression is then performed based on ANOVA results to develop predictive equations for case-depths in edge and middle plane (d_E and d_M respectively) as a function of power (P), heating time (T), axial gap (AG), and radial gap (RG). Here outputs are case-depths that termed dependent variable, and input parameters of P, T, AG, and RG are termed independent variables. The ANOVA conditions in this study are selected as stepwise method wherein interactions between factors are included. Stepwise method aims at excluding less important factors and interactions in each step giving more importance to the effective factors. Analyses were proceeded by including the most important interactions to prevent changing the meaning of the lower order coefficients. Furthermore, involving any redundant term to the model while the related P-value is higher than 0.05 could make the model more complicated [96].

P-Values for T, P, P×AG, and RG are respectively 0.001, 0.002, 0.030, and 0.060 as given in Table 14. Except for RG, all p-values are less than 0.05, hence, the null hypothesis is rejected. It can be observed that in d_E, the heating time (T) and machine power (P) are the most effective parameters on the case-depth and then, P×AG with less degree of importance regarding their descending quantity of p-values. P-Value of 0.030 for P×AG connotes

interaction between power and the axial gap was in such a way that combining these two independent variables gave a different effect on d_E. Table 15 introduces P, T, T×RG, and RG as the most effective variables in d_M concerning the P-Values (respectively 0.00, 0.005, 0.015, and 0.031). Results for both d_E and d_M proves the involving interactions as the P-values of P×AG and T×RG are respectively 0.030 and 0.015 from Table 14 and 7. The contribution of each variable and interaction is also defined in the edge and middle plane of the disc. From ANOVA results in Table 14 it can be concluded that in d_E, P and T have the main effect on the response as their contribution is respectively 40.31% and 43.69%. In d_M, the contribution of P and T indicates their dominant effect in the response slightly more than their effect in d_E as their ratios are respectively 44.81% and 48.98%.

Table 14. Results of ANOVA for micro-hardness tests in edge plane ($d_{E.}$)

Factors	DoF	Sum of squares	Contribution	F-Value	P-Value
P	1	0.48167	40.31%	46.21	0.002
T	1	0.52215	43.69%	66.03	0.001
RG	1	0.06695	5.60%	6.73	0.060
P*AG	1	0.09084	7.60%	10.86	0.030
Error	4	0.03345	2.80%		
Total	8	1.19505	100.00%		

Table 15. Results of ANOVA for micro-hardness tests in the middle plane ($d_{M.}$)

Factors	DoF	Sum of squares	Contribution	F-Value	P-Value
P	1	0.201667	44.81%	331.70	0.000
T	1	0.220417	48.98%	29.76	0.005
RG	1	0.014803	3.29%	10.76	0.031
T*RG	1	0.010607	2.36%	16.92	0.015
Error	4	0.002507	0.56%		
Total	8	0.450000	100.00%		

2.2.4.2 Main effect plot and predictive regression models

To define the correlation between each independent variable and dependent variable, main effect plots are drawn. Interpretation by plots provides us a visual trend of response variation with respect to parameter levels. This approach allows exploiting a goodness-of-fit model that describes the relationship between variables and predicting the case-depth with a combination of the input parameters. Main effect plots are drawn in Matlab^{TM} to describe the most effective parameters affecting the response. These plots show a general trend of how one parameter affects the response allowing their effectiveness comparison separately. This is performed by verifying the slope of each variation line between two levels in which the steeper the slope, the more effective the parameter on the response. The main effect plots of the responses (d_E and d_R) over the 3 levels of their parameters (P, T, RG, and AG) are shown in Figure 21. In this figure, d_E and d_R are presented with respectively blue and red lines. It can be observed from Figure 21 for d_E that P and T have a significant effect on the case-depth. The bigger domain of changing in response with steeper variation lines is the evidence of this interpretation. The effect of the axial and radial gap (AG and RG) on the case-depth at edge plane is less compared to P and T. This observation is based on the fact that the slope of AG and RG variation is less than the one of P and T. Like d_E, P and T are the effective parameters on d_M wherein the slopes of variations are steep. The effect of AG and RG on d_M can be interpreted as less than P and T since their variation slop is much smaller. Compared to AG, increasing in RG shows the opposite effect on the response as it is vivid from the negative slop from levels 1 to 3.

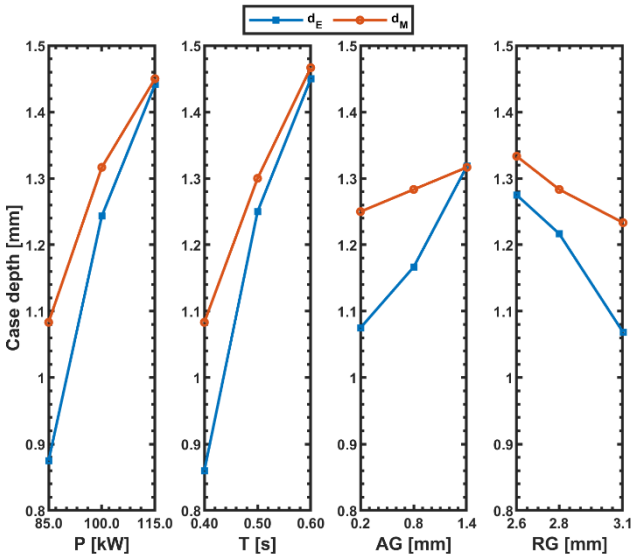

Figure 21. Main effect plots of case-depth on middle and edge planes (d_M and d_E).

The main effect plots are used to reveal the relationship of each independent variable on the dependent variables. The interaction between the parameters is also studied base on ANOVA as a combination of interacting variables because the effect of one variable depends on the value of the other [55]. Studying the interaction of variables indicates that P and AG (P×AG) in edge plane (d_E) and T and RG (T×RG) in middle plane (d_M) present interactions. To this end, a predictive linear regression of case-depth, which is a function of the important input parameters and interactions is exerted for the edge and middle plane. These predictive functions ate respectively presented in equations (1) and (2).

$$d_E = -1.130 + 0.01725 \times P + 3.042 \times T - 0.386 \times RG + 0.002046 \times P \times AG \quad (1)$$

$$d_M = -3.269 + 0.012450 \times P + 7.73 \times T + 0.829 \times RG - 2.053 \times T \times RG \quad (2)$$

The coefficient of determination (R^2) concerning the regression equation of d_E is 97% which declares that the predictive equation represents 97% of the response behavior based on the presented factors and their interactions. The R^2 of d_M is calculated 99% which means that the predictive regression equation represents almost perfectly the variation of response (d_M) in the range of experimentations. The accuracy of regression equations can also be

estimated based on the residual evaluations. In this regard, the difference between predicted and measured values represent the possible regression error (residual). Using Equation (3) the relative error of predicted models can be calculated. Our study's outcomes indicate a good agreement between experimentally measured and predicted model for case-depths at the edge plane (d_E) and the middle plane (d_M). The estimated errors of d_E are less than 4% except for test 2 where it reaches approximately 12% while the error of d_M is less than 4% for all tests.

$$Error\ (\%) = \frac{|\ Predicted - Measured\ |}{Measured} \times 100 \qquad (3)$$

The goodness of fit, which visually represents the level of agreement between the measured experiments and predicted models, is depicted in Figure 22.a and b for d_E and d_M case-depths respectively. Predicted values that agree exactly with measured values would fall on the red line, while the dispersion of these values (blue points) with respect to the red line represent the lack of fitness. The plots of Figure 22 illustrate a very good agreement between the experimental values and predictive models, forwhich the predicted model of d_M fits better than d_E.

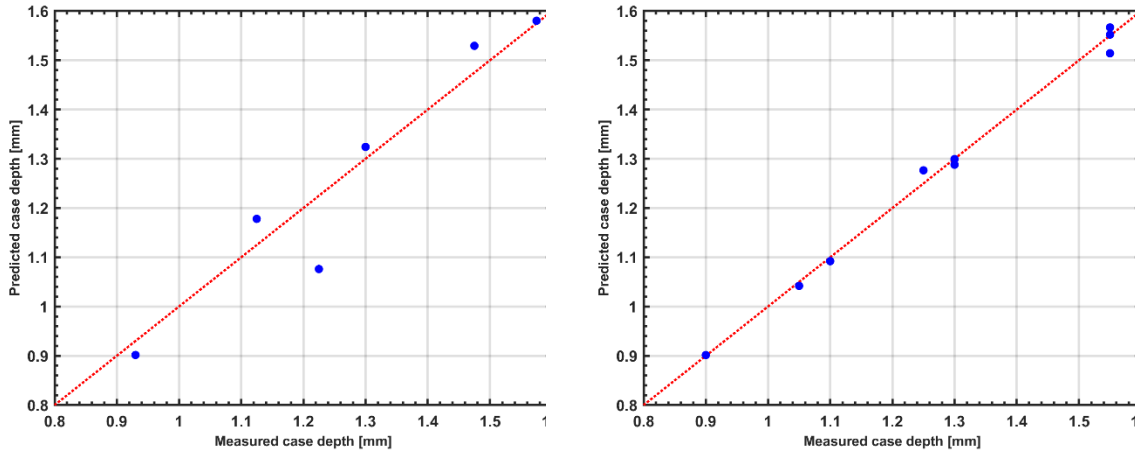

(a) (b)

Figure 22. Case-depth measured by experiments versus predicted by regression equations in (a) edge plane (d_E) and, (b) middle plane (d_M).

2.2.4.3 Response surfaces and sensitivity analysis

For empirical modeling, Response Surface Methodology (RSM) is applied whereby the results are shown by contour plots. Contour plots are 3D diagrams that the response curve is projected on the plane of variables. In this regard, the response is shown by contours (color gradient and isolines) on the plane of variables. Here the variables are P, T, AG, and RG, and responses are d_E and d_M. The results of RSM are displayed in Figure 23 for d_E and in Figure 24 for d_M. It should be noted that the non-presented parameters in the plots are considered as a constant independent variable in their medium level of 100 kW, 0.5 s, 0.8 mm, and 2.8 mm for P, T, AG, and RG respectively.

Contour plot of case-depths in edge plane (d_E) versus P and T is illustrated in Figure 23.a wherein the maximum values of case-depth (1.7 mm) in the upper right corner of the plot corresponds to the highest values of both P and T. The minimum value of case-depth (0.7 mm) in this graph corresponds with the lowest values of both P and T. In other words, both T and P have an increasing effect on the case-depth value as well as approximately the same impact on the cade depth enhancement. The same trend can be observed in Figure 23.b and c for P and AG as well as T and AG, but the case-depth value is affected more by changes

in P and T than AG in these plots. As it is already explained in section 3.2 and can be observed in Figure 23.d, RG shows the opposite effect on the case-depth when it is compared with other parameters and the maximum case-depth happens at minimum RG. This is demonstrated in contour plot of case-depths at edge plane versus AG and RG. As a conclusion, the highest case-depth can be achieved by increasing P, T, and AG whereas decreasing RG.

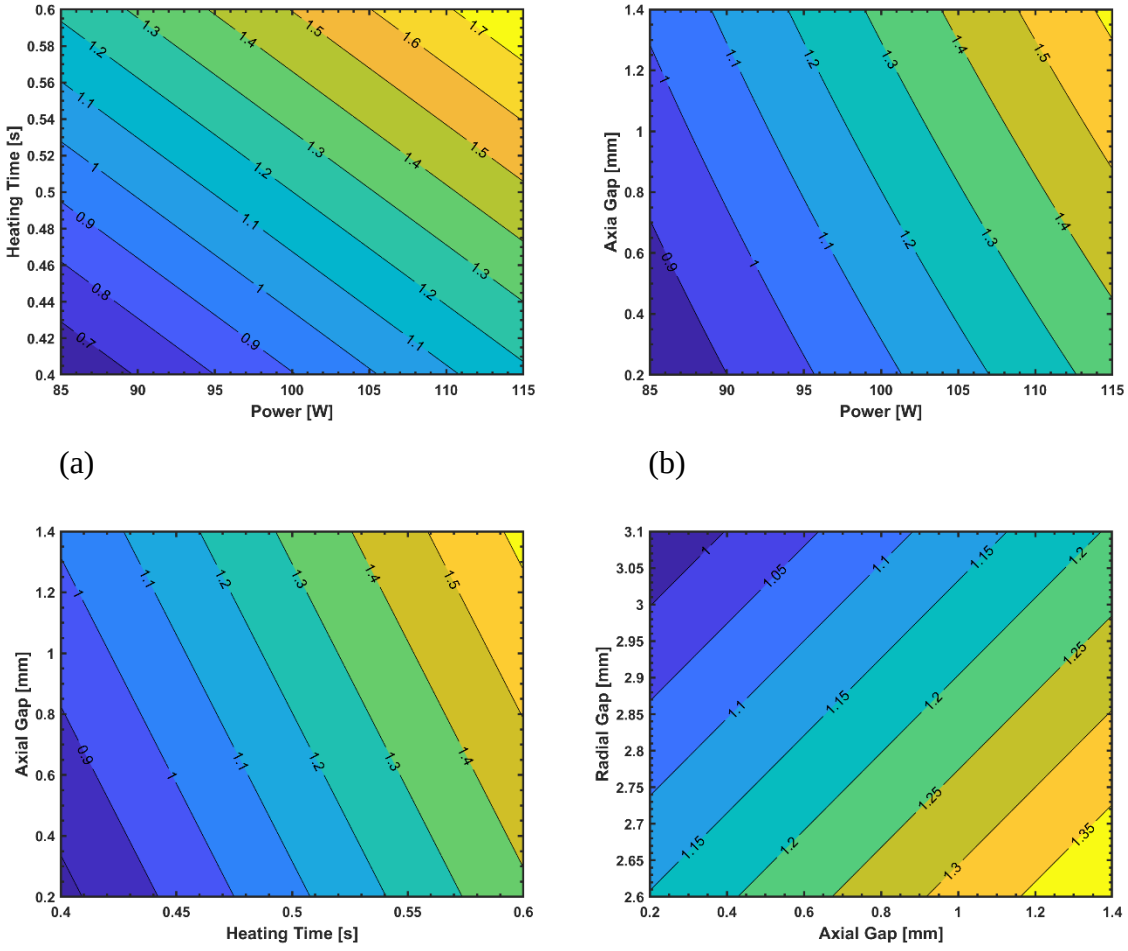

Figure 23. Contour plots of P, T, AG, and RG versus case-depths at edge plane of discs (d_E).

Based on ANOVA in section 3.1, the most effective parameters of case-depths in middle plane (d_M) are defined as P, T, and RG in which their contour plots are presented in

Figure 24. The increase of P and T results in the case-depth increase as shown in Figure 24.a. Similar to d_E, RG has an inverse effect on d_M as illustrated in Figure 24.b and c. It can be concluded from Figure 24 that case-depth in middle plane of discs is mainly affected by the P and T in which their increase would increase the case-depth

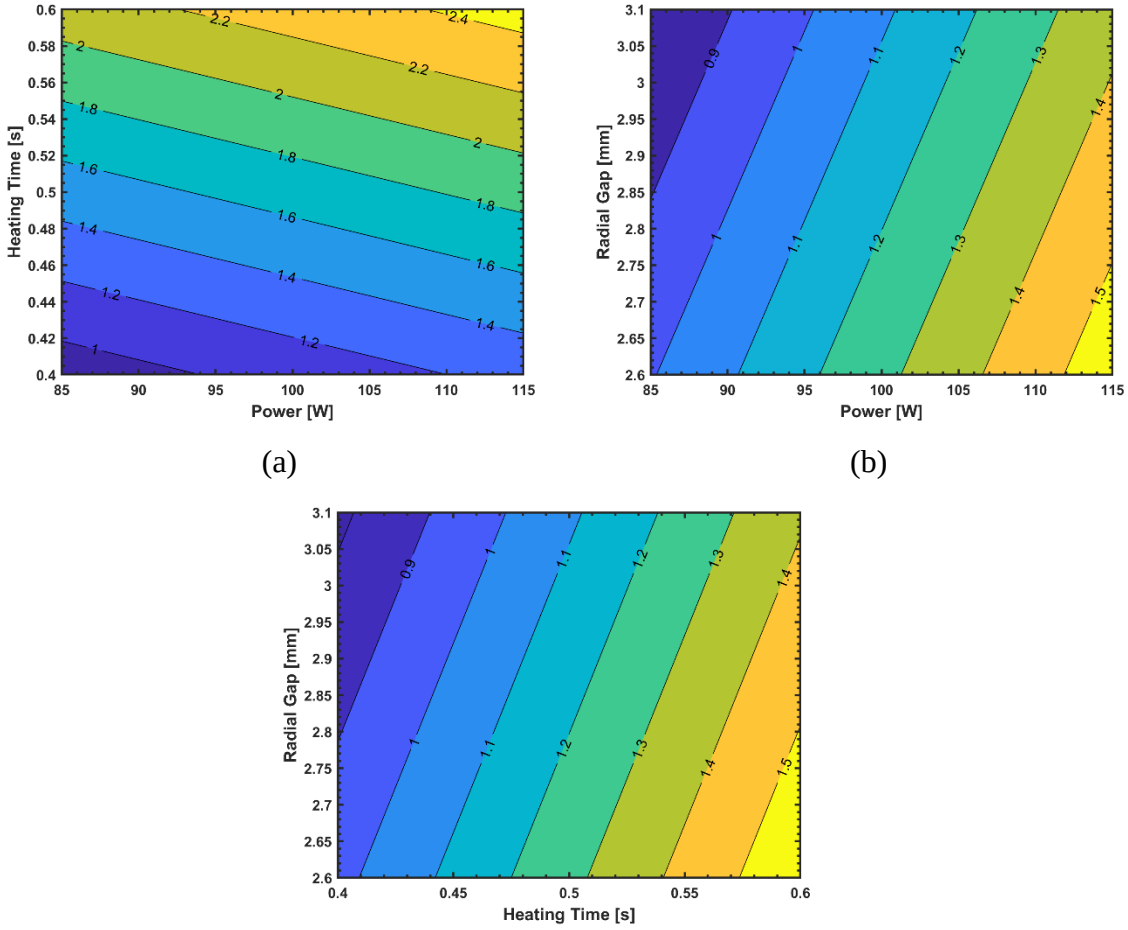

(a) (b)

(c)

Figure 24. Contour plots of P, T, and RG versus case-depths at middle plane of discs (d_M).

2.2.5 Edge effect discussion

Considering the principle of magnetic fields, they are denser near the source of the field. Consequently, moving from the outer diameter of the disc towards the center of the disc, hardness profile is reduced considerably to around the initial hardness of material as is

shown in Figure 20. Loops of induced electrical currents, namely "eddy currents" arising from changes in the magnetic field, tend to be stuck in corners that lead to non-uniform thermal distribution through the disc. Therefore, a non-uniform hardness profile and finally a different case-depth profile in edge plane versus the middle plane are formed. To make a comparison of case-depth profiles in the edge and middle planes, in this section, the middle plane is considered as the reference plane and the differences between the planes ($\Delta d = d_E - d_M$) present the edge effect. The ultimate purpose of this study is to determine the best combination of process parameters that maximized the case-depth with minimum edge effect utilizing flux concentrators. To this end, the less Δd the less edge effect, that results in more desirable uniform case hardening.

The effects of induction hardening process parameters (P, T, RG, and AG) on the case-depth profile have been already discussed separately in the middle and edge planes. Results showed that the case-depth profile is mainly affected by P and T, while other parameters including RG, AG participated less. In this study, the interaction of parameters is also considered and regarding ANOVA, only P×AG and T×RG are effective parameters in case-depth. Applying the concept of Δd, and presenting it in Figure 25, a reducing trend in edge effect from test 1 to test 9 can be observed. The minimum edge effect is then noted in test 7 and test 5. The experiment parameters, P, T, AG, and RG for test 7 are 85 kW, 0.6 s, 1.4 mm, and 2.8mm respectively which refers to the low-level of machine power, the maximum level of T and AG, and mid-level of RG. The process parameters of test 5 are 100 kW, 0.6 s, 0.8 mm, and 2.6 mm, respectively for P, T, AG, and RG. They refer to the maximum level of P and T as well as the mid-level of AG and RG. It worth mentioning that the average case-depth in test 7 is 1.30 mm while in test 5 is 1.56 mm. Although the best case-depth results in test 9, the edge effect is also considerable. It could be concluded that the best scenario, deeper case-depth, and less edge effect, is occurred in tests 5 and 7 where the heating time is tuned in its maximum level, the machine power, and radial gap are in low and mid-level, and the axial gap in its maximum and mid-level.

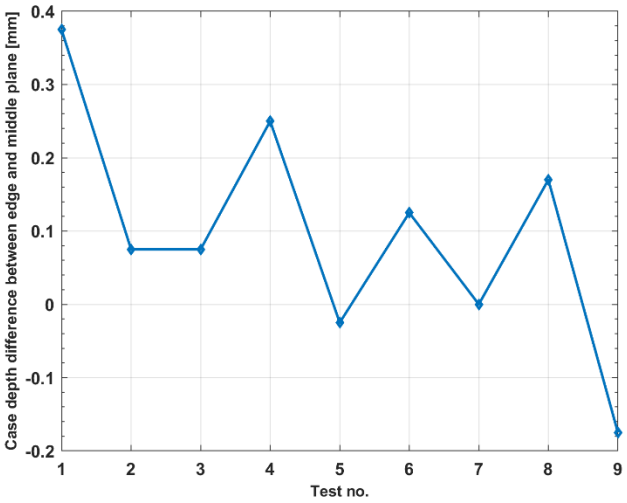

Figure 25. Case-depth difference between middle plane and edge plane (Δd) resulted from the 9 arrays of experiments.

2.2.6 Conclusions

4340 steel discs are used in this study to investigate the effects of induction hardening process parameters on the case-depth and edge effect with the presence of magnetic concentrators. The process parameters, machine power (P), heating time(T), the axial gap between disc and concentrator (AG), and the radial gap between disc and coil (RG) are considered to evaluate two responses, case-depth in edge and middle of discs (d_E and d_M). Taguchi design method is employed to plan nine tests (L_9) in three-parameter variation levels. Micro-hardness test and consequently the case-depths are then analyzed by Analysis of Variance (ANOVA). Using linear regression, predictive models are then developed for d_E and d_M with the coefficient of determination (R^2) of 97% and 99% respectively. The analyses show that heating time and machine power are dominant parameters to control the case-depth in d_E and d_M as far as the contribution percentage of T and P for d_E are respectively 43.69% and 40.31%. taking into account the effect of parameter interactions, P×AG is contributed 7.60%. in d_E variation. The contribution of T, P, RG, and T×RG in the variation of d_E is 48.98%, 44.81%, 3.29%, and 2.36%. Moreover, contour plots based on Response Surface Methodology (RSM) show that setting independent variables of P, T, and AG at maximum

level and RG at minimum level would enhance the case-depths (d_E and d_M). The edge effect, which presents the non-uniformity of case-depth in the edge plane with respect to the middle plane, is then analyzed in which tests 5 and 7 present the minimum edge effect. Based on the test results, maximum heating time, medium machine power, and radial gap, as well as maximum axial gap help reducing the edge effect. It worth mentioning that the average case-depth in tests 5 and 7 reaches 1.56 and 1.30 mm respectively. The results of this study can also be used in disc-shaped parts such as gears.

Although the results of this study are promising, some improvements and applications can be foreseen. Future works can study can the generator frequency fluctuation according to the variation of geometrical factors (thickness, axial and radial gaps) as an induction machine factor. Moreover, the concentration thickness can be optimized during the extensive design of experiments. To optimize surface treatment of the other parts like bevel gears, and helical gears which have different and more complex shapes, experimental test benches as well as predictive models can be developed. In this regard, applying artificial intelligence to create and enhance the models could be the next project to perform.

CHAPITRE 3
ÉTUDE SUR L'APPLICATION DE LA MÉTHODE SÉQUENTIELLE À DOUBLE FRÉQUENCE DANS LE CHAUFFAGE PAR INDUCTION POUR LA TREMPE DU PROFIL D'UN ENGRENAGE DROIT EN ACIER 4340 PAR SIMULATION 3D ET ANALYSE PAR ÉLÉMENTS FINIS

3.1 RESUME EN FRANÇAIS

Dans cette recherche, la simulation 3D par éléments finis a été utilisée pour modéliser le procédé de chauffage par induction appliqué à des engrenages en acier 4340. Le modèle développé tient en compte le mode de chauffage de chauffage monofréquence et à double fréquence séquentielle. Il améliore le profil de dureté de l'engrenage droit, en envisageant de produire le moins de chaleur possible pour aider à une meilleure trempe et en produisant un effet de bord autant que possible. Le logiciel multiphysiques Comsol est couplé au logiciel Matlab pour l'extraction de données utiles de la simulation. Par cette procédure, la température produite (°C) en fonction du temps (s) et la dureté (HRC) en fonction de la profondeur (mm) ont été analysées pour trouver la méthode avantageuse entre les deux deux modes de chauffage.

Mots clés **- Chauffage par induction, Simulation, Fréquence séquentielle-duelle. Effet de bord, Engrenage droit en acier 4340**

Ce troisième article, intitulé " Study on applying Sequential Dual-Frequency Method in Induction Heating for Hardening the Profile of 4340 Steel Spur Gear Through 3D Simulation and Finite Element Analysis est co-écrit par moi-même, le professeur Noureddine Barka et Ahmed Al Salkhady. En tant que premier auteur, ma contribution à ce travail est la recherche sur l'état de l'art, le développement de la méthode, la gestion des données et des résultats, et la rédaction de l'article. Le professeur Noureddine Barka a fourni l'idée originale

et a également contribué à la recherche sur l'état de l'art, au développement de la méthode et à la révision de l'article. Ahmed Al Salkhady a contribué au développement de la méthode, à la création des modèles de simulation et de prédiction et à la gestion des données.

3.2 STUDY ON APPLYING SEQUENTIAL DUAL-FREQUENCY METHOD IN INDUCTION HEATING FOR HARDENING THE PROFILE OF 4340 STEEL SPUR GEAR THROUGH 3D SIMULATION AND FINITE ELEMENT ANALYSIS

3.2.1 ABSTRACT

Finding the best set of parameters in a specific approach of induction heating, which is applied for surface hardening of the metal parts with a particular geometry always is demanding. The finite element method and simulation are verified tools to accomplish the mentioned objective. In this research, 3D modeling was applied to generate the single frequencies (medium frequency and high frequency, separately) and the sequential-dual frequency of induction heating. The goal is to give a comparison between the two. It enhances the hardened profile of the spur gear, by considering producing the less possible heat to help better quenching and producing edge effect as much as possible. the material. 4340 steel alloy is the chosen material for this study which is known for its reliability for industrial applications because of its suitable specification in this field. Employing MATLAB's plotting of function coupled to the simulation model to ease extracting useful data from simulation and its results. By this procedure, produced temperature (°C) vs time (s) and hardness (HRC) vs depth (mm) were analyzed to find the advantageous method between the two methods of a single frequency and sequential-dual frequency.

Keywords **- Induction heating, Simulation, Sequential-dual frequency, Edge effect, 4340 steel spur gear**

3.2.2 Introduction

Some parts with spherical and cylindrical mass are needed to be wear and fatigue resistant more on their surface rather than inside which can be accomplished by surface

hardening. This approach has several advantages such as shortening the heating and quenching time process and reducing the creation of residual stress in traditional methods when those generate more heat in the center or interior layer of the parts. In this regard, induction hardening is a reputable surface hardening method with numerous privileges such as creating high power density at a specific region on the surface of the metal part, productivity, energy efficiency, and being environment-friendly [26, 100, 121]. Besides, compared to laser and flame hardening which are other mass-productive methods, possess the advantages of more controlling of the depth of the generated heat and lower cost [71, 122]. Further features of the induction hardening method that make it proper for manufacturing include easily integrated into the production line, minimizing distortion and deformation of the final products with repeatable quality. Because of the proven reliability of this technology, it is widely used in the automotive, electron, railway transportation, and aerospace industries [123]. Mechanical characteristics of the result in this method are strongly related to the 1-physical-chemical attribute of the material, 2-inductor design, 3-induction heating process parameters, and condition, and 4-geometry of the part, thus, achieving [34] the best result is bound to optimize mentioned parameters. Regarding physicochemical properties of the base material, AISI 4340 steel is studied in this research which is a martensitic steel low-alloy steel known for maintaining its high strength during heat treating conditions and having high fatigue resistance. The traditional method for hardening the steel is to heat the intended region of the part beyond austenitizing temperature (Ac3) to make material ready to be formed to the martensitic structure after quenching. Adjusting the machine process parameter according to the geometry of the part will improve the wear resistance and fatigue life of the surface while the temperature of the core of the part remains below the Ac3 point. About the second-mentioned case, the design of the inductor should correspond to the geometry of the hardened part to guarantee the heat treat quality. Needless to say, the design of the inductor for hardening of the parts like splines is completely different and includes more calculations. These issues along with setting proper induction heating process parameters (frequency, induced current density, and heating time) make the process uphill. The difficulty of hardening parts like gears is, due to the varied

distance of the tip and root of the gears to the coil, the surface of these parts is exposed to diverse and uneven flux density. As the result, the surface of the final product will have an unwelcome hardness profile. Therefore, achieving a desirable surface hardness profile brings more complexity to the process [26, 81, 120, 124-126]. In the case of this study which is spline, because of the length of the part, additional complication of the movement of the coil (or part) adds some extra elaboration to the setting [127]. As the result, using the experimentation method to produce the part with favorable quality leads to time-consuming, expensive, and inefficient procedures of trial and error. To avoid this circumstance, utilizing simulation plays a key role to frame and planning appropriate qualitative and quantitative tests. Moreover, the numerical method helps to understand and enhance induction hardening and ease process development [100, 125]. In the last decade, striving to find a more productive and efficient method to enhance induction heating ends up changing the word "helpful" to the word "necessary" in applying computer modeling. However, Still through the literature reviews can access a great deal of research about all applications of the induction whether in heating, melting, or (and in) hardening fields [128]. A developed model by means of simulation can be created and it allows analysis of the hardness profile as a function of the material and environmental properties along with controller parameters of the induction machine.

Multiple studies are carried out on effectual parameters of the induction hardening process by utilizing simulation software. Each one tries to promote the precision of the predictions in a variety of models in a different situation in a more genuine and efficient way than the previous one, or to cover the new demanded field. Using the finite element method to investigate a variety of coupling techniques is almost a new concept that has been introduced in recent years to facilitate multifunctional properties. K. Sadeghipour et al.[48] ran the ANSYS program to investigate induction heating process parameters and the results were compared to the experimental. Developing the numerical simulation tool and its features are overviewed to demonstrate how the frequency and power of the induction machine influence the temperature distribution[129]. The effects of machine parameters (power, frequency, and air gap) as independent variables on the final hardened profile of the spindle

are studied based on ANSYS [130]. Mathematical modeling of direct induction heating along with the general optimization problem and numerical results for ultra-weak coupling procedure is provided. The goal is to prove the efficiency and robustness of the adjoint model in optimizing induction heating processes[131]. An open-type magnetizer is used in a three-dimensional finite element method to reduce measuring time and calculated heating profiles for different shapes of the inductor are compared to the measured [132]. The finite element model created by COMSOLTM is capable to take several physical rules into the account and develop a reliable model while reducing time and eliminating wasting parts and material and results are giving credit to the experiment results of the laboratory (ETS) by comparison [133]. A multiphysics approach for modeling can demonstrate the hardness profile of the ring gear, while the real cooling rate of the quenchant and both magnetic saturation and Curie transition effects are considered [28]. The result of the computer simulation for the creation of the undesirable residual stresses in surface hardening of forming rolls heated by induction is examined and compared with two experimental methods to show which one gives credit to the simulation results [134]. Another study tries to optimize the induction machine parameter according to the dimensions of gear considering the non-linear behavior of material properties in different temperatures by modeling software (COMSOL) [49]. A 3D model is built to study and calculate the hardness profile of the gear as some machine parameters (current density and the heating time) and geometrical factors (coil width and gap between coil and gear) in medium (MF) and high frequencies (HF) are assigned [81]. In a similar approach, a 3D model is built with COMSOL software helping to understand more about the dissymmetry effect of the induction hardening process of the helical gear [50]. Chan-Man Jeong et al. [113] try to predict the deformations of the curved plates during the forming process with the high-frequency induction heating with the finite element method (FEM) and find the relation between heating parameters and the initial conditions and angular deformations of the curved plates. Is shown how computer simulations can be beneficial for a number of induction hardening applications as the goal is to manage stress and strain in hardened parts to enhance fatigue strength, avoid cracks, and minimize distortion [9]. thermal rules and problems can be coupled with eddy currents rule through

FLUX-2D package program in studying of individual treatment of pinions tooth to reduce the experimentation process and time and giving a better knowledge of the process [135]. It is shown which type of induction processes express the strong preference for the finite element analysis, what is the limitation of the commercial software, and what is the tips while the finite element method is used [136]. FLUX 3D is supplemented with two nonlinear partial differential equations to describe the distributions of magnetic and temperature fields in the induction hardening of gear wheels [46]. When it comes to induction hardening of the parts with complex geometries, and complicated algorithm of the moving inductor, several studies have been done; Andrzej Fraczek et al. [137] examines the effect of moving inductors along the cylinder axis on reducing pick-to-pick temperature amplitude. In another study, our team has conducted research to investigate the effects of induction heating process parameters, environmental conditions, and geometrical futures of the part and inductor with the finite element method. In the mentioned study, a 3D simulation and experimental validation of the induction heating for AISI 4340 steel spline shafts with a non-stationary scanning method is conducted [20]. However, to the best of our knowledge, all the mentioned methods approach to applying high and medium frequency for induction heating without succession. As a result, there would be a delay as a dwell time between applying two frequencies in the absence of applied energy. It is known as a classical method of using dual-frequency, yet it is important cognition basic knowledge of using dual-frequency in induction heating [34, 138]. Although, it has been shown that it cannot be useful for all purposes or all workpieces through a study by Vl Rudnev [139]. This study is conducted to investigate the effects of applying the sequential dual-frequency on spur gear with and without utilizing the concentrators by COMSOL software. Thereby, the results give a better knowledge of induction process parameter and their effectiveness in having a uniform case depth for a part with complex geometry like spur gear.

This research is focused on the idea of sequential-dual frequency by dint of running a modeling simulation software. However, the idea of exploiting the dual-frequency is not completely new, but practically, there is a considerable difference between what used to be known as dual-frequency and what has been utilized currently. The idea of using two

different frequencies to have a more uniform hardened profile was brought in the late 1950s. But first dual-frequency hardening machine was made in 1986. Since then, companies try to produce a more polished version of these types of machines [139].

To achieve this objective, this study is carried out in the following steps: finding the right arrangement for the range of induction parameters can be employed for simulation in two frequencies of medium and then high separately. Collected data and literature reviews of previous studies are reliable sources to obtain this information. Performing simulation is the next step which reveals flaws of applying single frequencies of high and medium in the induction hardening process and its effects on austenitizing in different spots of the workpiece. The importance of this step originates from avoiding having the melted tip when the high-frequency current is necessitated to achieve austenite transformation in the root of the gear because of generated high temperature while using medium frequency ends up incomplete austenite transformation in the root. the subsequent step of sequential dual-frequency strategy resulting from experimental feasibility is carried out to determine the maximum and minimum temperature limitation based on the level of frequencies to produce the desired uniform hardened case depth in all surfaces of the gear (in roots and tops simultaneously). Frequency, heating time, the current density, the gap between the workpiece and the flux concentrators, the gap between the workpiece and the coil are the parameters to be tuned in this step.

3.2.3 Theorical background

Needless to say, the induction machine's function is based on using alternating current to induce electrical conductive charge [140]. Generally, numerical modeling employs Maxwell's and Fourier equations to simulate actual phenomena of electromagnetic and temperature fields and temperature transition throughout the workpiece in the form of space–time-temperature equations [141, 142]. In the hiring of the single frequency, Maxwell's time-dependent electromagnetic equations are harmoniously oscillatory, and conduction current density is much greater than the displacement current density, Thus, displacement fields can

be considered negligible [140], and magnetic vector potential A is related to the magnetic flux, therefore, electromagnetic equations are summarized to following diffusion equation:

$$J_S = A(j\omega\sigma - \frac{1}{\mu_r\mu_0}\nabla^2) \quad (1)$$

With μ_r, σ, μ_0, J_S, and ω describe respectively the relative magnetic permeability, electrical conductivity of the material, the vacuum permeability, the source current density in the coil and the angular frequency of the current whereas ω (rad/s) = $2\pi f$, and f is the current frequency of the power generator.

The term J_e known as eddy current density is the result of the electromagnetic analysis which is declared in terms of the magnetic vector potential A and it appears in eq(1) where:

$$J_e = -j\omega\sigma A \quad (2)$$

In continuation, to measure the produced heat inside the workpiece due to the Joule-Lenz heating rule, the following equation is applied:

$$Q_{ind}^{\circ} = \int_{\mathrm{v}} \frac{|J_e|^2}{\sigma} . dv \quad (3)$$

Which designates Q_{ind}° Joule heat as the result of electromagnetic phenomena. To measure heat transformation inside the workpiece during phase change, the time-dependent heat transfer equation is manipulated.

According to the joule heating rule, produced heat inside the workpiece is calculated by:

$$\mathrm{C_\rho}\frac{\partial\theta}{\partial\mathrm{t}} = \frac{[\nabla.(\mathrm{k}\nabla\theta)+Q_{ind}^{\circ}]}{\gamma} \quad (4)$$

where θ is the temperature, and k, $C\rho$, and γ are respectively representative for the thermal conductivity of the material used in the workpiece, the specific heat, and mass density which all three are non-linear temperature-dependent physical properties.

Having some energy wasted by conviction and radiation during the process because of the temperature variation of the workpiece and surrounding air, it is essential measuring these two terms, however, the hardening process of the steel 4340 is carried out at a high temperature of +350°, and compare to this temperature, wasted energy by radiation and conviction are negligible [26, 130], and duration of these two forms of transitions are very short, but to create the closest simulation to practical experience, taking these two form of wasting energy into the account is necessary. To this end, the term heat flux Φ_{th} is applied to indicate the realistic boundary conditions for the two ways of losing heat (radiation and convection from the workpiece surface to the surrounding air):

$$\dot{Q}_{rad}^{-1} = \frac{\dot{Q}_{con}}{\Phi_{\mathrm{th}}} \tag{5}$$

And from Newton's cooling law, the convection heat flux loss equation is calculated by the following equation:

$\dot{Q}_{con} = \alpha_c(\theta - \theta_a)\ \dot{Q}_{rad}$ where α_c , θ, and θ_a are respectively convection coefficient, the temperature of the surface and temperature the surrounding ambient both in Celsius temperature unit. In addition to this, wasted heat by radiation $\dot{Q}_{rad}$ is provided by Stefan–Boltzmann equation:

$$\dot{Q}_{rad} = \varepsilon\sigma_s(T^4 - T_a^4) \tag{6}$$

In which ε, σ_s, T^4, and T_a^4 are respectively brought for emissivity, Stefan–Boltzmann constant, absolute temperatures of the surface, and temperatures of the surrounding ambient. For the used material of the presented study which is 4340 carbon steel, Isothermal transformation diagrams (known as T-T-T diagrams) are the baseline data in this study which in brief, are plots of temperature versus time for specific alloy steel helps have better knowledge of the transformations of steel in its heating process [143]. For induction heating, these plots are a handful tool to predict the outcomes of the set induction process parameters to avoid happening over tempering by monitoring the pattern of hardened case depth. In this connection, the terms used to describe the procedure through the diagram include case depth

given by ds as it is produced in temperature higher than A_{c3} (critical point with the temperature of 850℃), low hardness value determined by d_L, and it results from heating workpiece between two critical temperatures of Ac_1(825℃) and A_{c3}, and general term for the heated region above 600℃ presented by d_C. Consequently, the over tempered area is specified by differentiation of d_S and d_C.

3.2.4 Simulation Model

As previously mentioned, there are some advantages and disadvantages of using the induction heating method for hardening of the spur gear: capability for surface heating of the workpiece without affecting the core fits the expectation for hardening of the workpiece. Through this method, residual stress resulting from quenching the hot core can be avoided [38]. Furthermore, the ability to do surface hardening for complex geometries like the gears is another beneficial future of the induction hardening method. In contrast, there are some disadvantages to be mentioned as the distinctive gap between coil and gear's tip from coil and gear's root and simultaneously, between the edge and the middle of the tooth, execution of single frequency will result in having a different hardened profile pattern between root and tip. In addition, there is a heating limitation during the process because of the avoiding reaching a temperature above the critical point Ac3 for the root of the gears. At that temperature, the tip can end up crossing the melting point which is another issue that can happen because of the over or under-heating of the different spots of the workpiece. Nevertheless, It appears to be the necessity of a change in this procedure which is the objective of this study. Reaching the point Ac3 for the root of the gears is intended, the tip can end up reaching the melting point, so, another issue comes from over and under heating of the different spots of the workpiece. Nevertheless, It appears to be the necessity of a change in this procedure which is the objective of this study. The idea of induction hardening is to heat the surface of the part to the temperature necessary to convert the metallurgy structure of the material to the austenitic structure and avoid overheating in the main sprocket above

the melting temperature. The main goal in this effort is to use metallurgical knowledge alongside the simultaneous dual-frequency induction heating to attain the closest hardened amount of the different spots on the surface of the gear by creating a uniform austenitic structure throughout the surface of the spur gear.

3.2.4.1 Geometries of the gear, concentrators, and coil

The benefits of applying flux concentrators are given by recent studies by Barka et al [53]. The spur gear and flux concentrators used in the present research to validate the sequential dual-Frequency approach in induction heating have the same geometry specifications containing the outer diameter of 104.3 mm, and a thickness of 6.5 mm. In the state of applying flux concentrators, the gear is symmetrically positioned between two magnetic flux concentrators. The axial gaps between the workpiece and both flux concentrators which act as slave gears have been established at 2 mm. Either with or without concentrators, the radial gap between the workpiece and the coil is set at 2 mm.

The coil is made of copper with a geometrical detail of 140 mm for the outer diameter, 110 mm for the inner diameter, and a thickness of 2 mm. Figure 26. Schematic presentation of a trimmed spur gear [102] presents a schematic position of the magnetic flux concentrators, gear, and coil.

The finite element approach is taken by using COMSOL Multiphysics software (3D Model) to perform a study on electromagnetic phenomena produced by induction method, and generation, and transmission of the heat inside the spur gear. To make the simulation closest to the experimentation, the gear-concentrators-coil combination is surrounded by Air which possesses dielectric permeability (μ_r) and vacuum permittivity (ε_r) of one.

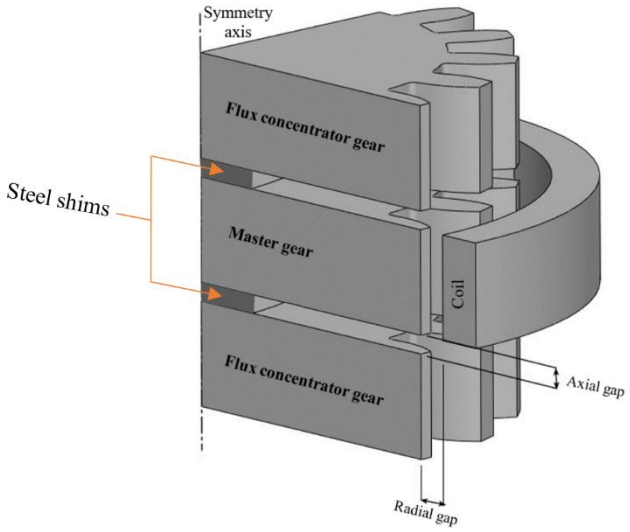

Figure 26. Schematic presentation of a trimmed spur gear [102]

Two set conditions aid to prune the model into quarters which means a huge reduction in computation time and increase the accuracy of the final result: first, identical geometries of the gear and concentrators and symmetric conditions of electric and thermal insulation alongside the periodic conditions, and second, the periodic conditions. The Trimmed model is demonstrated in Figure 26.

3.2.4.2 Material

The workpiece is a spur gear known as the simplest but most common type of gear, made of 4340 steels. This type of gear is widely used to deliver the transmission via torque in rolling mills, power units such as pumps and motors. Thus, needless to emphasize the importance of toughness, ductility, wear, and fatigue resistance in this type of gear due to the necessity of being heavy-duty according to mentioned applications [144]. Some cations should be taken utilizing 4340 for spur gear because the thermic and electric specifications of this steel are drastically changed by shifting the temperature [86] (Table 16 and Figure 27).

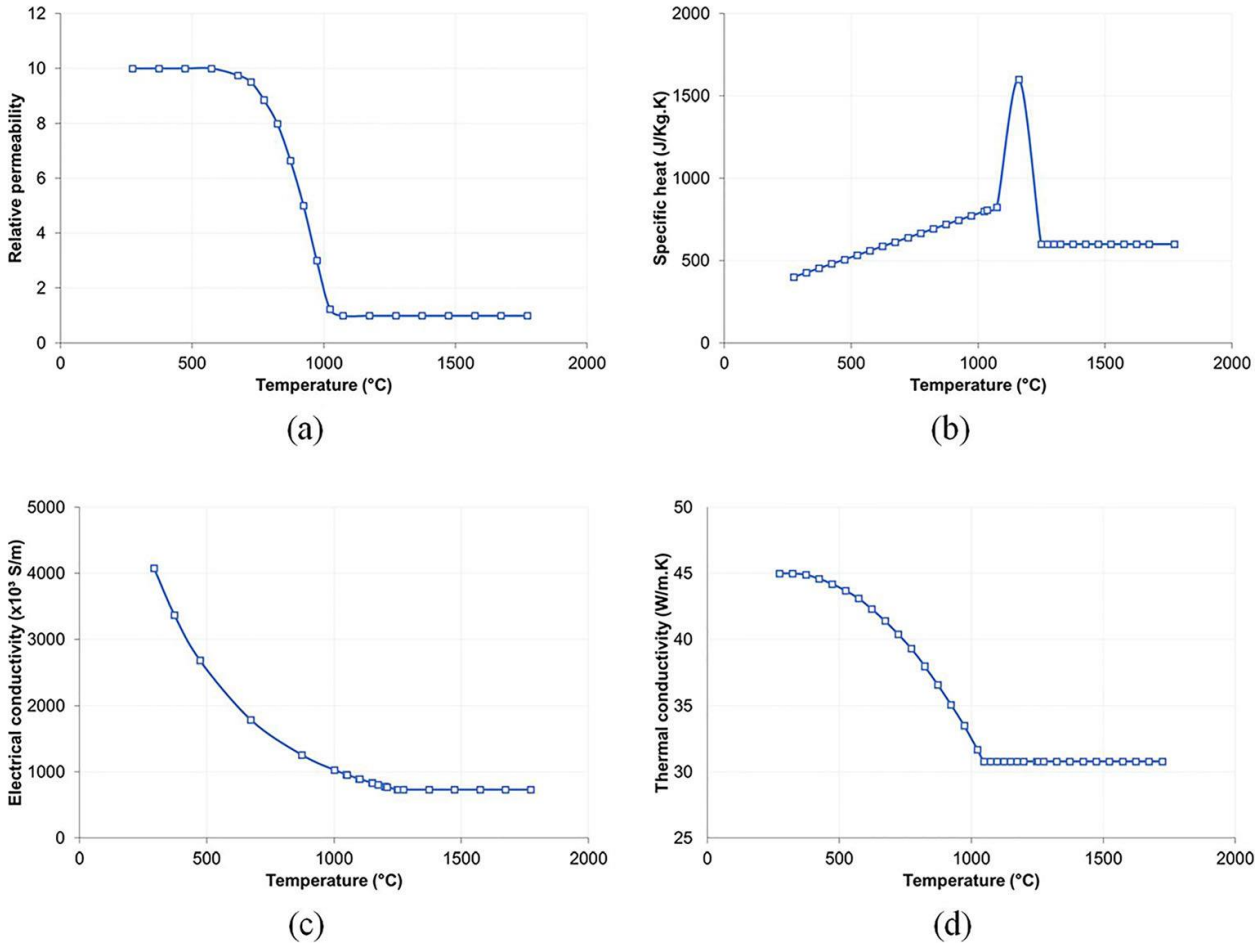

Figure 27. Changing the specifications of a steel alloy by Temperature (a), Relative Permeability (b), Specific heat (c), Electrical conductivity (d), and Thermal conductivity

[145]

Table 16. AISI 4340 steel chemical composition in wt% [86]

Element	Ni	Cr	Mn	C	Mo	Si	S	P
Content (%)	1.65–2.00	0.70–0.90	0.60–0.80	0.38–0.43	0.20–0.30	0.15–0.30	0.04	0.035

3.2.4.3 Meshing

As described earlier, to facilitate the simulation procedure and increase its accuracy, the rotational and the symmetrical planar shape of the gear and coil is regarded through the execution of COMSOL Multiphysics software. In addition, the appliance of the convergence study in this research permits setting the ideal mesh size for the simulation. To initiate the computing process, it is essential to choose the right parameters of meshes helping to split the problem at hand into several partitions as shown in Figure 28.

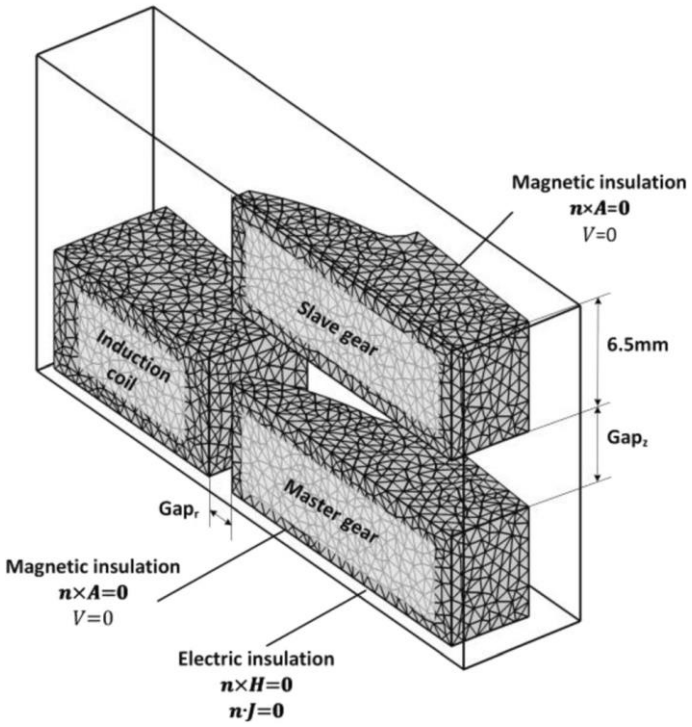

Figure 28. Schematic presentation of induction heating of spur gear with magnetic flux concentrators.

In this try, a range of 0.1mm to 1mm is chosen while 0.05 mm as size for each step between these two ends is applied. Worth mentioning setting the right size of mesh adds up more reliance and accuracy to the final result and shortens the simulation time. Then, further

adjustment of mesh size resulted in having 0.5 mm as the best size of mesh which provided an exalted computation time effort.

3.2.4.4 Model validity

The presented study is a continuation of former investigations conducted by our team: Khalifa et al. [124] applied 3D modeling to reduce edge effect by flux concentrators via response surface methodology and artificial neural network modeling for spur gear. In a later study, he tried to find the link between the experimentation results and axis-symmetric simulation to minimize the edge effect of 4340 steel workpieces while a set of concentrators was utilized [83]. And finally, a COMSOL axisymmetric model was conducted to optimize induction heating process parameters in presence of the concentrators. These studies are taken into the account for validation of the data and induction heating process parameters in this research.

3.3 SINGLE FREQUENCY

To have a uniform hardened layer on a spur gear, both tip and root must reach the Austenite temperature range that for 4340 steel this temperature is 815 – 845 ° C [43]. Consequently, the root will not meet the austenite temperature. Even with increasing the heating time, current density, or frequency pushing the root to the intended temperature range, the tip can end up over-heating up to the melting point. The idea of exploiting the sequential-dual frequency is to target the tip of the root with a medium frequency. Simultaneously, the high frequency is more focused on heating the root. However, there are some precautions to be taken; A rule of thumb in induction heating of the gears is the medium frequency is more focused on the roots while high frequency focuses on the tips, therefore, to have perfect coverage of the two frequencies for having an austenitic structure in whole teeth setting the parameters to be set for each medium and high in sequential-dual frequency are different than using each one separately. To simplify describing this issue, considering the process as sequential-dual frequency (with zero delays between the two) is helpful: at the

first step of applying the double-frequency, gear is heated by a medium frequency. This step should be terminated when the root obtains less temperature than the austenite point. The reason is continuing the process steadily with the high frequency) increases the temperature in both root and tip. Thus, adding more temperature to the already austenitic root will push its temperature to the melting territory.

To grasp the point of using the combination of the two frequencies of medium and high instead of separately using single frequencies first and foremost is to have the outcomes of using each frequency independently for comparison. At the first step, the aim is to reach the minimum austenitic temperature in root through the medium frequency, and in the tip by the high frequency. Then, the disparity of the temperatures between the tip and root for each frequency is determined. These measures give the comparison of the effectiveness of the single frequencies to the sequential-dual frequency in terms of the lower edge effect and produced temperature.

3.3.1 Results of single frequencies (MF and HF, separately)

To find the lowest temperature for creating the austenite structure on spur gear, temperature distribution on the surface of the spur gear should be considered. Numerous combinations of the parameters for both MF and HF had been tested to find the best current density J_0, heating time t_c, G_A (Axial Gap/ the gap between each concentrator and the part), and G_R (Radial Gap/ the gap between the coil and part) for reaching the austenitic temperature. The terms ET, MT, ER, and MR, all used in the figures respectively represent the temperature of the edge of the tip, middle of the tip, edge of the root, and middle of the root. Other mentioned terms in these figures are depth of the maximum hardness, minimum hardness, and depth of the whole heat-treated area are respectively H_{Max}, H_{Min}, and H_T. To determine H_{max}, H_{min}, and H_T, temperatures of the critical points of T_0(640°C), A_{C1}(825°C), and A_{C3} (850ºC) are considered all came from the Iron Phase diagram [146]. In Figure 29, the temperature distribution in the root and the tip in MF= 10 KHz is shown. The final set-up of parameters in this frequency considering the lowest temperature to reach the austenitic

temperature in the root are J_0=2.93×10^3 A.m^{-2}, t_c=0.3 s, G_A= 0.5mm, and G_R= 0.2mm. While the average temperature of the root reaches about 867ºC, the tip has approximately 298°C, which shows about 570 ºC difference between the temperature of the root and the tip.

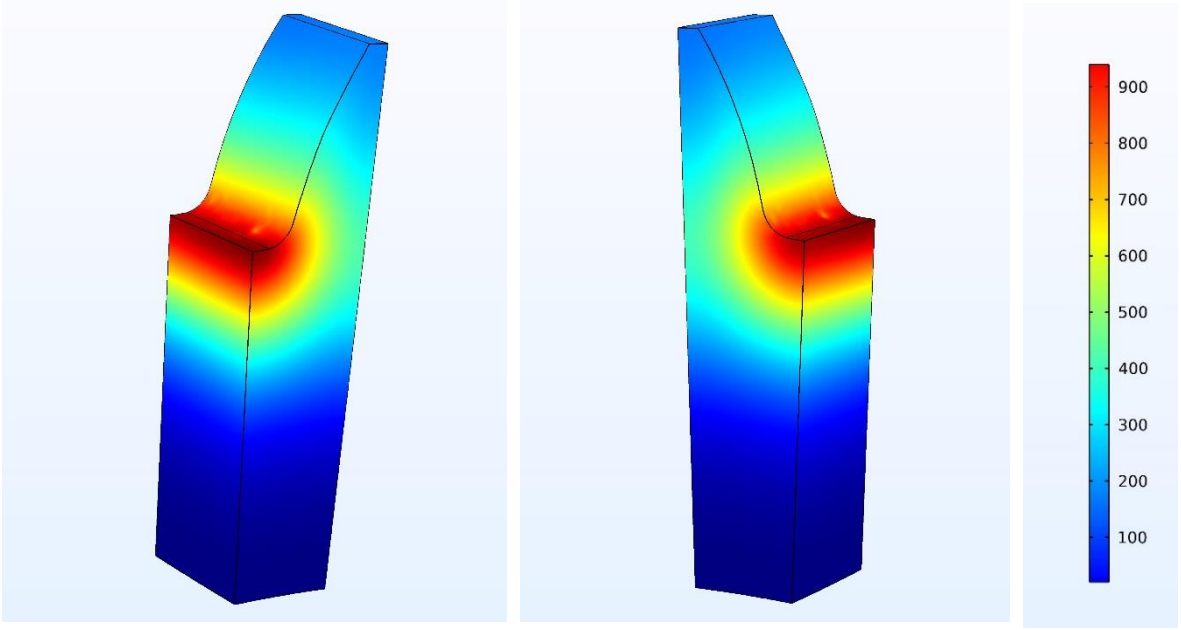

(a) (b)

Figure 29. Minimum austenitic temperature (ºC) with MF (a) in ER, (b) in MR

For results came from simulation for HF= 200 KHz, set parameters to have the best outcome in tip are J_0=14×10^3 A.m^{-2}, t_c=0.2 s, G_A= 0.5mm, and G_R= 0.2mm. Figure 30 demonstrates the temperature distribution with the mentioned combination of the parameter. The observed average temperature between the middle and edge of the tip is 850 °C, and between the middle and edge of the root is 638 ºC, which shows about 212 ºC diversity in produced temperature between the tip and root.

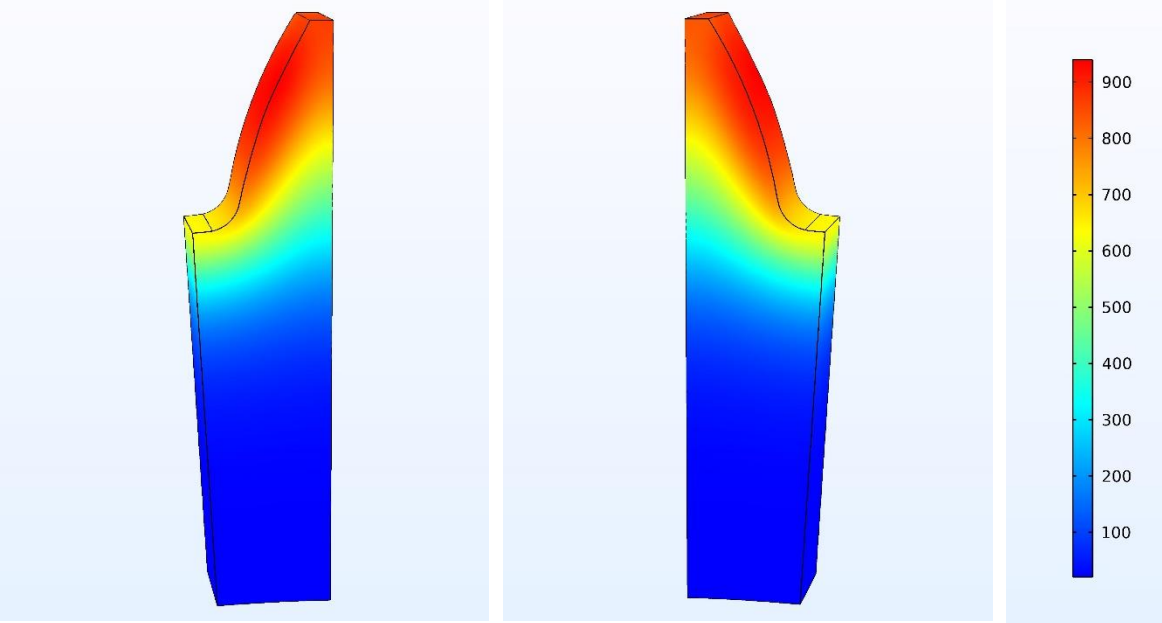

(a) (b)

Figure 30. Minimum austenitic temperature (ºC) with HF (a) in ET, (b) in MT

The data proves that despite the short length of the teeth in spur gears, and numerous tries to yield the best results, there is a big discrepancy in produced temperature between the root and the tip. These outcomes declare a big edge effect in tests that the study aims to avoid. Further increase in heating process in each of MF and HF has the effect of overheating of already-austenite areas while the temperature of the underheated areas is intended to push to the austenitic territory, and consequently, having the melting effect or ununiform hardened profile of the final result especially because of the additional temperature imposed to the quenching which itself, will lead to malformed austenitization or incomplete solution of alloy elements and uneven case depth [147].

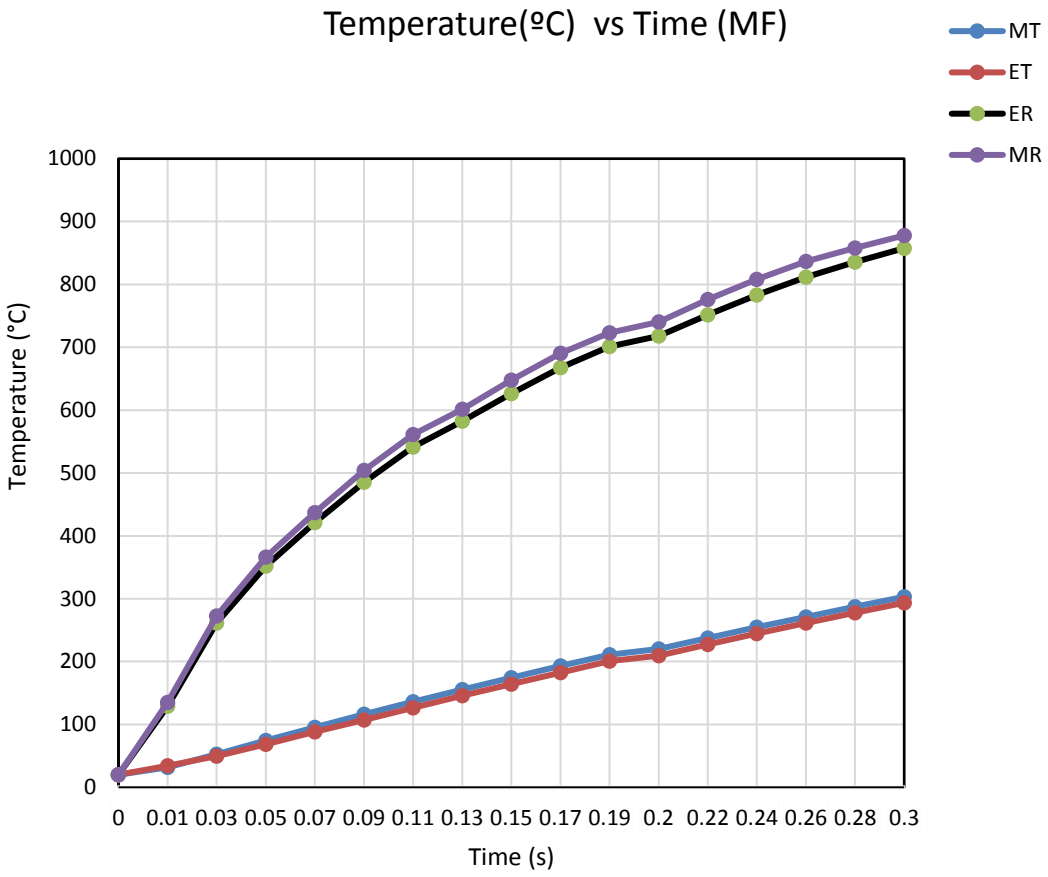

Figure 31. Temperature (ºC) vs Time (MF)

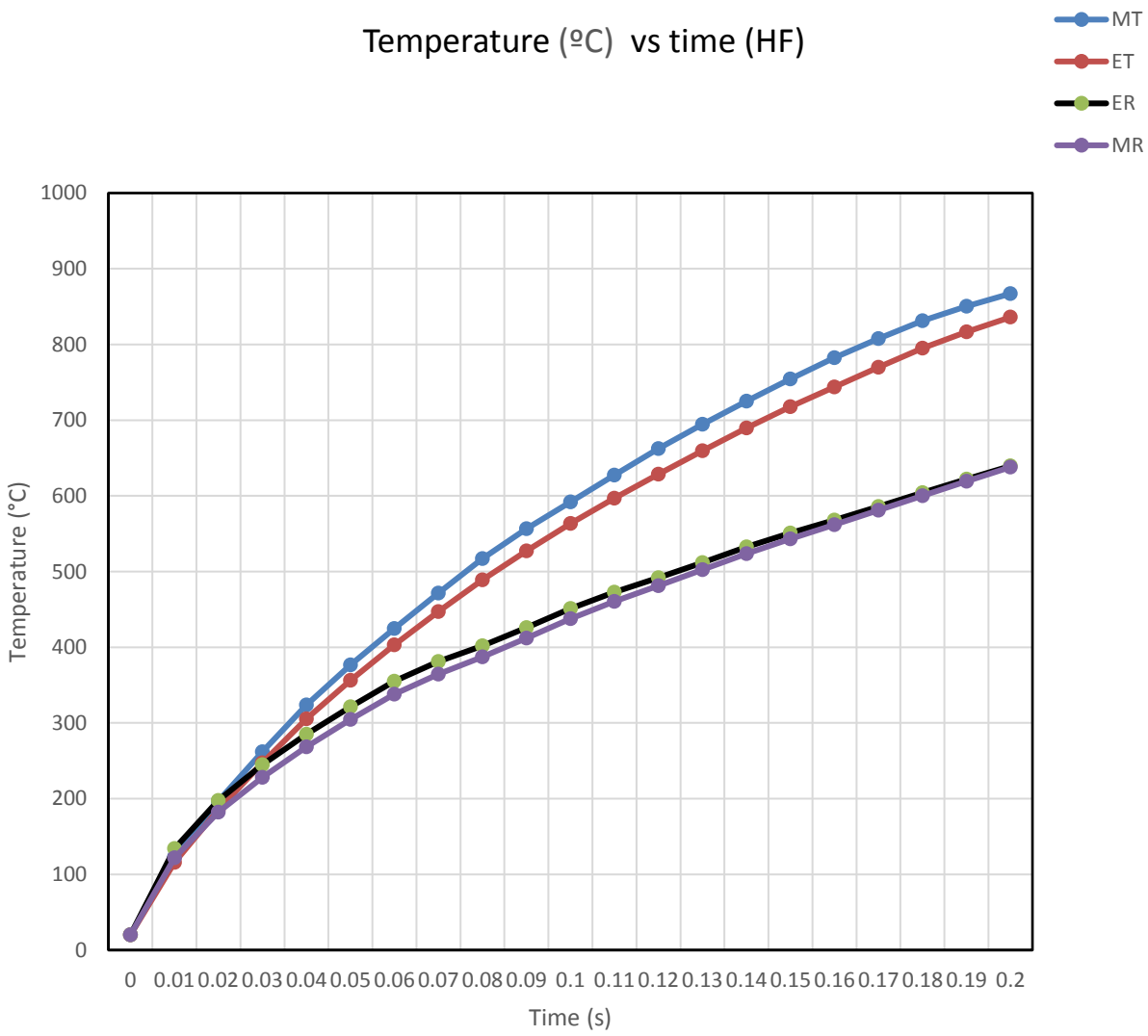

Figure 32. Temperature (ºC) vs Time (HF)

3.4 SEQUENTIAL DUAL FREQUENCY HEATING

As it showed with applying the single frequencies, reaching the austenitic temperature simultaneously in the low level of austenite bracket temperature (about 850) is not possible. Data declare big differences and uneven contour temperature over out layer of the gear based on the difference of the distance from the coil. As a result, to reach the austenitic structure

with single frequencies, more intense heating to reach more temperature in tip and root is inevitable.

In this section, sequential dual-frequency is applied and parameters used in this step are presented in Table 17. These parameters and their quantities are in reference to the simulation and experimentation expediency, mentioned previous studies and statistical method all in the frame of literature reviews. In this regard, the parameters in Table 17 are fixed optimized parameters. worth mentioning that for the optimization, several efforts with a temperature range of 850-1150 which is arranged to cover austenite to melting temperature for 4340 steel alloy. This range gave us the maximum and minimum of the range of parameters included in this study. Parameters of this table bring the best result for producing the minimum possible temperature simultaneously in the root and tip.

Table 17: Parameter's quantity in sequential-dual frequency

	Fr(KHz)	$J_0(A.m^{-2})$	$t_c(s)$	$G_A(mm)$	$G_R(mm)$
MF	10	1.5×10^3	0.3	0.7	2
HF	200	14.3×10^3	0.2	0.7	2

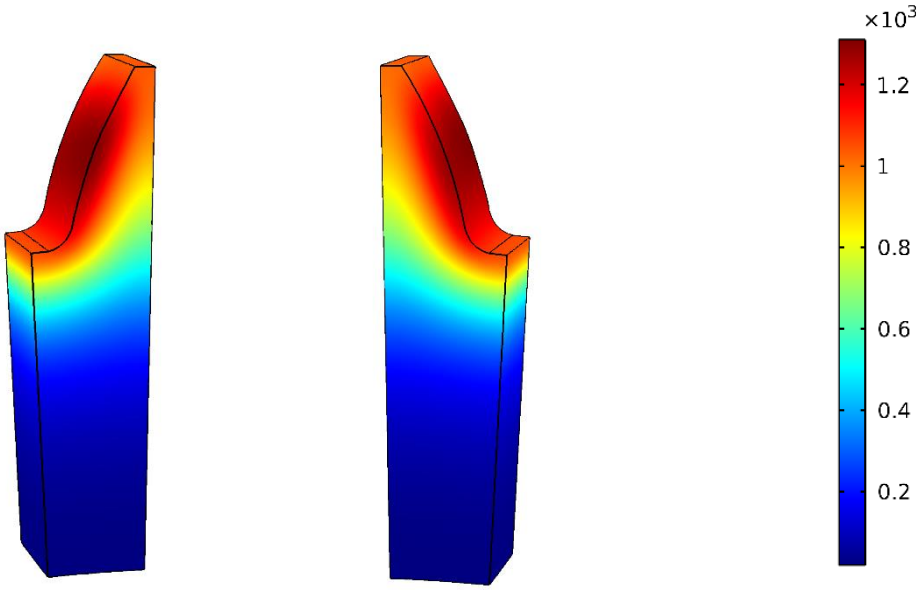

(a) (b)

Figure 33. Temperature distribution (ºC) for simultaneous applying of MF and HF in (a) edge plan, (b)middle plan

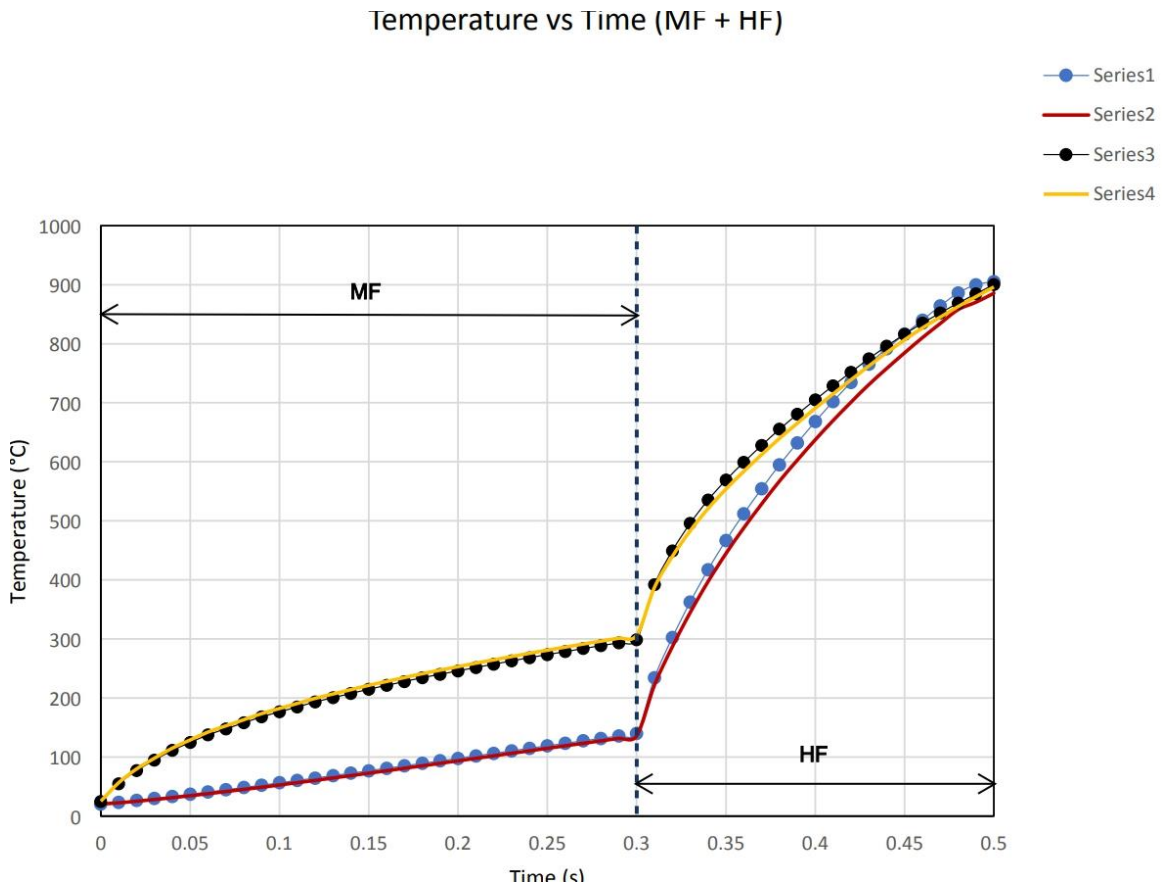

Figure 34. Temperature distribution (ºC) with time (s) within sequential-dual frequency approach

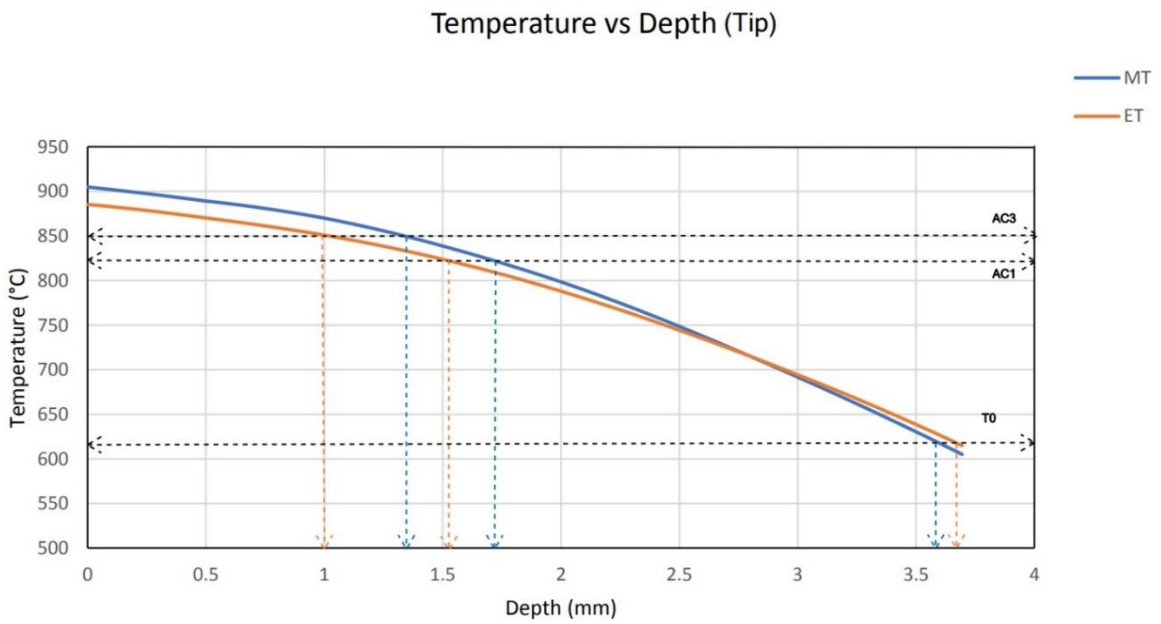

Figure 35: Temperature distribution (ºC) vs depth (mm) through sequential-dual frequency in tip

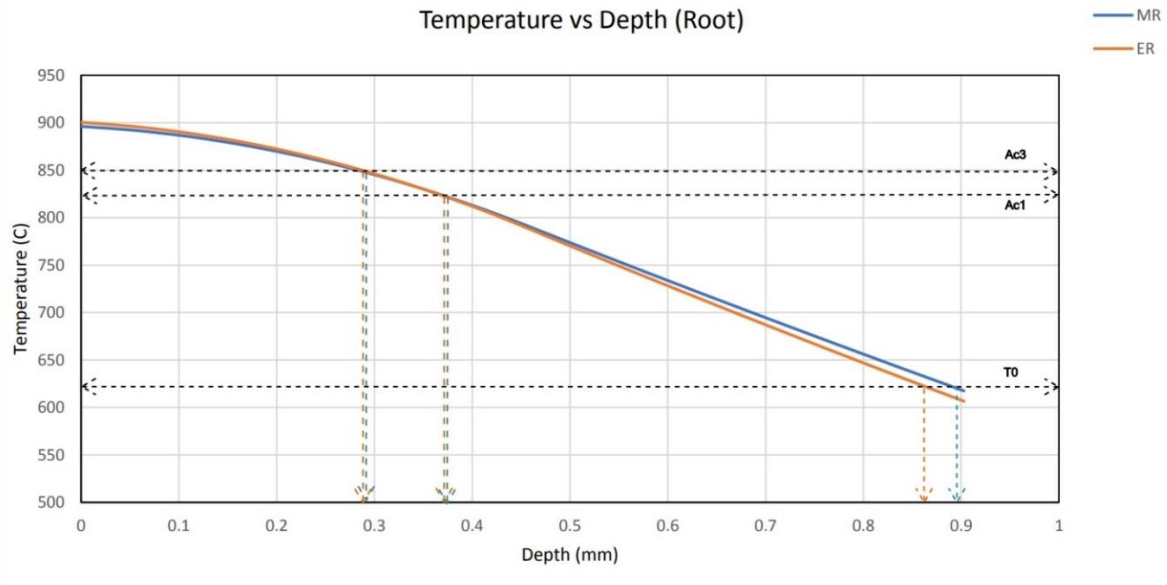

Figure 36. Temperature distribution (ºC) vs depth (mm)through sequential-dual frequency in Root

Results indicate that reaching the austenitic bracket temperature in both root and tip with sequential-dual frequency has an obvious improvement because of the negligible produced edge effects between tip-root and middle-edge.

3.5 CONCLUSION

To enhance the hardened profile of the 4340 spur gear in terms of reaching the Austenitic temperature range with a less possible edge effect, COMSOL finite element software was applied. To this end, finding the best method among single frequencies of the medium and high, and sequential-dual frequency was the objective to investigate. Numerous combinations of the induction heating parameters are examined to find the best for producing the highest case depth in the permitted temperature range of Austenite. Then, the best result of medium-high and sequential-dual frequencies are compared to each to reveal the advantageous method in terms of reduction of the edge effect, produced heat, and case depth. Results imply a clear improvement in generated edge effect and heat, which help the better result at the end of the quenching step. The outcome of this study can be beneficial for

induction hardening of the other complex parts like helical gear, bevel gear, screw gear and Worm Gear.

CONCLUSION GÉNÉRALE

Ce mémoire de maîtrise, préparé sous forme d'article, a été réalisé dans le cadre de l'étude des laboratoires de l'UQAR. Il est consacré à l'étude des effets des paramètres du procédé de chauffage par induction sur l'engrenage droit et le disque simple en alliage d'acier 4340 en appliquant un ensemble de concentrateurs de flux. Le premier objectif était d'améliorer la profondeur de carter de l'engrenage droit en acier 4340 et de minimiser les phénomènes indésirables d'effet de bord tout en utilisant un ensemble de concentrateurs de flux de la même géométrie que l'engrenage principal. Le second objectif était d'étudier l'impact de l'effet de bord sur des disques simples. En raison de la géométrie simple des disques, certaines difficultés de l'engrenage droit et de ses dents ont été éliminées. Le troisième objectif était de maximiser la profondeur de carter et de minimiser l'effet de bord sur l'engrenage droit en utilisant une double fréquence séquentielle (moyennes et hautes fréquences) en utilisant COMSOL pour créer un modèle 3D.

Les approches d'expérimentation comprenaient :

- La planification de l'essai expérimental sur la base de l'analyse de la littérature pour choisir les paramètres les plus efficaces, puis les soumettre à la méthode de planification Taguchi pour organiser les essais les plus efficaces.

- La validation expérimentale est effectuée par le laboratoire de test de dureté Rockwell afin de collecter les données importantes et utiles pour les analyses

- L'analyse des données par l'analyse statistique ANOVA, pour produire un modèle complet et pour identifier et évaluer les effets des paramètres du processus sur l'effet de bord de l'engrenage droit et du disque 4340 traités par induction, ce qui aide à utiliser les résultats à des fins industrielles. De plus, cette phase a permis d'avancer un modèle prédictif amélioré qui prévoit l'effet

des paramètres de la machine et de la géométrie sur la profondeur de trempe du disque et de l'engrenage droit trempé.

Pour l'engrenage droit, l'étude a montré que la puissance avec un pourcentage de contribution de 40,83%, 53,88%, 52,32%, 41,91%, et le temps de chauffage avec des pourcentages de contribution de 30,00%, 32,59%, 36,33%, et 51,51% pour d_{RM}, d_{RE}, d_{TM}, et d_{TE} sont les paramètres dominants dans la profondeur de cas. Cependant, l'écart axial n'a pas eu d'effet significatif sur La profondeur durcie.

Pour le disque, le temps de chauffage et la puissance de la machine sont les paramètres les plus efficaces pour contrôler La profondeur durcie dans d_E et d_M, en autant que le pourcentage de contribution de T et P pour d_E est respectivement de 43,69% et 40,31%. Cependant, contrairement à l'engrenage droit avec une géométrie plus complexe, dans la trempe du disque, l'interaction entre les paramètres a joué un rôle plus important dans La profondeur durcie puisque P×AG a contribué à 7,60% dans la variation de d_E, et la contribution de T×RG dans la variation de d_E était de 2.36%.

La simulation par éléments finis a démontré que les deux paramètres géométriques (écart entre chaque concentrateur et la pièce et l'écart entre l'inducteur et la pièce) ainsi que les paramètres machine de densité J_0, temps de chauffe t_c et fréquence (moyenne, haute et double fréquence simultanée) ont été inclus dans les simulations.

Pour avoir une gamme de structure austénitique pour l'acier 4340, la gamme de température de 815 – 845 ° C a été considérée. Pour une fréquence moyenne de MF= 10 KHz, J_0=2.93×103 A.m-2, tc=0.3 s, GA= 0.5mm, and GR= 0.2mm , la température moyenne de la racine a atteint environ 867ºC, la tête avait approximativement 298°C, ce qui montre une différence d'environ 570 ºC entre la température de la racine et de la tête.

Et pour la haute fréquence de HF= 200 KHz, les paramètres définis pour avoir le meilleur résultat dans la tête étaient J_0=14×10^3 A.m^{-2}, t_c=0.2 s, G_A= 0.5mm, and G_R= 0.2 mm, ce qui a créé la température moyenne de 850 °C entre le milieu et le bord de la tête est

et 638 ºC entre le milieu et le bord de la racine est, ce qui montre environ 212 ºC de diversité dans la température produite entre la tête et la racine.

Les résultats du mémoire présentée peuvent être résumés comme suit :

- L'étude sur l'engrenage droit a démontré que le profil de de dureté dans le plan médian est contrôlable par les paramètres de la machine, et que la gamme de paramètres la mieux exploitée peut maximiser la profondeur durcie tout en minimisant l'effet de bord.

- Durant la trempe de l'engrenage droit, la puissance de la machine la plus élevée et le temps de chauffage le plus long, associés au plus petit écart axial, contribuent à une profondeur durcie optimisée.

- En présence des concentrateurs de flux pour le chauffage par induction de l'engrenage droit, la puissance, le temps de chauffage et l'écart radial, la puissance et le temps de chauffage ont l'effet le plus dominant sur la profondeur durcie.

- En réglant la meilleure disposition des paramètres de la machine à induction, la profondeur durcie et l'effet de bord sont contrôlables. Dans ce cas, la plus grande profondeur durcie est produite lorsque la puissance est réglée au niveau le plus élevé, mais que le temps de chauffe et l'écart axial sont réglés au niveau le plus bas.

- Les résultats de l'étude sur le disque montrent que la disposition des paramètres doit être suivie comme maximale pour le temps de chauffage et l'écart axial, mais moyenne pour la puissance de la machine et l'écart radial, pour obtenir la plus grande réduction sur l'effet de bord.

- L'application du logiciel Multiphysiques COMSOL pour la modélisation donne une bonne perspective de comparaison entre la fréquence double séquentielle et la fréquence unique (à la fois élevée et moyenne), alors que

l'objectif est de produire moins de chaleur possible avec un effet de bord minimal (entre le plan du milieu et du bord, et la tête et la racine).

- Les résultats démontrent l’utilité d’utiliser le chauffage à double fréquence séquentielle par rapport au chauffage monofréquence, car elle permet d'atteindre la température austénitique avec une différence de chaleur plus faible entre la tête et la racine de la denture, et en même temps, entre le plan du bord et le plan du milieu, ce qui démontre une réduction de l'effet de bord. En même temps, le fait de générer moins de température sur la profondeur du boîtier permet un meilleur processus de trempe qui améliore directement le profil durci de la pièce à la fin.

Il convient de mentionner que l'utilisation de concentrateurs de flux a joué un rôle majeur dans l'obtention de meilleurs résultats pour la trempe de l'engrenage droit et du disque en acier 4340. Une piste intéressante pour les travaux futurs serait de mesurer les paramètres du processus d'induction sur la profondeur durcie des engrenages plus complexes comme les engrenages coniques droits, les engrenages à vis sans fin, les engrenages hypoïdes, les engrenages épicycloïdaux et , les engrenages hélicoïdaux. D'autres recherches pourraient être menées pour trouver les valeurs géométriques optimales en fonction du type spécifique d'engrenage choisi parmi les noms mentionnés. D'autres travaux futurs pourraient être effectués en adoptant des techniques de modélisation par réseau neural artificiel afin d'optimiser les paramètres machine pour la trempe par induction de ces types d'engrenages.

RÉFÉRENCES BIBLIOGRAPHIQE

[1] J. E. Neely, "Practical Metallurgy and Materials of Industry, (Book)," *John Wiley & Sons, 406,* p. 1984, 1984.

[2] J. S. Selvan, K. Subramanian, and A. Nath, "Effect of laser surface hardening on En18 (AISI 5135) steel," *Journal of Materials Processing Technology,* vol. 91, no. 1-3, pp. 29-36, 1999.

[3] R. S. Lakhkar, Y. C. Shin, and M. J. M. Krane, "Predictive modeling of multi-track laser hardening of AISI 4140 steel," *Materials science and engineering: a,* vol. 480, no. 1-2, pp. 209-217, 2008.

[4] H. R. Shercliff and M. Ashby, "The prediction of case depth in laser transformation hardening," *Metallurgical Transactions A,* vol. 22, no. 10, pp. 2459-2466, 1991.

[5] M. Lee, G. Kim, K. Kim, and W. Kim, "Control of surface hardnesses, hardening depths, and residual stresses of low carbon 12Cr steel by flame hardening," *Surface and coatings technology,* vol. 184, no. 2-3, pp. 239-246, 2004.

[6] M. Lee, G. Kim, K. Kim, and W. Kim, "Effects of the surface temperature and cooling rate on the residual stresses in a flame hardening of 12Cr steel," *Journal of materials processing technology,* vol. 176, no. 1-3, pp. 140-145, 2006.

[7] D. Coupard, T. Palin-luc, P. Bristiel, V. Ji, and C. Dumas, "Residual stresses in surface induction hardening of steels: Comparison between experiment and simulation," *Materials Science and Engineering: A,* vol. 487, no. 1-2, pp. 328-339, 2008.

[8] Y. Han, E.-L. Yu, and T.-X. Zhao, "Three-dimensional analysis of medium-frequency induction heating of steel pipes subject to motion factor," *International journal of heat and mass transfer,* vol. 101, pp. 452-460, 2016.

[9] D. Ivanov, L. Markegård, J. I. Asperheim, and H. Kristoffersen, "Simulation of stress and strain for induction-hardening applications," *Journal of materials engineering and performance,* vol. 22, no. 11, pp. 3258-3268, 2013.

[10] T. Munikamal and S. Sundarraj, "Modeling the case hardening of automotive components," *Metallurgical and Materials Transactions B,* vol. 44, no. 2, pp. 436-446, 2013.

[11] M. Tarakci, K. Korkmaz, Y. Gencer, and M. Usta, "Plasma electrolytic surface carburizing and hardening of pure iron," *Surface and Coatings Technology,* vol. 199, no. 2-3, pp. 205-212, 2005.

[12] M. Béjar and R. Henríquez, "Surface hardening of steel by plasma-electrolysis boronizing," *Materials & design,* vol. 30, no. 5, pp. 1726-1728, 2009.

[13] O. Asi, "Fatigue failure of a helical gear in a gearbox," *Engineering failure analysis,* vol. 13, no. 7, pp. 1116-1125, 2006.
[14] W. Xu, W. Ding, Y. Zhu, X. Huang, and Y. Fu, "Understanding the temperature distribution and influencing factors during high-frequency induction brazing of CBN super-abrasive grains," *The International Journal of Advanced Manufacturing Technology,* vol. 88, no. 1-4, pp. 1075-1087, 2017.
[15] B. Reul, "Method and device for brazing connections by induction heating," ed: Google Patents, 2012.
[16] P. Guerrier, G. Tosello, K. K. Nielsen, and J. H. Hattel, "Three-dimensional numerical modeling of an induction heated injection molding tool with flow visualization," *The International Journal of Advanced Manufacturing Technology,* vol. 85, no. 1, pp. 643-660, 2016.
[17] P. Guerrier, K. K. Nielsen, S. Menotti, and J. H. Hattel, "An axisymmetrical non-linear finite element model for induction heating in injection molding tools," *Finite Elements in Analysis and Design,* vol. 110, pp. 1-10, 2016.
[18] G. M. Mucha, D. E. Novorsky, and G. D. Pfaffmann, "Method for hardening gears by induction heating," ed: Google Patents, 1987.
[19] Y. Kawase, T. Miyatake, and K. Hirata, "Thermal analysis of steel blade quenching by induction heating," *IEEE transactions on magnetics,* vol. 36, no. 4, pp. 1788-1791, 2000.
[20] H. Hammi, A. El Ouafi, N. Barka, and A. Chebak, "Scanning based induction heating for AISI 4340 steel spline shafts-3D simulation and experimental validation," *Advances in Materials Physics and Chemistry,* vol. 7, no. 06, p. 263, 2017.
[21] R. E. Haimbaugh, *Practical induction heat treating*. ASM international, 2015.
[22] P. M. Unterweiser, H. E. Boyer, and J. J. Kubbs, *Heat treater's guide: standard practices and procedures for steel*. Asm International, 1982.
[23] K. C. Ltd, L. Koshuha Co., Ed. *"Heating with 2 different frequency waves.,"*. 2016.
[24] M. Khalifa, N. Barka, J. Brousseau, and P. Bocher, "Sensitivity study of hardness profile of 4340 steel disc hardened by induction according to machine parameters and geometrical factors," *The International Journal of Advanced Manufacturing Technology,* vol. 101, no. 1, pp. 209-221, 2019.
[25] V. Rudnev, "A common misassumption in induction hardening," *Heat Treat. Prog., ASM International,* pp. 23-25, 2004.
[26] V. Rudnev, D. Loveless, and R. L. Cook, *Handbook of induction heating*. CRC press, 2017.
[27] M. Forzan, S. Lupi, and E. Toffano, "Compensation of induction heating load edge-effect by space control," *COMPEL-The international journal for computation and mathematics in electrical and electronic engineering,* 2011.
[28] A. Candeo, C. Ducassy, P. Bocher, and F. Dughiero, "Multiphysics modeling of induction hardening of ring gears for the aerospace industry," *IEEE Transactions on Magnetics,* vol. 47, no. 5, pp. 918-921, 2011.
[29] X. Fu, B. Wang, X. Zhu, X. Tang, and H. Ji, "Numerical and experimental investigations on large-diameter gear rolling with local induction heating process,"

The International Journal of Advanced Manufacturing Technology, vol. 91, no. 1-4, pp. 1-11, 2017.
[30] K. Gao, Z. Wang, X.-p. Qin, and S.-x. Zhu, "Numerical analysis of 3D spot continual induction hardening on curved surface of AISI 1045 steel," *Journal of Central South University*, vol. 23, no. 5, pp. 1152-1162, 2016.
[31] C. Chaboudez, S. Clain, R. Glardon, D. Mari, J. Rappaz, and M. Swierkosz, "Numerical modeling in induction heating for axisymmetric geometries," *IEEE transactions on magnetics*, vol. 33, no. 1, pp. 739-745, 1997.
[32] M. Erdogan and S. Tekeli, "The effect of martensite particle size on tensile fracture of surface-carburised AISI 8620 steel with dual phase core microstructure," *Materials & design*, vol. 23, no. 7, pp. 597-604, 2002.
[33] R. Caruso, B. Gómez, O. De Sanctis, J. Feugeas, A. Dıaz-Parralejo, and F. Sánchez-Bajo, "Ion nitriding of zirconia coated on stainless steel: structure and mechanical properties," *Thin Solid Films*, vol. 468, no. 1-2, pp. 142-148, 2004.
[34] N. Barka, "Study of the machine parameters effects on the case depths of 4340 spur gear heated by induction—2D model," *The International Journal of Advanced Manufacturing Technology*, vol. 93, no. 1, pp. 1173-1181, 2017.
[35] N. Barka, P. Bocher, and J. Brousseau, "Sensitivity study of hardness profile of 4340 specimen heated by induction process using axisymmetric modeling," *The International Journal of Advanced Manufacturing Technology*, vol. 69, no. 9, pp. 2747-2756, 2013.
[36] P. Kochure and K. Nandurkar, "Mathematical modeling for selection of process parameters in induction hardening of EN8 D steel," *Power (kw)*, vol. 10, no. 12, p. 14, 2012.
[37] K.-Y. Bae, Y.-S. Yang, and C.-M. Hyun, "Analysis for the angular deformation of steel plates in a high-frequency induction forming process with a triangle heating technique," *Proceedings of the Institution of Mechanical Engineers, Part B: Journal of Engineering Manufacture*, vol. 227, no. 3, pp. 423-429, 2013.
[38] M.-S. Huang and Y.-L. Huang, "Effect of multi-layered induction coils on efficiency and uniformity of surface heating," *International Journal of Heat and Mass Transfer*, vol. 53, no. 11-12, pp. 2414-2423, 2010.
[39] H. B. Besserer *et al.*, "Induction Heat Treatment of Sheet-Bulk Metal-Formed Parts Assisted by Water–Air Spray Cooling," *steel research international*, vol. 87, no. 9, pp. 1220-1227, 2016.
[40] D. Rodman, C. Krause, F. Nürnberger, F.-W. Bach, L. Gerdes, and B. Breidenstein, "Investigation of the surface residual stresses in spray cooled induction hardened gearwheels," *International journal of materials research*, vol. 103, no. 1, pp. 73-79, 2012.
[41] H. Kristoffersen and P. Vomacka, "Influence of process parameters for induction hardening on residual stresses," *Materials & Design*, vol. 22, no. 8, pp. 637-644, 2001.
[42] P. Kochure and K. Nandurkar, "Application of taguchi methodology in selection of process parameters for induction hardening of EN8 D Steel," *Power (kw)*, vol. 10, no. 12, p. 14, 2012.

[43] D. Hömberg *et al.*, "Simulation of multi-frequency-induction-hardening including phase transitions and mechanical effects," *Finite Elements in Analysis and Design*, vol. 121, pp. 86-100, 2016.
[44] J. Montalvo-Urquizo, Q. Liu, and A. Schmidt, "Simulation of quenching involved in induction hardening including mechanical effects," *Computational materials science*, vol. 79, pp. 639-649, 2013.
[45] L. Jakubovičová, G. Andrej, K. Peter, and S. Milan, "Optimization of the induction heating process in order to achieve uniform surface temperature," *Procedia Engineering*, vol. 136, pp. 125-131, 2016.
[46] J. Barglik, A. Smalcerz, R. Przylucki, and I. Doležel, "3D modeling of induction hardening of gear wheels," *Journal of Computational and Applied Mathematics*, vol. 270, pp. 231-240, 2014.
[47] F. Cajner, B. Smoljan, and D. Landek, "Computer simulation of induction hardening," *Journal of materials processing technology*, vol. 157, pp. 55-60, 2004.
[48] K. Sadeghipour, J. Dopkin, and K. Li, "A computer aided finite element/experimental analysis of induction heating process of steel," *Computers in industry*, vol. 28, no. 3, pp. 195-205, 1996.
[49] N. Barka, P. Bocher, J. Brousseau, and P. Arkinson, "Effect of dimensional variation on induction process parameters using 2D simulation," in *Advanced Materials Research*, 2012, vol. 409: Trans Tech Publ, pp. 395-400.
[50] N. Barka, A. Chebak, and A. El Ouafi, "Simulation of helical gear heated by induction process using 3D model," in *Advanced Materials Research*, 2013, vol. 658: Trans Tech Publ, pp. 266-270.
[51] N. Barka, A. El Ouafi, P. Bocher, J. Brousseau, and A. Chebak, "Explorative study and prediction of overtempering region of disc heated by induction process using 2D axisymmetric model and experimental tests," in *Advanced Materials Research*, 2013, vol. 631: Trans Tech Publ, pp. 417-423.
[52] C. Myers, J. Osborn, C. Tiell, R. Goldstein, and R. T. Ruffini, "Induction Heat Treating-Optimizing Performance of Crankshaft Hardening Inductors-Using Fluxtrol A in crankshaft induction coils resulted in a 100% improvement in coil lifetime while improving," *Industrial Heating*, vol. 73, no. 12, pp. 43-50, 2006.
[53] N. Barka, A. Chebak, A. El Ouafi, M. Jahazi, and A. Menou, "A new approach in optimizing the induction heating process using flux concentrators: application to 4340 steel spur gear," *Journal of materials engineering and performance*, vol. 23, no. 9, pp. 3092-3099, 2014.
[54] M. Parvinzadeh, S. S. Karganroudi, N. Omidi, N. Barka, and M. Khalifa, "A novel investigation into the edge effect reduction of 4340 steel disc through induction hardening process using magnetic flux concentrators," *The International Journal of Advanced Manufacturing Technology*, pp. 1-13, 2021.
[55] V. Rudnev, "An objective assessment of magnetic flux concentrators," *Heat treating progress*, pp. 19-23, 2004.
[56] T. Zhu, P. Feng, X. Li, F. Li, and Y. Rong, "The study of the effect of magnetic flux concentrator to the induction heating system using coupled electromagnetic-

thermal simulation model," in *2013 International Conference on Mechanical and Automation Engineering*, 2013: IEEE, pp. 123-127.
[57] J. Grum, "Induction hardening," *Handbook of residual stress and deformation of steel*, vol. 2, pp. 220-247, 2002.
[58] M. Khalifa, "Étude du profil de dureté et de l'effet de bord des disques et engrenages droits traités thermiquement par induction en utilisant les concentrateurs de flux: prédiction et optimisation numérique et expérimentale," Université du Québec à Rimouski, 2019.
[59] V. Rudnev, "Spin Hardening of Gears Revisited," *Heat Treating Progress*, pp. 17-20, 2004.
[60] G. C. Iron, "Metals Handbook Desk Edition, JR Davis, Editor, p 309-314," 1998.
[61] M. Fisk, L.-E. Lindgren, W. Datchary, and V. Deshmukh, "Modelling of induction hardening in low alloy steels," *Finite elements in analysis and design*, vol. 144, pp. 61-75, 2018.
[62] T. Rajan, C. Sharma, and A. Sharma, *Heat treatment: Principles and techniques*. PHI Learning Pvt. Ltd., 2011.
[63] S. K. Putatunda, "Influence of austempering temperature on microstructure and fracture toughness of a high-carbon, high-silicon and high-manganese cast steel," *Materials & design*, vol. 24, no. 6, pp. 435-443, 2003.
[64] W. D. Callister and A. Morin, *Science et génie des matériaux*. Dunod, 2001.
[65] G. Doyon, V. Rudnev, C. Russell, and J. Maher, "Revolution-not evolution-necessary to advance induction heat treating," *ADVANCED MATERIALS & PROCESSES*, vol. 175, no. 6, pp. 72-80, 2017.
[66] V. Savaria, F. Bridier, and P. Bocher, "Predicting the effects of material properties gradient and residual stresses on the bending fatigue strength of induction hardened aeronautical gears," *International Journal of Fatigue*, vol. 85, pp. 70-84, 2016.
[67] S. Rao and D. McPherson, "Experimental characterization of bending fatigue strength in gear teeth," *Gear Technology*, vol. 20, no. 1, pp. 25-32, 2003.
[68] K. FUJITA, A. YOSHIDA, and K. AKAMATSU, "A study on strength and failure of induction-hardened chromium-molybdenum steel spur gears," *Bulletin of JSME*, vol. 22, no. 164, pp. 242-248, 1979.
[69] Z. Li and B. L. Ferguson, "Induction Hardening Process With Preheat to Eliminate Cracking and Improve Quality of a Large Part With Various Wall Thickness," in *International Manufacturing Science and Engineering Conference*, 2017, vol. 50725: American Society of Mechanical Engineers, p. V001T02A026.
[70] J. Barglik, "Identification of temperature and hardness distribution during dual frequency induction hardening of gear wheels," *Archives of Electrical Engineering*, pp. 913–923-913–923, 2018.
[71] K. Gao *et al.*, "Numerical and experimental analysis of 3D spot induction hardening of AISI 1045 steel," *Journal of Materials Processing Technology*, vol. 214, no. 11, pp. 2425-2433, 2014.
[72] D. Ivanov, J. I. Asperheim, and L. Markegård, "Residual Stress Distribution in Induction Hardened Gear," in *28th ASM Heat treating society conference*, 2015, pp. 29-34.

[73] J. Chovan and M. Slodička, "Induction hardening of steel with restrained Joule heating and nonlinear law for magnetic induction field: Solvability," *Journal of Computational and Applied Mathematics,* vol. 311, pp. 630-644, 2017.
[74] H. Tawa, "Method for manufacturing gear," ed: Google Patents, 2020.
[75] Y.-Q. Zhao, Y. Han, and Y. Xiao, "An asynchronous dual-frequency induction heating process for bevel gears," *Applied Thermal Engineering,* vol. 169, p. 114981, 2020.
[76] H. Wen, Y. Han, X. Zhang, F. Liu, and H. Zhang, "Study on electromagnetic heating process of wind power gear: temperature morphology and evolution," *Journal of Thermal Science and Engineering Applications,* vol. 13, no. 3, 2021.
[77] J. Barglik, S. Golak, A. Smalcerz, and T. Wieczorek, "Numerical modeling of induction hardening of gear wheels made of steel AMS 6419," *Metalurgija,* vol. 58, no. 1-2, pp. 143-146, 2019.
[78] M. Baldan, A. Nikanorov, and B. Nacke, "A parallel multi-fidelity optimization approach in induction hardening," *COMPEL-The international journal for computation and mathematics in electrical and electronic engineering,* 2019.
[79] H. Li, W. Zhou, H. Liu, Z. Li, and L. He, "Analysis of Phase Transformation and Mechanical Properties of 55CrMo Steel during Induction Hardening," *Journal of Testing and Evaluation,* vol. 49, no. 1, 2019.
[80] D. Tong, J. Gu, and G. E. Totten, "Numerical investigation of asynchronous dual-frequency induction hardening of spur gear," *International Journal of Mechanical Sciences,* vol. 142, pp. 1-9, 2018.
[81] N. Barka, A. Chebak, A. E. Ouafi, P. Bocher, and J. Brousseau, "Sensitivity study of temperature profile of 4340 spur gear heated by induction process using 3D model," in *Applied Mechanics and Materials*, 2012, vol. 232: Trans Tech Publ, pp. 736-741.
[82] M. Khalifa, N. Barka, J. Brousseau, and P. Bocher, "Reduction of edge effect using response surface methodology and artificial neural network modeling of a spur gear treated by induction with flux concentrators," *The International Journal of Advanced Manufacturing Technology,* pp. 1-15, 2019.
[83] M. Khalifa, N. Barka, J. Brousseau, and P. Bocher, "Optimization of the edge effect of 4340 steel specimen heated by induction process with flux concentrators using finite element axis-symmetric simulation and experimental validation," *The International Journal of Advanced Manufacturing Technology,* vol. 104, no. 9, pp. 4549-4557, 2019.
[84] G. Taguchi, "Introduction to quality engineering: designing quality into products and processes," 1986.
[85] M. J. Crawley, *Statistical computingan introduction to data analysis using S-Plus* (no. 001.6424 C73). 2002.
[86] H. Chandler, *Heat treater's guide: practices and procedures for irons and steels*. ASM international, 1994.
[87] W. Jamil *et al.*, "Mechanical properties and microstructures of steel panels for laminated composites in armoured vehicles," *International Journal of Automotive & Mechanical Engineering,* vol. 13, no. 3, 2016.

[88] J. Berk and S. Berk, *Quality management for the technology sector*. Elsevier, 2000.
[89] G. Taguchi, "Taguchi on Robust Technology Development. Bringing Quality Engineering Upstream, 1993," ed: ASME Press, New York.
[90] R. K. Roy, *A primer on the Taguchi method*. Society of Manufacturing Engineers, 2010.
[91] S. S. Karganroudi, V. B. F. Kemda, and N. Barka, "A novel method of identifying porosity during laser welding of galvanized steels using microhardness pattern matrix," *Manufacturing Letters*, vol. 25, pp. 98-101, 2020.
[92] N. Barka, S. Sattarpanah Karganroudi, R. Fakir, P. Thibeault, and V. B. Feujofack Kemda, "Effects of Laser Hardening Process Parameters on Hardness Profile of 4340 Steel Spline—An Experimental Approach," *Coatings*, vol. 10, no. 4, p. 342, 2020.
[93] D. C. Montgomery, G. C. Runger, and N. F. Hubele, *Engineering statistics*. John Wiley & Sons, 2009.
[94] W. Y. Fowlkes and C. M. Creveling, *Engineering methods for robust product design: using Taguchi methods in technology and product development*. Addison-Wesley, 1995.
[95] D. C. Montgomery, "Design and analysis of experiments. John Wiley & Sons," *Inc., New York*, vol. 1997, p. 200.1, 2001.
[96] S. A. S. K. Grace-Martin, "Data analysis with SPSS: A first course in applied statistics," *Statistics*, vol. 4, p. 27, 2010.
[97] J. Frost, "Regression Analysis. An Intuitive Guide for Using and Interpreting Linear Models," *ebook*, 2019.
[98] H. Shokouhmand and S. Ghaffari, "Thermal analysis of moving induction heating of a hollow cylinder with subsequent spray cooling: Effect of velocity, initial position of coil, and geometry," *Applied Mathematical Modelling*, vol. 36, no. 9, pp. 4304-4323, 2012.
[99] S. L. Semiatin and D. E. Stutz, "Induction heat treatment of steel," 1985.
[100] H. Hammi, A. El Ouafi, and N. Barka, "Study of frequency effects on hardness profile of spline shaft heat-treated by induction," *Journal of Materials Science and Chemical Engineering*, vol. 4, no. 03, p. 1, 2016.
[101] V. Rudnev, "Induction hardening of gears and critical components," *Gear Technology*, pp. 58-63, 2008.
[102] S. S. K. Mahyar Parvinzadeh, Narges Omidi, Noureddine Barka, Mohamed Khalifa "A novel investigation into edge effect reduction of 4340 steel spur gear during induction hardening process," *The International Journal of Advanced Manufacturing Technology*, pp. 1-15, 2021, doi: 10.1007/s00170-021-06639-w.
[103] J. Grum, "Influence of induction surface heating and quenching on residual stress profiles, followed by grinding," *International Journal of Materials and Product Technology*, vol. 29, no. 1-4, pp. 211-227, 2007.
[104] K. Kurek and D. M. Dolega, "Numerical simulation of superficial induction hardening process," *International Journal of Materials and Product Technology*, vol. 29, no. 1-4, pp. 84-102, 2007.

[105] A. Pokrovskii, V. Leshkovtsev, A. Polushin, and E. Bochektueva, "Simulation of structural state and stresses in forming rolls subjected to hardening with induction heating," *Metal Science and Heat Treatment,* vol. 52, no. 9-10, pp. 442-445, 2011.
[106] G. Balachandran, A. Vadiraj, B. Sharath, and B. Krishnamurthy, "Studies on induction hardening of gray iron and ductile iron," *Transactions of the Indian Institute of Metals,* vol. 63, no. 4, pp. 707-713, 2010.
[107] A. Polushin, S. Kamantsev, V. Gryzunov, and M. Y. Minakov, "Kinetics of hardened layer formation with induction hardening," *Metal Science and Heat Treatment,* vol. 52, no. 7-8, pp. 388-392, 2010.
[108] V. Dutka, A. Maistrenko, V. Lukash, O. Mel'nichuk, and L. Virovets, "Computer-aided and experimental study of hardness distribution in cutting tool steel body due to phase transformations during induction hardening," *Journal of Superhard Materials,* vol. 34, no. 2, pp. 131-140, 2012.
[109] D. Rodman *et al.*, "Induction hardening of spur gearwheels made from 42CrMo4 hardening and tempering steel by employing spray cooling," *steel research international,* vol. 82, no. 4, pp. 329-336, 2011.
[110] K. Clarke, C. Van Tyne, C. Vigil, and R. Hackenberg, "Induction hardening 5150 steel: effects of initial microstructure and heating rate," *Journal of materials engineering and performance,* vol. 20, no. 2, pp. 161-168, 2011.
[111] E. Santos, K. Kida, T. Honda, H. Koike, and J. Rozwadowska, "Fatigue strength improvement of AISI E52100 bearing steel by induction heating and repeated quenching," *Materials Science,* vol. 47, no. 5, pp. 677-682, 2012.
[112] T. G. K. Hirsch, A. da Silva Rocha, and R. M. Nunes, "Distortion Analysis in the Manufacturing of Cold-Drawn and Induction-Hardened Components," *Metallurgical and Materials Transactions A,* vol. 44, no. 13, pp. 5806-5816, 2013.
[113] C.-M. Jeong, Y.-S. Yang, K.-Y. Bae, and C.-M. Hyun, "Prediction of deformation of steel plate with forced displacement and initial curvature in a forming process with high frequency induction heating," *International Journal of Precision Engineering and Manufacturing,* vol. 14, no. 5, pp. 785-790, 2013.
[114] M. H. Nateq, S. Kahrobaee, and M. Kashefi, "Use of eddy-current method for determining the thickness of induction-hardened layer in cast iron," *Metal Science and Heat Treatment,* vol. 55, no. 7-8, pp. 370-374, 2013.
[115] V. Nemkov, R. Goldstein, J. Jackowski, L. Ferguson, and Z. Li, "Stress and distortion evolution during induction case hardening of tube," *Journal of materials engineering and performance,* vol. 22, no. 7, pp. 1826-1832, 2013.
[116] M. Schwenk, J. Hoffmeister, and V. Schulze, "Experimental determination of process parameters and material data for numerical modeling of induction hardening," *Journal of materials engineering and performance,* vol. 22, no. 7, pp. 1861-1870, 2013.
[117] M. Hayne, P. Anderson, K. Findley, and C. Van Tyne, "Effect of Microstructural Banding on the Fatigue Behavior of Induction-Hardened 4140 Steel," *Metallurgical and Materials Transactions A,* vol. 44, no. 8, pp. 3428-3433, 2013.
[118] M. Spezzapria, M. Forzan, and F. Dughiero, "Multiphysical-Multiscale FEM Simulation of Contour Induction Hardening on Aeronautical Gears," 2015.

[119] V. Bukanin, A. Zenkov, A. Ivanov, and V. Nemkov, "Simulation of induction heat treatment of steel articles with the help of ELTA 6.0 and 2DELTA software," *Metal Science and Heat Treatment,* vol. 58, no. 7-8, pp. 493-497, 2016.
[120] H. Hammi, N. Barka, and A. El Ouafi, "Effects of induction heating process parameters on hardness profile of 4340 steel bearing shoulder using 2D axisymmetric model," *International Journal of Engineering and Innovative Technology,* vol. 4, pp. 41-48, 2015.
[121] "Induction Heat Treating," in *Induction Heating and Heat Treatment,* vol. 4C, V. Rudnev and G. E. Totten Eds.: ASM International, 2014, p. 0.
[122] A. Leatherman and D. E. Stutz, *Induction Heating Advances: Applications to 58000 F*. Technology Utilization Division, National Aeronautics and Space Administration, 1969.
[123] M. S. A. Nezhad and A. H. Ardakani, "A study of joint quality of aluminum and low carbon steel strips by warm rolling," *Materials & Design,* vol. 30, no. 4, pp. 1103-1109, 2009.
[124] M. Khalifa, N. Barka, J. Brousseau, and P. Bocher, "Reduction of edge effect using response surface methodology and artificial neural network modeling of a spur gear treated by induction with flux concentrators," *The International Journal of Advanced Manufacturing Technology,* vol. 104, no. 1, pp. 103-117, 2019.
[125] A. Chebak, N. Barka, A. Menou, J. Brousseau, and D. Ramdenee, "Simulation and validation of spur gear heated by induction using 3D multi-physics model," *World Academy of Science, Engineering and Technology,* vol. 59, pp. 893-897, 2011.
[126] S. Semiatin, *Elements of induction heating: design, control, and applications*. Asm International, 1988.
[127] V. Demidovich and Y. Y. Perevalov, "Increase in Efficiency of Heat Treatment of Large-Sized Mill Rolls by Simulating Thermal Conditions of Hardening," *Metallurgist,* vol. 63, no. 5, pp. 617-626, 2019.
[128] C.-Y. Lin, M. Wu, J. A. Bloom, I. J. Cox, M. L. Miller, and Y. M. Lui, "Rotation, scale, and translation resilient watermarking for images," *IEEE Transactions on image processing,* vol. 10, no. 5, pp. 767-782, 2001.
[129] E. Wrona and B. Nacke, "3D-Modelling for the Solution of Sophisticated Induction Harden-ing Tasks," 2003.
[130] J. Yuan, J. Kang, Y. Rong, and R. D. Sisson Jr, "Development of a Computer Model for Induction Hardening of Steel," in *ASME International Mechanical Engineering Congress and Exposition*, 2003, vol. 3719, pp. 15-21.
[131] Y. Favennec, V. Labbé, and F. Bay, "Induction heating processes optimization a general optimal control approach," *Journal of computational physics,* vol. 187, no. 1, pp. 68-94, 2003.
[132] H. Kawaguchi, M. Enokizono, and T. Todaka, "Thermal and magnetic field analysis of induction heating problems," *journal of materials processing technology,* vol. 161, no. 1-2, pp. 193-198, 2005.
[133] N. Barka, A. J. Khelalfa, P. Bocher, J. Brousseau, and S. Sundararajan, "Analysis of the effect of frequency using numerical modeling of induction hardening

process," in *1st International Conference on Sustainable Manufacturing, Montreal, Canada*, 2007.
[134] A. Pokrovskii, V. Leshkovtsev, A. Polushin, and E. Bochektueva, "Simulation of structural state and stresses in forming rolls subjected to hardening with induction heating," *Metal Science and Heat Treatment,* vol. 52, no. 9, pp. 442-445, 2011.
[135] G. Cheregi and M. Arion, "About the analisys of simultaneous induction hardening method of pinions with circular coil," *Journal of electrical and electronics engineering, University of Oradea,* pp. 26-29, 2008.
[136] V. Rudnev, "Unique Computer Modeling Approaches for Simulation of Induction Heating and Heat-Treating Processes," *Journal of materials engineering and performance,* vol. 22, no. 7, pp. 1899-1906, 2013.
[137] A. Frązyk, P. Urbanek, and J. Kucharski, "Control algorithms for inductors movement in induction heated calenders," *Image Processing & Communications,* vol. 17, no. 4, pp. 51-57, 2012.
[138] J. Barglik, A. Smalcerz, and A. Smagor, "Induction hardening of small gear wheels made of steel 50CrMo4," in *8th International Conference on Electromagnetic Processing of Materials*, 2015.
[139] V. I. Rudnev, "Single-coil dual-frequency induction hardening of gears," *Heat treating progress,* vol. 9, pp. 9-11, 2009.
[140] S. Lupi, M. Forzan, and A. Aliferov, "Induction and direct resistance heating," *Switzerland: Springer*, 2015.
[141] S. Dokos, *Modelling organs, tissues, cells and devices: using MATLAB and COMSOL multiphysics*. Springer, 2017.
[142] E. Rapoport and Y. Pleshivtseva, *Optimal control of induction heating processes*. CRC Press, 2006.
[143] W. D. Callister and D. G. Rethwisch, *Materials science and engineering: an introduction*. Wiley New York, 2018.
[144] K. Vučković, I. Čular, R. Mašović, I. Galić, and D. Žeželj, "Numerical model for bending fatigue life estimation of carburized spur gears with consideration of the adjacent tooth effect," *International Journal of Fatigue,* vol. 153, p. 106515, 2021.
[145] A. Senhaji, "Simulation numérique de la chauffe par induction électromagnétique d'un disque en AISI 4340," École de technologie supérieure, 2017.
[146] J. L. Dossett and H. E. Boyer, *Practical heat treating*. Asm International, 2006.
[147] G. E. Totten, C. E. Bates, and N. Clinton, *Handbook of quenchants and quenching technology*. ASM international, 1993.